

QC851
.C47
no.54
ATMOS

ISSN No. 0737-5352-54

**CHARACTERIZATION OF CARBONACEOUS AEROSOL DURING THE BIG
BEND REGIONAL AEROSOL AND VISIBILITY OBSERVATIONAL STUDY**

Steven G. Brown, Pierre Herckes, Sonia M. Kreidenweis and Jeffrey L. Collett, Jr.

Department of Atmospheric Science
Colorado State University
Fort Collins, CO

Funding Agency:
National Park Service
CA2380-99-001 T001-52
CA2350-97-001 T098-07

December, 2001

CIRA Cooperative Institute for Research in the Atmosphere

**Colorado
State
University**

CHARACTERIZATION OF CARBONACEOUS AEROSOL DURING THE
BIG BEND REGIONAL AEROSOL AND VISIBILITY OBSERVATIONAL
STUDY

Steven G. Brown, Pierre Herckes, Sonia M. Kreidenweis and Jeffrey L. Collett, Jr.

Department of Atmospheric Science

Colorado State University

Fort Collins, CO

Funding Agency:

National Park Service

#CA2350-97-001 T098-07

#CA2380-99-001 T001-52

December, 2001



018402 2636437

QC
851
.C47
NO. 54
ATMOS

ABSTRACT

CHARACTERIZATION OF CARBONACEOUS AEROSOL DURING THE BIG BEND REGIONAL AEROSOL AND VISIBILITY OBSERVATIONAL STUDY

The Big Bend Regional Aerosol and Visibility Observational (BRAVO) study was a four month field campaign (July-October 1999) to investigate aerosol particle properties, sources, and impacts on regional visibility in Big Bend National Park, Texas. Daily PM_{2.5} aerosol samples were collected on pre-fired quartz fiber filters for detailed molecular analysis of the aerosol organic carbon fraction. Aerosol black carbon concentrations during BRAVO were measured with an aethalometer.

The molecular characterization of the organic carbon fraction of aerosol present during the BRAVO study was performed using gas chromatography – mass spectroscopy (GC-MS). Organic carbon concentrations on individual days were too low for a detailed analysis by GC-MS. Therefore, multi-day composite samples, selected based on common air mass trajectories and temporal proximity, were extracted and analyzed for numerous compounds, including n-alkanes, polycyclic aromatic hydrocarbons (PAH), and alkanolic acids.

Low alkane Carbon Preference Indices (CPIs) during July through September reflect similar concentrations of n-alkanes containing odd and even numbers of carbon atoms and indicate that anthropogenic emissions were important contributors to carbonaceous aerosol during this period, when air masses generally were advected from the east over Texas and Mexico. In October, CPIs increased, reflecting increased influence of odd carbon numbered alkanes and

suggesting a predominant biogenic aerosol influence with air masses arriving from the north and the south. Plant wax contributions to odd carbon number alkanes (C₂₅-C₃₃) were estimated to range between 26% and 78%, with the highest contributions occurring in October with air masses arriving from the north and south. Periods with transport from eastern Texas and northeastern Mexico had much smaller plant wax contributions.

Alkanoic acids were the most abundant compound class, with CPIs that were high throughout the study. The high acid CPI suggests that the alkanolic acids may be largely biogenic in origin, a finding consistent with other studies. Caution is required in interpreting the acid CPI, however, as alkanolic acids can also be formed as secondary products of atmospheric reactions. Polycyclic aromatic hydrocarbons (PAH) were usually not found in abundance, suggesting that upwind combustion emissions were not important contributors to carbonaceous aerosol or that PAH were removed by reaction or deposition in transit. Higher PAH concentrations during one period indicated a more significant contribution from fresh combustion emissions.

Molecular source tracer (hopanes for vehicle emissions, levoglucosan for wood combustion, cholesterol for meat cooking) concentrations were generally not detected. Based on analytical detection limits for these species, it was estimated that wood smoke contributed no more than 1% of the total Organic Carbon (OC) present, vehicle exhaust contributed no more than 4%, and smoke from meat cooking contributed less than 13%. The presence of other wood smoke tracer molecules, however, suggests a possibly greater influence from wood combustion and possible chemical instability of levoglucosan during multi-day transport in an acidic atmosphere.

Several observations suggest that secondary production contributed significantly to BRAVO carbonaceous aerosol. Examination of ratios of aerosol organic carbon to elemental carbon indicates that secondary organic aerosol may have contributed between 45% and 90% of the total BRAVO aerosol organic carbon. High ratios of saturated/unsaturated C₁₈ acids, an abundance of nonanoic acid, and high concentrations of 6,10,14 trimethylpentadecan-2-one (an

indicator of secondary aerosol production from vegetation emissions) all support the conclusion that secondary aerosol formation was important in the region.

Total black carbon (BC) concentrations ranged from below detection limit (71 ng/m^3) to 267 ng/m^3 , averaging 129 ng/m^3 . Fine ($<1 \mu\text{m}$) aerosol BC concentrations averaged 114 ng/m^3 , and comprised 89% of the total BC. BC concentrations correlated reasonably well with aerosol sulfate concentrations, suggesting similar source regions for these species.

ACKNOWLEDGMENTS

This work was supported by the National Park Service under contracts #CA2350-97-001 T098-07 and #CA2380-99-001 T001-52. We would like to thank the BRAVO team members of Dr. Jenny Hand, Taehyoung Lee and D. Eli Sherman, whose diligent field work made this study possible. We'd also like to thank Laurie Trenary and Dr. Mike P. Hannigan for valuable advice. We thank Dr. Lowell Ashbaugh and the University of California, Davis for the IMPROVE data, Air Resource Specialists for providing logistical support for the BRAVO study, and Derek Day for NPS aethalometer data. We are grateful to Dr. Ken Reardon from the Department of Chemical and Bioresource Engineering for helpful comments on this work.

TABLE OF CONTENTS

List of Figures ix

List of Tables xii

1	Introduction.....	1
1.1	BRAVO Project Motivation and Objectives	1
1.2	Carbonaceous Aerosol: Organic Carbon	3
1.2.1	Visibility Degradation from Organic Aerosol	4
1.2.2	Sources of Organic Aerosol.....	6
1.3	Alkanes: Carbon Preference Indices.....	7
1.4	Alkanoic Acids : Carbon Preference Indices.....	10
1.5	Plant Wax Influence	11
1.6	Other Carboxylic Acids: Alkanoic Diacids and Oleic Acid.....	13
1.7	Polycyclic Aromatic Hydrocarbons.....	16
1.8	Tracers : Source Tracers.....	18
1.9	Tracers: Wood Smoke Tracers	19
1.10	Tracers : Secondary Biogenic Aerosol	20
1.11	Tracers: Coal and Fossil Fuel Usage	21
1.12	Secondary Organic Aerosol.....	22
1.13	Carbonaceous Aerosol: Black Carbon.....	23
1.14	Project Objectives and Layout.....	26
2	Methodology.....	27
2.1	Collection Setup	27
2.2	Filter Preparation, Loading, Unloading and Storage	28
2.3	Establishment of BRAVO Groups.....	28
2.3.1	Organic Carbon Concentrations During BRAVO	28
2.3.2	TOR Combustion Analysis.....	30
2.3.3	Use of the NOAA Hysplit Model	34
2.3.4	Development of an IDL Code to Chart Multiple Trajectories.....	35
2.3.5	Composite Descriptions.....	36
2.4	GC-MS Analytical Method	45
2.4.1	GC-MS Specifications.....	45
2.4.2	Gas Chromatography – Mass Spectroscopy Theory	46

2.5 Extraction Methods.....	48
2.5.1 DCM Extraction Method.....	49
2.5.2 Comparison of DCM Extraction Method with Hexane/Benzene/IPA Extraction Method.....	51
2.5.3 Calculations of Variances for Extraction Methods.....	52
2.5.4 Statistical Comparison between Extraction Methods.....	55
2.5.5 Methylation for Acid Analysis.....	58
2.5.6 Silylation for Sugars and Alcohols.....	60
2.5.7 Extraction of Blank Filters.....	61
2.6 Calculations of Source Influences from Tracer Concentrations.....	62
2.6.1 Contributions from Vehicular Exhaust Calculations.....	63
2.6.2 Contributions from Meat Smoke Calculations.....	64
2.6.3 Contributions from Wood Smoke Calculations.....	65
2.6.4 Extraction of Source Samples.....	67
2.7 Estimations of Secondary OC.....	68
2.8 Aethalometer Sampling of Black Carbon.....	69
2.8.1 Aethalometer Setup.....	69
2.8.2 Aethalometer Sampling Principles.....	70
2.8.3 Aethalometer Data Assimilation.....	71
3 Results and Discussion.....	72
3.1 General Characterization of Organic Aerosol During BRAVO.....	72
3.1.1 Characterization of Compound Classes.....	73
3.1.2 Typical Distributions of Alkanes and Alkanoic Acids.....	75
3.2 Carbon Preference Indices.....	77
3.2.1 Plant Wax Influences on the n-Alkanes and n-Alkanoic Acids.....	79
3.3 PAH 81	
3.4 n-Alkanoic Diacids and C18 Ratio.....	83
3.5 Tracers: Maximum Influences of Sources.....	87
3.5.1 Source contribution estimates from tracer concentrations.....	87
3.5.2 Sensitivity Analysis of Source Influences.....	88
3.6 Tracers: Other Wood Smoke Markers.....	92
3.7 Estimated Source Contributions from Consideration of Alternative Tracers.....	94
3.7.1 Calculations Using Vanillin as a Source Tracer for Wood Smoke.....	94
3.7.2 Calculations of Vehicle Influence Using EC as a Source Tracer.....	96
3.8 Tracers: Other Compounds.....	98
3.8.1 Secondary Biogenic Aerosol.....	98
3.8.2 Coal and Fossil Fuel Markers.....	99
3.8.3 Citric Acid.....	100
3.9 Secondary Organic Aerosol Estimations.....	101
3.10 Black Carbon.....	106
3.10.1 Calculation of the Aethalometer Detection Limit.....	107
3.10.2 Comparison of CSU Aethalometer BC with NPS Aethalometer BC and IMPROVE EC.....	109
3.10.3 Aethalometer Black Carbon and Inorganic Species.....	112

4 Conclusions.....	116
5 Future Work.....	121
References.....	124
Appendix A - Daily flow rates, total sampling times and volume collected on organics sampler during BRAVO.....	133
Appendix B – IDL codes.....	137
Appendix C – Daily Air Mass Trajectories.....	143
Appendix D – Error Calculations and Propagation.....	165
Appendix E – Concentrations of Species.....	165

LIST OF FIGURES

Figure 1.1 Map of the area surrounding Big Bend N. P.	2
Figure 1.2 Typical mass and scattering distribution over particle size (from Malm, 1999).	5
Figure 1.3 Annual average (a) extinction in inverse megameters due to OC and (b) percent contribution of organic carbon to total extinction (from Malm, 1994).....	6
Figure 1.4 Structure of C18 alkane – octadecane.	8
Figure 1.5 Structure of C12 alkanolic (dodecoic) acid.	10
Figure 1.6 Structure of Oleic acid (C18:1).	13
Figure 1.7 Breakdown of oleic acid into nonanoic (C9 acid) and azelaic (C9 diacid) acid.....	14
Figure 1.8 Structures of alkanolic diacids: succinic and azelaic acid.....	16
Figure 1.9 Structures of PAH: anthracene, phenanthrene, 1-methylphenanthrene, 9-methylanthracene, pyrene, fluoranthene, benzo[b]fluoranthene and benzo[a]pyrene.....	17
Figure 1.10 Structures of several source tracer species: hopanes, levoglucosan, and cholesterol.	18
Figure 1.11 Structures of wood smoke markers: vanillin, syringaldehyde, abietic acid and retene.....	20
Figure 1.12 Structure of 6,10,14-trimethylpentadecan-2-one.....	21
Figure 1.13 Structures of fossil fuel tracers: picene, phytane and pristane.....	22
Figure 1.14 Annual mean BC (a) concentrations and (b) as percent of total aerosol mass (from Seinfeld and Pandis, 1998).	25
Figure 1.15 Percent contribution of BC toward light extinction in the U.S. (from Malm, 1994).	25
Figure 2.1 Daily IMPROVE OC concentrations and estimated CSU μg OC collected	29
Figure 2.2 Daily IMPROVE OC concentrations and daily CSU OC (μg) remaining for analysis.....	30
Figure 2.3 Volatilization/combustion area of DRI TOR carbon analyzer (from Chow et al., 1993).....	31
Figure 2.4 An example of a DRI thermal/optical reflectance carbon analyzer thermogram (from Chow et al., 1993).....	33
Figure 2.5 BRAVO groups' daily trajectories: Border July, Mid July, TxMxJuly, Mx July, Border Aug, SBorder Aug.....	38
Figure 2.6 BRAVO groups' daily trajectories: EtxMxAug, Border Loop, XBorder, BorderSA, ETxMxSept, SW Sept1, SW Sept2.....	38
Figure 2.7 BRAVO groups' daily trajectories: TxMx Dip, ETxMx Oct, Central Mexico, SSE October, North Texas 1, North Texas 2.....	39
Figure 2.8 Graphical representation of the temperature scheme used for GC analysis	46
Figure 2.9 Flow chart of extraction and derivatization techniques.....	49
Figure 2.10 Diagram of diazomethane generating system, from Kimble Glassware Catalogue, part #767200.....	59

Figure 3.1 Mass budget of PM _{2.5} aerosol during BRAVO.....	72
Figure 3.2 Percent of total OCM identified as alkanes, PAH and alkanolic acids and total identified compounds percentage; error bars represent a 8.6% error for alkanes, 4.6% error for PAH and 7.3% error for alkanolic acids, and 12.2% error for total identified compounds, all of which are one standard deviation	74
Figure 3.3 Alkane Concentrations for MxJuly, BorderSA and SSEOct; error bars represent a 34.6% (one standard deviation) error for alkanes for the DCM extraction method.....	76
Figure 3.4 Concentrations of alkanolic acids in the sample groups MxJuly, BorderSA and SSEOct; error bars represent a 20.4% error (one standard deviation) for quantifying alkanolic acids with the DCM extraction method.....	77
Figure 3.5 BRAVO groups' alkane CPIs; error bars represent one standard deviation, an average error in the alkane CPI calculation of 22.2%.....	78
Figure 3.6 BRAVO groups' alkanolic acid CPIs; error bars represent a 17.7% error (one standard deviation) in calculating alkanolic acid CPIs with the DCM extraction method.....	79
Figure 3.7 Average percentage contributions of odd n-alkanes (C25-C33) derived from plant wax; error bars represent an average 49.2% error (one standard deviation) for the plant wax percentage calculation	80
Figure 3.8 Average influence (%) of plant wax on even alkanolic acids (C12-C30) for BRAVO groups; error bars represent a 29.0% error (one standard deviation) for calculating alkanolic acid CPIs	81
Figure 3.9 BRAVO groups' PAH concentrations, grouped by compound mass; error bars signify a 14.1% error (one standard deviation) in quantifying PAH with the DCM extraction method.....	82
Figure 3.10 BRAVO groups' concentrations of alkanolic diacids and oleic acid; error bars represent a 20.4% error (one standard deviation) for alkanolic acids with the DCM extraction method.....	83
Figure 3.11 BRAVO groups' C18:0 / C18:1 ratios; error bars represent a 28.8% error (one standard deviation) in calculating this ratio	84
Figure 3.12 Graph of average temperature and C18 ratio for BRAVO groups	85
Figure 3.13 Percentage of total alkanolic acid that is C9 acid; error bars represent a 22.2% error (one standard deviation) in calculating this ratio.	86
Figure 3.14 C18 ratio vs. C9 alkanolic acid concentration (ng/m ³).....	86
Figure 3.15 Maximum estimated influences for BRAVO groups for vehicular exhaust, meat cooking and wood smoke: using Rogge (1993) for autos and Schauer (1999) for diesel, Rogge (1991) for meat cooking, and Nolte (2001) for wood smoke.....	88
Figure 3.16 Sensitivity study using for vehicular exhaust using Rogge et al. (1993); varying the ratio between catalyst, non-catalyst and diesel emissions.....	89
Figure 3.17 Sensitivity analysis of vehicular exhaust influence using Rogge et al. (1993) for auto and Schauer et al. (1999) for diesel emissions	90
Figure 3.18 Sensitivity analysis for meat cooking: varying the ratio of charbroiling:frying meat.....	91
Figure 3.19 Sensitivity analysis for wood smoke: varying the ratio between pine and oak smoke	92
Figure 3.20 BRAVO groups' concentrations of wood smoke markers; error bars represent a 14.1% error (one standard deviation) in quantifying PAH	93
Figure 3.21 Acid-catalyzed hydrolysis of levoglucosan in acidic cloud drops.....	94
Figure 3.22 Influence of wood smoke (%) on total OC: comparison of using vanillin versus levoglucosan as tracer using source profiles from Schauer et al. (2001).....	95

Figure 3.23 Maximum influence on the BRAVO OC from vehicles, based on EC	97
Figure 3.24 BRAVO groups' 6,10,14-trimethylpentadecan-2-one concentrations; error bars represent a 34.6% error (one standard deviation) in quantifying alkanes with the DCM method.....	98
Figure 3.25 BRAVO groups' concentrations of 6,10,14 trimethylpentadecan-2-one normalized by OC in ppm; error bars represent a 40% error in this calculation (one standard deviation).....	99
Figure 3.26 Structure of citric acid	100
Figure 3.27 Citric acid concentrations during BRAVO; error bars represent a 20.4% error (one standard deviation) in quantifying acids with the DCM extraction method.....	101
Figure 3.28 Percentage of OC that is secondary during BRAVO, assuming an $OC/EC_{min} = 1.95$ (average winter (Dec-Feb, 1988-1998) ratio at BBNP); error bars represent a 30.5% error (one standard deviation) for this calculation	102
Figure 3.29 Secondary OC Percentage vs. OC/EC ratio for BRAVO groups, assuming a primary OC/EC ratio of 1.95 (average winter ratio at BBNP).....	103
Figure 3.30 EC concentration vs. secondary OC percentage, using an OC/EC ratio of 1.95 (average winter ratio at BBNP).....	104
Figure 3.31 Graph of Estimated Secondary OC % ($OC/EC=1.95$) vs. 6,10,14trimethylpentadecan-2-one divided by total OC	105
Figure 3.32 Graph of Estimated Secondary OC % ($OC/EC=1.95$) vs. C18 Ratio.....	105
Figure 3.33 CSU Aethalometer Daily Black Carbon Concentrations (ng/m^3): Total BC, Fine BC (1 μm aerodynamic diameter cut), and Coarse BC (Total – Fine). The aethalometer detection limit, calculated based on the average blank plus three standard deviations, was estimated as 71 ng/m^3	107
Figure 3.34 CSU Aethalometer Total BC (ng/m^3) versus NPS Aethalometer Total BC (ng/m^3)	109
Figure 3.35 CSU Aethalometer Fine Black Carbon (1 μm aerodynamic diameter cut) versus IMPROVE fine EC from TOR analysis (2.5 μm aerodynamic diameter cut)	110
Figure 3.36 IMPROVE Fine Elemental Carbon (2.5 μm aerodynamic diameter size cut) versus NPS Aethalometer Total Black Carbon.....	111
Figure 3.37 CSU Aethalometer Fine Black Carbon (1 μm size cut) versus CSU Fine (2.5 μm size cut) SO_4^{2-}	112
Figure 3.38 CSU Aethalometer Fine BC (1 μm size cut) vs CSU total fine N[-III] (2.5 μm size cut).....	113
Figure 3.39 CSU Aethalometer Fine BC (1 μm size cut) vs. CSU Fine K^+ (2.5 μm size cut)	114
Figure 3.40 CSU Aethalometer Total BC vs. CSU Fine K^+ (2.5 μm size cut)	114
Figures C1-122 Charts of Daily Air Mass Trajectories During the BRAVO Study.....	142-161

LIST OF TABLES

Table 1.1 CPIs of n-alkanes and n-alkanoic acids for various aerosol sources	9
Table 1.2 Percentage of alkanes derived from plant wax reported from previous studies	13
Table 1.3 C18:0/C18:1 ratios for various locations and time of year	15
Table 1.4 Listing of Secondary OC % and correlation between EC and Secondary OC.....	23
Table 2.1 Trajectory Groupings: dates included, trajectory description, total OC (μg), and OC/EC; * denotes extracted and analyzed groups	37
Table 2.2 Deuterated standards used for quantification: their concentrations and amounts added	48
Table 2.3 Sample Method Comparison Table	52
Table 2.4 Comparison of Extraction Methods for Alkanes, PAHs and Alkanoic Acids	55
Table 2.5 Differences between average concentrations measured by the DCM and Hx/Bz/IPA extraction methods for alkanes; values above the critical value of 835 at 95% confidence level (and therefore showing a significant difference between the methods) are denoted in bold.....	57
Table 2.6 Differences between the DCM and Hx/Bz/IPA extraction methods for alkanic acids; values above the critical value of 1172 at 95% confidence level (and therefore showing a significant difference between the methods) are denoted in bold	57
Table 2.7 Differences between the average concentrations measured by the DCM and Hx/Bz/IPA extraction methods for PAH; values above the critical value of 41969 at 95% confidence level (and therefore showing a significant difference between the methods) are denoted in bold.....	58
Table 2.8 Source Profile for Vehicular Fine Particle Emissions (adapted from Rogge et al., 1993a; diesel from Schauer et al., 1999).....	63
Table 2.9 Source Profile for Meat Cooking Emissions (adapted from Rogge et al., 1991 and Schauer et al., 1999).....	65
Table 2.10 Source Profile for Wood Burning Emissions (adapted from Schauer et al., 2001, Fine et al., 2001, and source extracts).....	66
Table 2.11 Refractive indices of some atmospheric substances at $\lambda = 589 \text{ nm}$ unless otherwise noted (adapted from Seinfeld and Pandis, 1998; and Finlayson-Pitts and Pitts, 1999)	71
Table 3.1 Percentage of total OCM that has been identified as specific compounds in previous source sample and ambient studies and this BRAVO study (range of percent identified in parentheses)	75
Table 3.2 Listing of Secondary OC % and correlation between EC concentration and Secondary OC	103
Table 3.3 Aethalometer Blank Run Concentrations, Average Concentration, Standard Deviation, and Detection Limit (Avg + 3 SD).....	108
Table A1: Daily flow rate, total sampling time, channel, and total volume collected.....	133
Table D1 Error propagation in arithmetic calculations (from Skoog et al., 1992)	165
Tables E1-E4 Concentrations of Species in each BRAVO Composite Sample.....	165

1 Introduction

The Big Bend Regional Aerosol and Visibility Observational Study (BRAVO) was conducted in Big Bend National Park, Texas, July through October 1999. Although Big Bend is very remote, it has some of the poorest visibility among national parks (Gebhart et al., 2000). The goals of the study included determining the physical and chemical characteristics of the aerosol present, the importance of various particle sources, and their impacts on visibility degradation in the park. Specific areas of interest discussed here include the characterization of the molecular composition of the organic aerosol present in the park in order to evaluate the relative importance of different carbonaceous aerosol source types, and a characterization of the black carbon present during the study.

1.1 BRAVO Project Motivation and Objectives

Big Bend National Park is a national park on the Texas – Mexico border encompassing over 800,000 acres. Along the park's southern boundary, the Rio Grande has cut a large canyon in the middle of the Chihuahuan desert near the Chisos Mountain range. The park is the largest protected area of the Chihuahuan desert, which stretches from Texas into central Mexico. Artifacts over 9,000 years old have been discovered here, as well as fossils from the Cretaceous and Tertiary periods. A map of the area surrounding Big Bend N. P. is shown in figure 1.1.

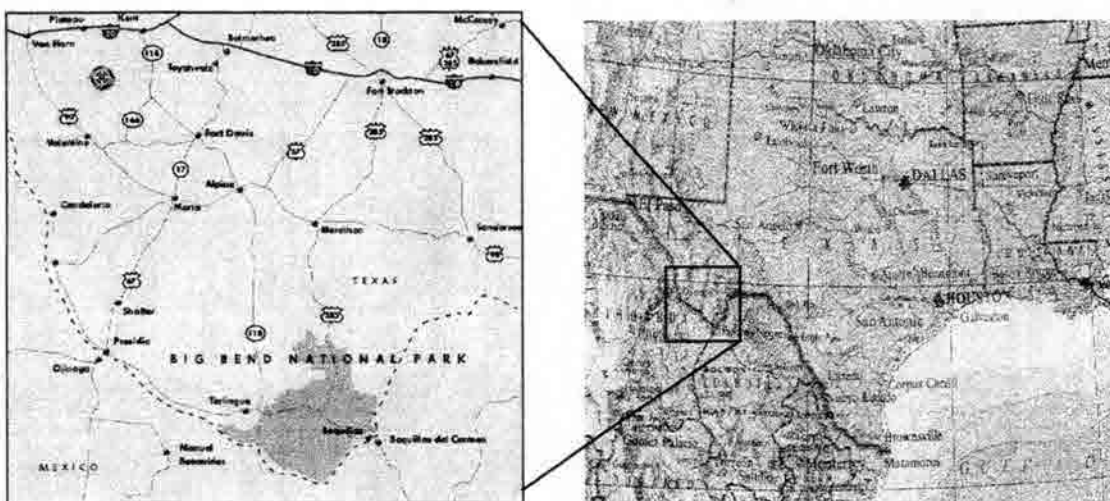


Figure 1.1 Map of the area surrounding Big Bend N. P.

Despite being one of the most remote areas in the United States, the park has poor air quality and visibility (Gebhart et al., 2000). Initially, a U.S./Mexico bilateral group was established in 1993 to investigate the impact of two major Mexican coal power plants, Carbon I and II, on nearby Big Bend Park. After a preliminary study in 1996 (Big Bend Air Quality Work Group, 1999; Gebhart et al., 2000), it was recommended that an extensive field study be launched, which led to the initiation of the Big Bend Regional Aerosol and Visibility Observational (BRAVO) study. BRAVO was conducted from July through October of 1999. The main objectives of this study included the full characterization of the fine and coarse aerosol mass, atmospheric optical properties, gaseous pollutants and meteorology present in Big Bend National Park.

Specific tasks of the study were to identify and quantify the major source regions impacting the park, notably focusing on: the coal burning plants Carbon Plants I and II; industrial emissions along the Texas Gulf coast and near Monterrey, Mexico; refineries and coal-fired power plants in Texas and New Mexico; and the major sulfur dioxide emitters in the southeastern

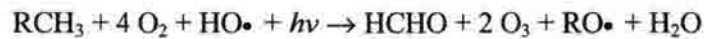
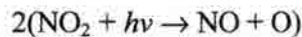
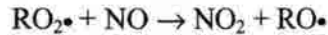
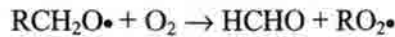
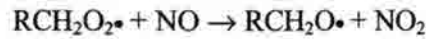
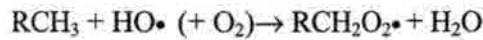
US. The chemical and physical characteristics of the aerosol and the impact on light scattering were to be examined. Pathways of pollutant advection were studied, as well as the role of meteorology. The organic carbon fraction was to be analyzed to help assess contributions from individual source types. Scattering and absorption contributions to the Big Bend haze were also to be estimated, as well as relationships between particle composition, concentration and light extinction.

1.2 Carbonaceous Aerosol: Organic Carbon

The organic carbon (OC) fraction of atmospheric aerosol consists of a complex mixture of hundreds of compounds in both rural and urban environments (Simoneit et al., 1982, 1988, 1995; Simoneit, 1989; Rogge et al., 1991, 1993a,b; Schauer et al., 1996, 2000; Jacobson et al., 2000). This includes many different compound classes, such as n-alkanes, n-alkanoic acids, polycyclic aromatic hydrocarbons (PAH), n-alkanoic diacids, alcohols, alkanones and others (Rogge et al., 1991, 1993a,b, 1998; Oros et al., 1999b; Schauer et al., 1999, 2001; Nolte et al., 2001; Fine et al., 2001). After sulfates, organic compounds are usually the second most abundant fraction of fine aerosol (Jacobson et al., 2000), and as such play an important role in determining the aerosol's chemical composition and physical properties.

Organic compounds can have impacts on human health, climate, cloud nucleation, tropospheric ozone production, and visibility. For instance, PAH are extremely toxic and carcinogenic, even in low concentrations (Payne, 1982; Stanley et al., 1990; Eskinja et al., 1996). Penner et al. (1992) have given an estimate of -2.0 W/m^2 radiative forcing due to organic aerosol, though the overall aerosol effect on climate is still highly uncertain. Many highly and slightly soluble organic compounds can be cloud active (Kulmala et al., 1996), as well as causing delays in droplet formation (Bigg, 1986) and evaporation (Gill et al., 1983). Aliphatic hydrocarbons (RCH_3) can react with hydroxyl radical to form intermediary peroxy radicals (RO_2); these peroxy

radicals then react with NO, converting it to NO₂. NO₂ photolysis yields atomic oxygen, which reacts with molecular oxygen (O₂) to form ozone (O₃) (Seinfeld and Pandis, 1998):



Other hydrocarbon oxidation mechanisms contribute to ozone formation in analogous ways (Finlayson-Pitts and Pitts, 1999). These reactions show that tropospheric ozone production is sensitive to the amount and speciation of organic carbon and NO_x present. Additionally, since organic aerosols are also a product of volatile organic compound (VOC) oxidation, photochemical smog episodes are often associated with higher OC (Gray et al., 1986, Hildemann et al., 1994).

1.2.1 Visibility Degradation from Organic Aerosol

Visibility degradation results from particles and gases scattering and absorbing light. Visibility is reduced when there is significant scattering or absorption of the light transmitted between an object and an observer. This decreases the contrast between the object and the background sky, thus reducing visibility. Fine aerosol (< 2.5 μm aerodynamic diameter) is particularly effective at light scattering, as shown in figure 1.2, due to Mie scattering, where fine particle diameters are close to the wavelengths of visible light that they scatter.

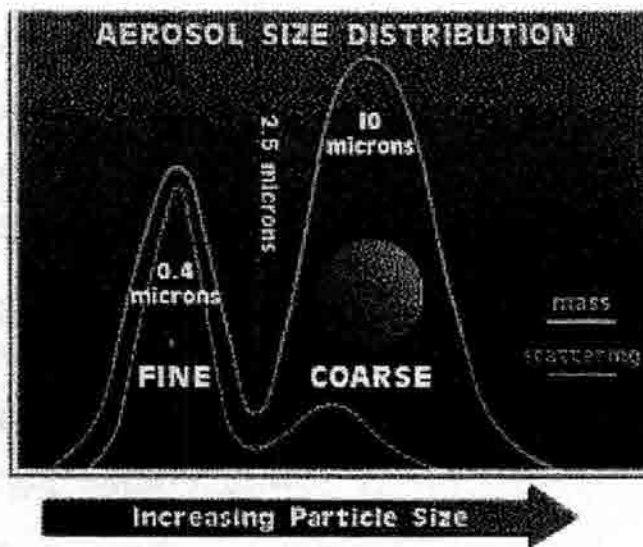


Figure 1.2 Typical mass and scattering distribution over particle size (from Malm, 1999).

Organic aerosol has been reported to be responsible for as much as 60% of the fine-particle scattering (Jacobson et al., 2000), especially in urban environments in the western U.S. Figure 1.3 shows yearly average contributions of organic aerosol to total light extinction in the U.S., as measured at Interagency Monitoring of PROtected Visual Environments (IMPROVE) sites.

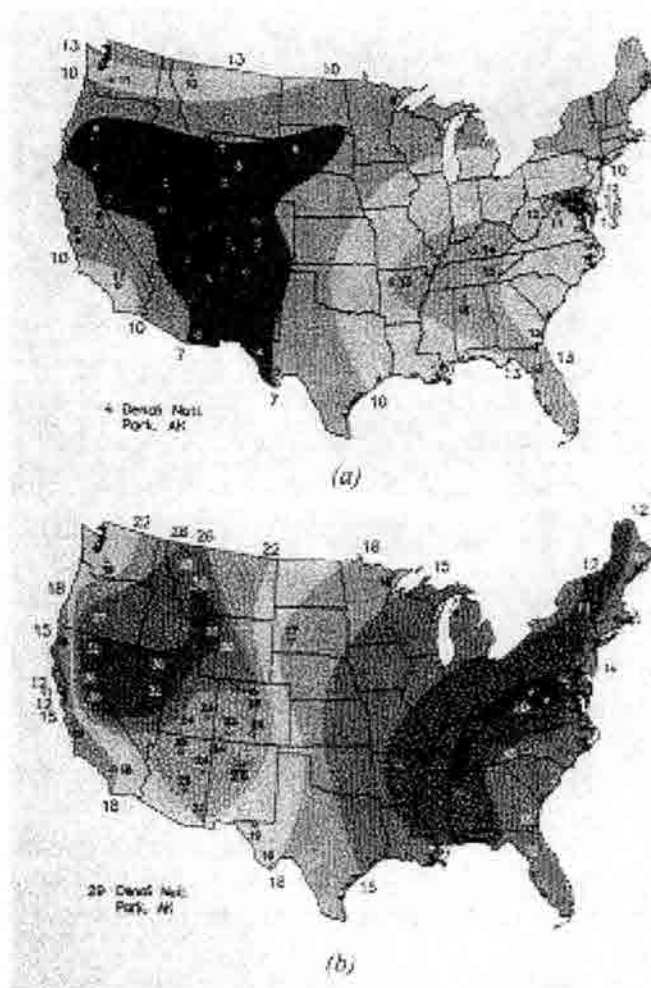


Figure 1.3 Annual average (a) extinction in inverse megameters due to OC and (b) percent contribution of organic carbon to total extinction (from Malm, 1994)

The effect of organic compounds on visibility ranges from 9% to 36% of the total light extinction at the IMPROVE sites, which are situated mainly in rural environments, including national parks. From figure 1.3, it is estimated that organics on average contribute 19% of the total light extinction in Big Bend N.P. annually.

1.2.2 Sources of Organic Aerosol

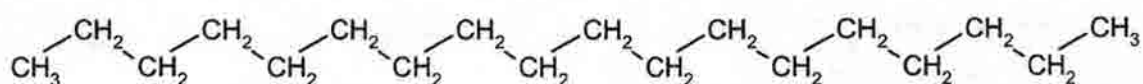
Organic aerosol particles can either be emitted directly from a source as a primary emission, or can be formed in the atmosphere from volatile species as a secondary product.

Primary aerosol emissions can also be altered by atmospheric oxidation to form secondary products. Anthropogenic sources of primary organic aerosol include meat cooking, cigarette smoke, and various combustion processes (vehicles, power plants, coal and wood burning). Primary biogenic sources include plant waxes, fungi, bacteria, pollen, algae and biomass burning (Matsumoto and Hanya, 1980; Simoneit and Mazurek, 1982; Limbeck and Puxbaum, 1999). Relative contributions of primary versus secondary emissions depend on the types of local emissions, meteorology and atmospheric chemical conditions.

In urban environments, there is generally a large amount of organic aerosol primary emissions, with significant contributions from anthropogenic sources (Simoneit 1989, Simoneit et al., 1991a; Schauer et al., 1996; Zheng et al., 1997, 2000; Azevedo et al., 1999; Fang et al., 1999b; Kavouras et al., 1999; Didyk et al., 2000; Kendall et al., 2001). Rural environments usually have a larger contribution from biogenic aerosol compared to urban areas, but may also have a significant contribution from anthropogenic sources (Simoneit et al., 1982, 1988, 1991b; Gogou et al., 1996; Castro et al., 1999; Schauer et al., 2000; Pio et al., 2001). The degree of anthropogenic contributions at rural sites depends on air advection patterns, distance from sources and local meteorology. Rural sites can also have a higher content of secondary organics than urban areas if precursor emissions from non-local sources are transported to the rural site; during transport, the aerosol is subject to atmospheric oxidation and can be altered from its primary form (Castro et al., 1999).

1.3 Alkanes: Carbon Preference Indices

One class of compounds analyzed in BRAVO aerosol samples was the homologous series of n-alkanes. The n-alkanes are comprised of saturated straight carbon chains designated by the number of carbon atoms in a chain. For example, the alkane C-18 has eighteen carbon atoms linked in a chain, as seen in figure 1.4.



C18 alkane - octadecane

Figure 1.4 Structure of C18 alkane – octadecane.

One useful characterization of n-alkanes is the carbon preference index, defined as the ratio of molecules containing odd to even numbers of carbon atoms. Carbon preference indices (CPIs) have been used as indicators of biogenic and anthropogenic contributions to organic aerosol (Simoneit 1978, 1989; Simoneit and Mazurek, 1982; Simoneit et al., 1990, 1991a,b,c, 1999; Rogge et al, 1993b; Abas et al., 1995; Zheng et al., 1997; Fang et al., 1999a,b; Didyk et al., 2000).

The alkane CPI is defined as the sum of the concentrations of odd carbon number alkanes divided by the sum of the concentrations of the even carbon number alkanes:

$$\text{Alkane CPI} = \frac{\sum \text{OddCarbonNumberAlkanes}}{\sum \text{EvenCarbonNumberAlkanes}} \quad (1.1)$$

If there is no odd or even carbon preference, this ratio will be one. Although n-alkanes are emitted by many source types, their CPI can provide some insight as to what source types (anthropogenic versus biogenic) are most strongly influencing the alkane composition. Alkane CPIs greater than one, indicating an odd carbon number preference, are observed in biogenic emissions (Simoneit, 1978, 1989; Simoneit and Mazurek, 1982; Simoneit et al., 1990, 1991a,b; Rogge et al, 1993b; Abas et al., 1995; Azevedo et al., 1999; Kavouras et al., 1999). The odd carbon number alkanes in biogenic emissions are derived from the decarboxylation or carbonyl reduction of even carbon number alkanic acids, which are preferentially synthesized in

biological processes (Stryer et al., 1988; Prescott et al., 1999). The even carbon number alkanolic acids are preferentially synthesized because malonyl-CoA, a three-carbon chain attached to coenzyme A, is used to elongate the four-carbon chain fatty acid precursor; with the loss of CO₂ during the process, the result is an even carbon number chain after each elongation step, which leads to an odd carbon number alkane chain after decarboxylation.

Table 1.1 CPIs of n-alkanes and n-alkanoic acids for various aerosol sources

Type	n-alkane CPI	n-alkanoic acid CPI	Reference
Urban Western US	1.2-2.8	8.0-23.0	Simoneit 1989
Santiago, Chile	1.11-1.28	N/A	Didyk et al. 2000
Hong Kong	1.2-1.9	4.4-15.2	Zheng et al. 2000
Eastern Mediterranean, Urban	1.3-1.6	6-9.5	Gogou et al. 1996
Vehicular Exhaust : Cars	0.93	N/A	Simoneit 1989
Vehicular Exhaust : Diesel	1.02	N/A	Simoneit 1989
Rural Western US	1.6-8.4	5.0-12.0	Simoneit 1989
Eastern Mediterranean, Rural	1.6-3.3	5-10	Gogou et al. 1996
Vascular Plant Wax	6-10	7-20	Simoneit 1989
Natural Fire Smoke	1.2-10	13-20	Simoneit 1989
Oceanic Aerosol : Atlantic	5-10	4-10	Simoneit 1989
Oceanic Aerosol : Pacific	2-4	10-14	Simoneit 1989

Table 1.1 includes alkane CPI values for several aerosol source types. As reported by Simoneit (1989), purely anthropogenic emissions, such as vehicular exhaust, have CPIs close to 1, while vascular plant wax aerosol has much higher CPIs (6-10). This strong biogenic carbon preference allows for comparison of the relative importance of biogenic contributions between aerosol samples. For example, urban CPIs in the western US have been observed between 1.2 and 2.8, while rural site CPIs have been found to be between 1.6 and 8.4. The lower values for

the urban sites reflect a larger degree of anthropogenic input from fossil fuel combustion than found in the rural atmosphere, whereas CPIs are higher in rural areas due to higher vegetative emissions.

Alkane CPIs can be broken down further into two classes (Mazurek and Simoneit, 1982; Abas and Simoneit, 1996; Pio et al., 2001). C12 to C25 n-alkanes are often considered microbial or algal in origin, while C26 to C35 n-alkanes are from higher plant waxes and are a strong indicator of vegetative origin. Generally, the C12 to C25 CPI is 0.8 – 2.0 in rural atmospheres and 0.9 to 1.3 in urban atmospheres, while the C26 to C35 CPI can vary between 1.5 and 13.0 for rural and from 2 to 3.3 for urban atmospheres in the western U.S. (Simoneit, 1989). The higher CPIs for C26 to C35 indicate that plant wax is the main contribution in this range of alkanes.

1.4 Alkanoic Acids : Carbon Preference Indices

Another series of compounds analyzed were the n-alkanoic acids. n-Alkanoic acids are similar in structure to n-alkanes as they are characterized by long carbon chains, but containing a carboxyl group (consisting of a carbon, two oxygens and a hydrogen, -COOH) at one end. Alkanoic acids can also be named by their carbon number. For example, a C12 acid is a compound with a carbon chain of eleven carbons and a carboxylic acid group on one end, as shown in figure 1.5.

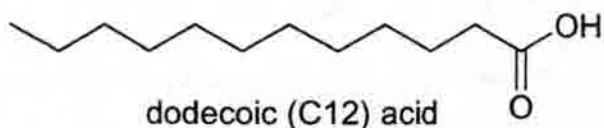


Figure 1.5 Structure of C12 alkanoic (dodecoic) acid.

Alkanoic acids also exhibit a carbon number preference with regard to biological source emissions. In this case a biogenic preference is shown by even carbon numbers. A CPI for

alkanoic acids is defined in equation 1.2 (Mazurek and Simoneit, 1982; Simoneit, 1989; Lawrence and Koutrakis, 1996):

$$\text{Acid CPI} = \frac{\sum \text{EvenCarbonNumberAcids}}{\sum \text{OddCarbonNumberAcids}} \quad (1.2)$$

This equation is analogous to the inverse of the alkane CPI equation, since even carbon number acids are preferentially emitted from biological sources. As with the alkanes, a larger CPI is indicative of more biogenic influence on the aerosol composition (Simoneit and Mazurek, 1982; Simoneit, 1989; Rogge et al, 1993b; Zheng et al., 1997; Mayol-Bracero et al., 2001). As seen in Table 1.1, alkanolic acid CPIs are usually high for both rural and urban sites, indicating that these acids are mainly biogenic in origin (Simoneit 1989; Zheng et al., 1997). Additionally, alkanolic acids have been reported as a major constituent of marine aerosol, and their abundance can indicate marine influence (Sicre et al., 1990; Stephanou, 1992; Gogou et al., 1994; Novakov et al., 1997; Limbeck et al., 1999). However, these acids can also be secondary products of oxidation reactions of higher-molecular weight compounds (Simoneit and Mazurek, 1982; Lawrence and Koutrakis, 1996); alkanolic acids can, therefore, not always be assumed to originate as primary emissions.

1.5 Plant Wax Influence

Since n-alkanes emitted from fossil fuel combustion generally have a CPI of about one (Simoneit, 1984, 1988, 1989), especially for homologs larger than n-C₂₄, the amount of alkanes that raise the CPI above one can be designated as purely biogenic (Simoneit et al., 1982, 1990, 1991a,b,c; Zheng et al., 1997). A numerical evaluation based on CPIs has been developed and used to distinguish plant wax influence from fossil fuel derived alkanes (Schneider et al., 1983;

Sicre et al., 1987; Simoneit et al., 1990, 1991a,b,c; Gougou et al., 1996; Fang et al., 1999b; Kavouras et al., 1999; Xie et al., 2000; Zheng et al., 2000; Pio et al., 2001). Concentrations of plant wax alkanes are calculated via subtraction of the average of the concentrations of the next higher and lower even carbon numbered homologs from the concentration of the odd carbon number alkane:

$$\text{Plant Wax } C_n = [C_n] - \left[\frac{(C_{n+1}) + (C_{n-1})}{2} \right] \quad (1.3)$$

Negative values were taken as zero. This running average calculation assumes that the wax n-alkanes are derived directly from vegetative emissions and that soil detritus is not a significant fraction of the alkanes. For each odd n-alkane, the percentage of plant wax influence was calculated by dividing the Plant Wax C_n from equation 1.3 by the total C_n alkane concentration and multiplying by 100% :

$$\text{Plant Wax Percentage for } C_n = \text{Wax } C_n / \text{Total } C_n * 100\% \quad (1.4)$$

To obtain the average contribution of plant waxes to the alkanes for an entire sample, these percentages of plant wax influence on each odd alkane were averaged for C25-C33. One thing to note is that this calculation only finds the plant wax influence on the odd carbon number alkanes. Since both odd and even carbon number alkanes are emitted from biogenic sources, this is an underestimation of the total biogenic influence, and can be viewed as a lower limit of total plant wax influence.

Plant wax contributions are generally low for urban atmospheres (< 25%) while rural environments can have more than 50% of alkanes derived from plant wax. Table 1.2 details the plant wax influences reported for previous urban and rural studies.

Table 1.2 Percentage of alkanes derived from plant wax reported from previous studies

Location	% Plant Wax	Reference
Rio de Janeiro	2.5-9.8%	Azevedo et al., 1999
Beijing	10%	Simoneit et al., 1991a
Santiago, Chile	4.6-20.8%	Kavouras et al., 1999
Heraclion, Greece (urban)	13-25%	Gougou et al., 1996
Finokalia, Greece (rural)	30-50%	Gougou et al., 1996
Giesta, Portugal (semi-rural)	24%	Pio et al., 2001

1.6 Other Carboxylic Acids: Alkanoic Diacids and Oleic Acid

In addition to saturated alkanoic acids, mono-unsaturated acids can be found. The difference between these is the presence of a double bond in the carbon chain of mono-unsaturated acids, shown in figure 1.6.

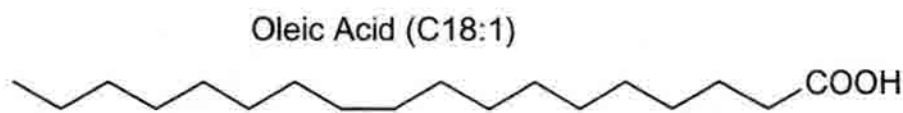


Figure 1.6 Structure of Oleic acid (C18:1).

One method that has been used to gauge the age of aerosol is to take the ratio of saturated C18 acid to the mono-unsaturated C18 acid, oleic acid (Mazurek and Simoneit, 1982; Simoneit et al., 1988; Simoneit et al., 1991a; Abas and Simoneit, 1996; Zheng et al., 1997; Fang et al., 1999a,b; Zheng et al., 2000). This ratio is used as an aerosol age indicator since the mono-unsaturated acid breaks down much faster by atmospheric oxidation than the saturated analog (Simoneit et al., 1988; Simoneit et al., 1990; Simoneit et al., 1991a; Kawamura et al., 1996 a,b;

Lawrence and Koutrakis, 1996; Zheng et al., 1997; Fang et al., 1999a,b; Kawamura and Sakaguchi, 1999; Zheng et al., 2000). The degradation of oleic acid is presented in figure 1.7. The abundance of the saturated acid compared to the mono-unsaturated analog can therefore indicate a relative decomposition rate. Table 1.3 presents observations of this ratio for a number of sites and seasons.

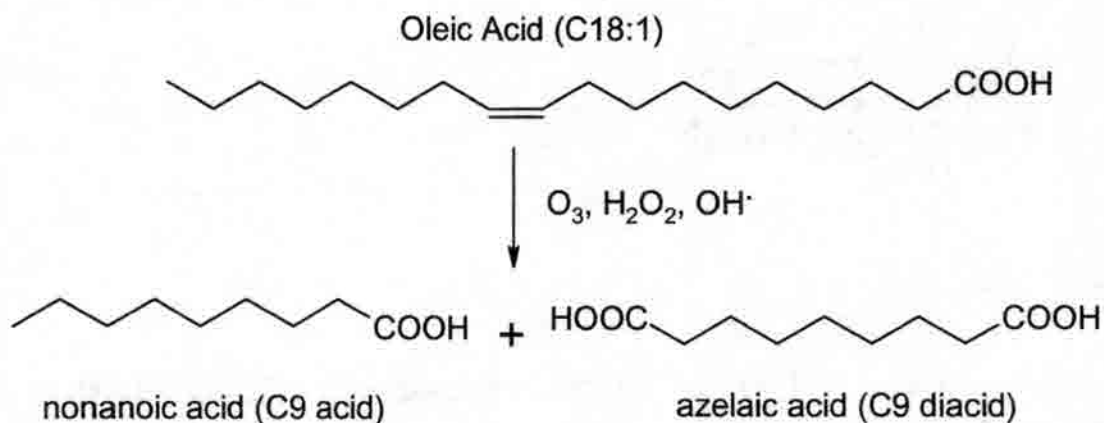


Figure 1.7 Breakdown of oleic acid into nonanoic (C9 acid) and azelaic (C9 diacid) acid

In urban environments where fresh ambient aerosol is sampled, such as during studies in Hong Kong and urban China, this ratio was found to be close to, or even below, 1. The large amount of oleic acid present in these studies was attributed to meat cooking (Rogge et al., 1991; Simoneit et al., 1991; Zheng et al., 1997, 2000). In the Lake Tahoe and Mt Lassen areas in California, average ratios for the summer were reported to be approximately 13, while the average ratio in the winter was reported to be around 6 (Mazurek and Simoneit, 1982).

Table 1.3 C18:0/C18:1 ratios for various locations and time of year

Location	Site Description	Time of Year	C18:0/C18:1 ratio	Source
Beijing, China	Urban, near traffic and smoke	June	2.1	Simoneit et al. 1991a
Guangzhou China	Suburban, natural vegetation, vehicular and coal emissions	March	2.5	Simoneit et al. 1991a
Hong Kong	Urban, vehicle and cooking emissions	Summer	0.52 (reported as C18:1/C18:0)	Zheng et al. 2000
Hong Kong	Urban, vehicle and cooking emissions	Winter	1.5 (reported as C18:1/C18:0)	Zheng et al. 2000
California Mountains	Rural, some vehicle emissions	Summer	13.0	Simoneit and Mazurek 1982
California Mountains	Rural, some vehicle emissions	Winter	6.5	Simoneit and Mazurek 1982
Mt. Keira, Australia	Rural, some vehicle emissions	Winter	4.2	Simoneit et al. 1991c

Oleic acid is degraded to C9 (nonanoic) acid by the breaking of the double bond in the middle of the chain (Kawamura et al., 1987a), as shown in figure 1.7. An abundance of C9 acid can indicate that the aerosol has been subject to atmospheric processing (Rogge et al., 1993b; Gogou et al., 1996; Kawamura and Sakaguchi, 1999).

Another family of organic acids studied is the alkanolic dicarboxylic acids, which have a carboxylic acid group on both ends of the carbon chain, shown in figure 1.8. These diacids can be directly emitted into the atmosphere by fossil fuel combustion and biomass burning (Kawamura et al., 1987b; Legrand and De Angelis, 1996) and can also be formed by secondary photochemical oxidations of both biogenic and anthropogenic compounds (Satsumabayashi, et. al., 1990; Kawamura and Ikushima, 1993). The presence of diacids as oxidation products in photochemical smog has been documented (Appel et al., 1980; Hatakeyanma et al., 1985, 1987; Jacobson et al., 2000). However, determining which of these processes is responsible for the presence of diacids is difficult.

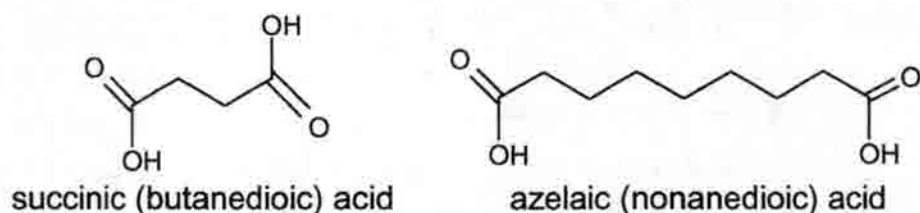


Figure 1.8 Structures of alkanedioic acids: succinic and azelaic acid

Many diacids exhibit semivolatile behavior, and their distribution between the gas and particle phases is not dependent solely on their vapor pressures, but also on the temperature, relative humidity and chemical properties of the particles (McDow and Huntzicker, 1990; Limbeck, et. al., 2001). Additionally, diacids can be an abundant species in the water-soluble fraction of organic aerosols (Sempere and Kawamura, 1994; Kawamura et al., 1996a) and have a potential of being rained out (Sempere and Kawamura, 1996; Novakov et al., 1997; Kawamura and Sakaguchi, 1999). Since the diacids can originate as primary emissions as well as secondary photochemical oxidation products, and can be effectively removed from the particulate fraction, they are generally not used for source apportionment.

1.7 Polycyclic Aromatic Hydrocarbons

Polycyclic aromatic hydrocarbons (PAH) are emitted from both biogenic and anthropogenic combustion sources (Simoneit, et. al., 1991; Rogge et al., 1991, 1993a,b; Hawthorne et al., 1992; Oros and Simoneit, 2000). They can be used as combustion tracers (Rogge et al., 1993a,b; Schauer et al., 1996; Schauer and Cass, 2000), though they can be altered by atmospheric processes and therefore can be short lived (Simoneit et. al., 1990). The absence of the PAH benzo(a)pyrene has been used as an indicator of aged aerosol (Simoneit et. al., 1988, 1990, 1991a). Unless combustion sources are located near the sampling site, PAH may not be found in the samples, even though combustion aerosol is present.

The BRAVO samples were analyzed for 30 different PAH, and were grouped by mass to charge ratio (m/z). This means that, for example, the two PAH with m/z 178, phenanthrene and anthracene, were grouped together as PAH 178. These two species are both condensed three ring aromatics and have similar properties. Similarly, PAH of m/z 192 (methyl-phenanthrenes and anthracenes), 202 (four ring condensed aromatics), and 252 (five ring condensed aromatics) were grouped together and reported as the total concentration for each m/z . Example structures of these compound types are shown in figure 1.9.

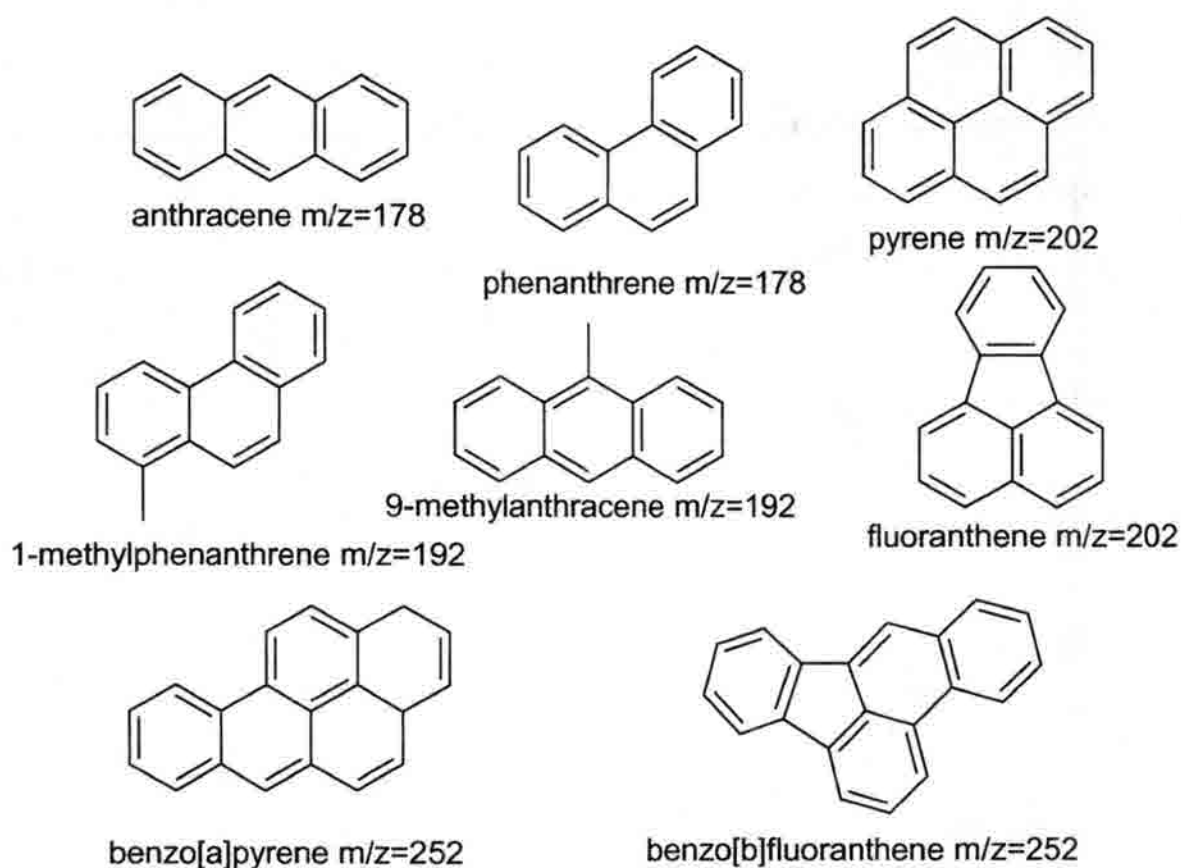


Figure 1.9 Structures of PAH: anthracene, phenanthrene, 1-methylphenanthrene, 9-methylanthracene, pyrene, fluoranthene, benzo[b]fluoranthene and benzo[a]pyrene.

1.8 Tracers : Source Tracers

BRAVO aerosol samples were also analyzed for source-specific molecular tracers in order to evaluate the contribution of specific source types to BRAVO organic aerosol concentrations. Source profiles have been previously analyzed for vehicle exhaust (Rogge et al., 1993a; Schauer et al., 1999b) and meat cooking (Rogge et al., 1991; Schauer et al., 1999a), and unique molecular tracers were found for both sources. Rogge et al. (1993a) have profiled catalyst-equipped and non-catalyst-equipped car and diesel truck emissions, finding that 17 α 21 β -hopane, originating from lubricating oil, was a unique molecular marker for vehicles. However, this tracer can also come from the utilization of fossil fuels, such as in coal power plants, so calculations of vehicle exhaust using this tracer may be an overestimation. Similarly, meat smoke from charbroiling and frying hamburgers was profiled by Rogge et al. (1991), who found that cholesterol was a unique molecular marker for meat smoke. The structures of these tracer species are found in figure 1.10.

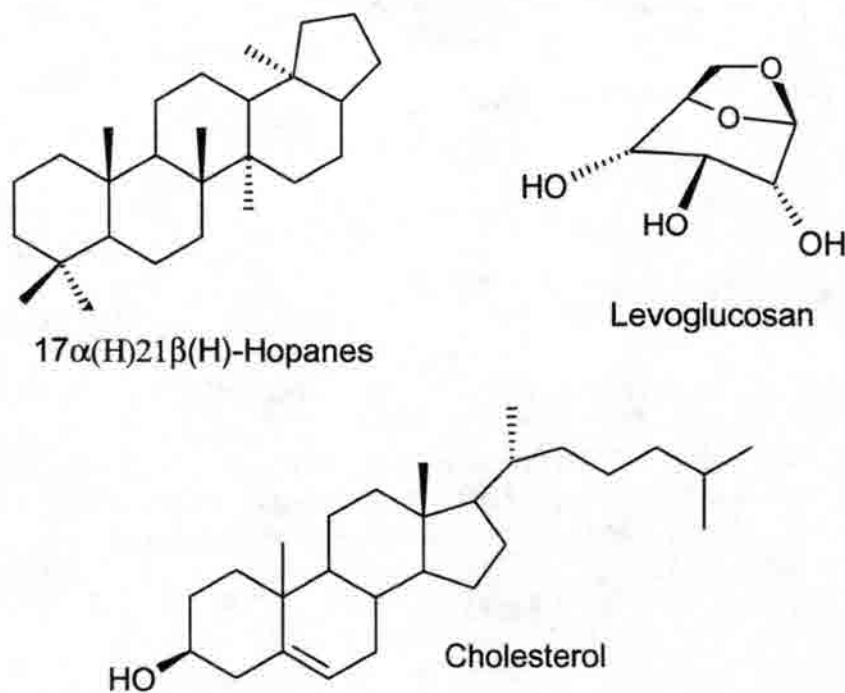


Figure 1.10 Structures of several source tracer species: hopanes, levoglucosan, and cholesterol.

Assuming that these source tracers are not altered during transport, source profiles can be used to calculate fine aerosol OC contributions from different source types, based on the concentrations of the tracers found. If the tracer concentrations are at or below detection limits, a detailed source apportionment is not possible; however, by using the tracer species' detection limits as upper bounds to tracer concentrations, an estimate of the maximum contribution of the associated source type to the aerosol composition can be obtained. The calculations of source impacts are discussed further in section 2.6.

1.9 Tracers: Wood Smoke Tracers

Levoglucosan has recently been used as a molecular marker for wood smoke since it is a unique combustion product of wood lignin (Rogge et al., 1998; Oros et al., 1999b; Simoneit et al., 1999; Simoneit, 1999; Fine et al., 2001; Schauer et al., 2001). Levoglucosan accounts for 3% to 18% (Fine et al., 2001; Schauer et al., 2001) of the fine particulate emissions from wood burning, with an average of 100 ± 40 mg of levoglucosan per gram of fine particulate OC emitted (Fine et al., 2001). This compound can be used as a wood smoke tracer analogous to the use of vehicle and meat cooking tracers described above.

There are additional compounds that have also been used as wood smoke tracers. For instance, sugar anhydrides from lignin combustion that are similar to levoglucosan, such as mannosan and galactosan, can be used (Oros et al., 1999b; Simoneit et al., 2000; Elias et al., 2001; Fine et al., 2001; Nolte et al., 2001). Other wood smoke markers include retene from coniferous (softwood) combustion (Ramdahl, 1983), methoxyphenols, such as vanillin (for softwood) and syringaldehyde (for hardwood), and resin acids such as pimaric and abietic acid (Hawthorne et al., 1988, 1989, 1992; Edye and Richards, 1991; Sagebiel and Seiber, 1993;

Simoneit et al., 1993; Rogge et al., 1998; Oros et al., 1999b; McDonald et al., 2000; Nolte et al., 2001; Schauer et al., 2001; Fine et al., 2001). Structures for some of these wood smoke markers are shown in figure 1.13. Use of vanillin for calculating wood smoke influence is discussed in section 3.7.

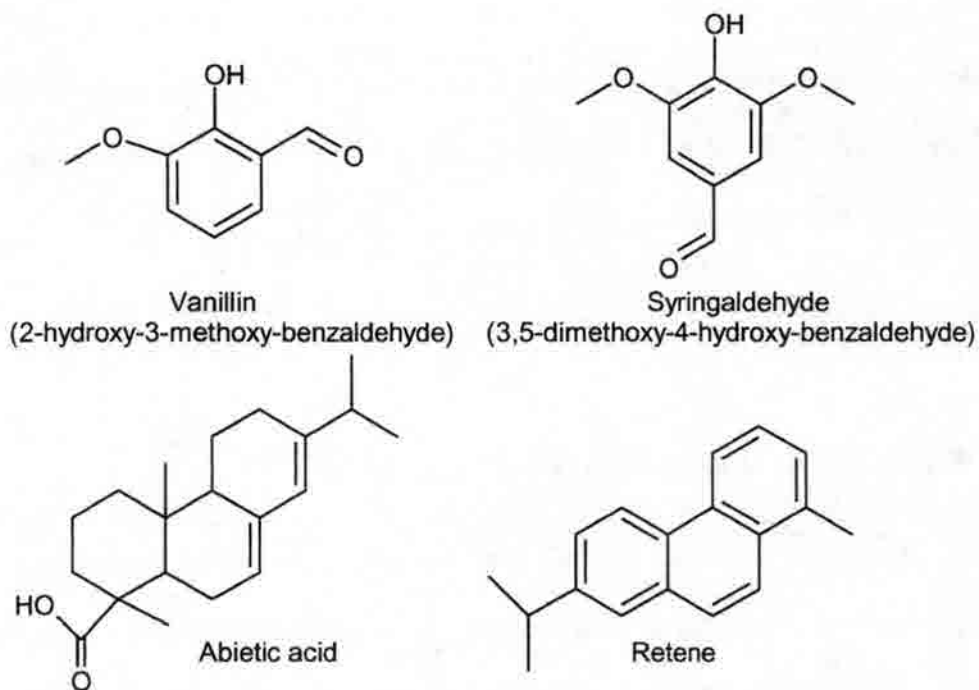
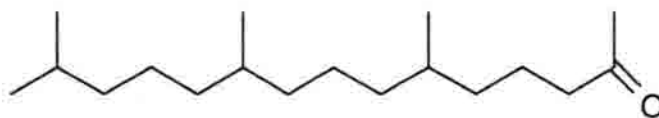


Figure 1.11 Structures of wood smoke markers: vanillin, syringaldehyde, abietic acid and retene

1.10 Tracers : Secondary Biogenic Aerosol

The compound 6,10,14-trimethylpentadecan-2-one has been proposed as a marker for secondary biogenic aerosol (Mazurek and Simoneit, 1982; Simoneit et al., 1988; Simoneit et al., 1991b; Abas et al., 1995; Pio et al., 2001a,b). The structure is shown in figure 1.12. This compound is produced by thermal alteration and oxidation of phytol, emitted from plants (Simoneit et al., 1988; Abas et al., 1995; Alves et al., 1999; Pio et al., 2001a,b). Microbial sources also generate this compound (de Leeuw et al., 1977), but their contribution in the

atmosphere is negligible (Abas et al., 1995). Relative abundance of 6,10,14-trimethylpentadecan-2-one can suggest greater secondary biogenic influences in an aerosol sample.



6,10,14-Trimethylpentadecan-2-one

Figure 1.12 Structure of 6,10,14-trimethylpentadecan-2-one.

1.11 Tracers: Coal and Fossil Fuel Usage

The burning of coal and other fossil fuels can significantly increase the input of particulate organic carbon into the atmosphere (Simoneit, 1994; Zheng et al., 1997). Pristane (2,6,10,14-tetramethylpentadecane) and phytane (2,6,10,14-tetramethylhexadecane) are geologically mature compounds found in oil and coal formed over millions of years (Simoneit, 1978, 1985). These branched hydrocarbons petroleum residues that can be used as biomarkers for fossil fuel usage (Simoneit, 1985, 1994; Simoneit et al., 1990; Abas et al., 1995). Their structures are shown in figure 1.13. Their presence in aerosol suggests input from fossil fuel utilization. Vehicle emissions, fuel oil combustion and coal combustion are all possible sources of these compounds. An abundance of picones has been proposed as a molecular tracer for coal smoke (Oros and Simoneit, 2000). Their structures are also shown in figure 1.13. The ratio between 17 α 21 β -hopane and 22R-17 α 21 β -hopane was found to be different between coal smoke and vehicle exhaust in this study, and this ratio was proposed as an additional indicator of coal smoke.

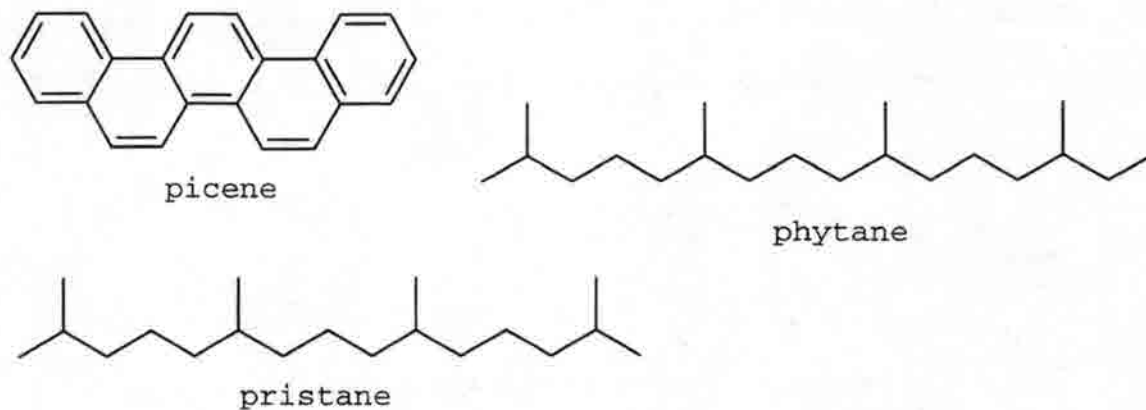


Figure 1.13 Structures of fossil fuel tracers: picene, phytane and pristane.

1.12 Secondary Organic Aerosol

The amount of secondary organic aerosol present in an ambient aerosol sample has previously been estimated by examining the ratio of total organic carbon to total elemental carbon (EC) (Turpin et al., 1991a,b, 1995; Lee and Huang, 1993; Castro et al., 1999; Lin and Tai, 2001). By assuming a minimum value for the OC/EC ratio that represents purely primary emissions, and that this ratio remains constant between samples, the concentration of secondary organic carbon can be estimated using the equation:

$$OC_{\text{sec}} = OC_{\text{total}} - (OC/EC)_{\text{minimum}} * EC \quad (1.9)$$

Table 1.4 shows the amount of secondary OC calculated by this approach from previous studies. While there is a wide variety of sampling locations and seasons, the overall trend is higher secondary OC levels in rural areas compared to urban areas, and during the summer months compared to the winter. The higher amount found at rural areas is probably due to atmospheric oxidation processes during transport. Higher temperatures and more intense solar radiation during the summer months are favorable conditions for photochemical activity and

secondary OC production. The large amount of secondary OC in Taiwan, L.A. and Portugal relative to Birmingham is attributed to warmer temperatures and more sunlight in the former locations compared to Birmingham.

Table 1.4 Listing of Secondary OC % and correlation between EC and Secondary OC

Location	Secondary OC %	r^2 between EC and OC_{sec}	Reference
Los Angeles (summer)	40%-80%	N/A	Turpin et al. 1991a
Birmingham, UK (urban winter)	17%	0.11	Castro et al. 1999
Taiwan (urban winter)	40%	N/A	Lin et al. 2001
Oporto, Portugal (urban summer)	47%	0.38	Castro et al. 1999
Areão, Portugal (rural winter)	45%	0.83	Castro et al. 1999
Areão, Portugal (rural summer)	78%	0.96	Castro et al. 1999
Tabua, Portugal (rural summer)	68%	0.63	Castro et al. 1999

1.13 Carbonaceous Aerosol: Black Carbon

The other part of the carbonaceous aerosol fraction is black carbon (BC), also referred to as elemental carbon (EC) or light absorbing carbon (LAC). These names all refer to the fraction of carbonaceous aerosol that absorbs light and is insoluble in polar as well as non-polar solvents (Seinfeld and Pandis, 1998). The term "black carbon" will be used to refer to measurements obtained from an aethalometer, detailed in section 2.6, while elemental and light absorbing carbon will be used to refer to results from thermal/optical reflectance (TOR) method analyses of ambient BRAVO samples, discussed in section 2.3.2.

Black carbon is produced only from combustion sources (Chen et al., 1997; Seinfeld and Pandis, 1998; Park et al., 2001), including vehicular exhaust, power plant emissions, and biomass burning. Diesel trucks (Rogge et al., 1993a; Schauer et al., 1999) and wood burning in fireplaces (Fine et al., 2001; Schauer et al., 2001) are the most efficient sources for BC per equivalent of fuel burned.

BC is the major contributor to light absorption in the atmosphere (Japar et al., 1986; Adams et al., 1990a,b), and these light absorbing properties make BC very effective at reducing visibility. BC has a refractive index of approximately $1.96 - 0.66i$ at 550 nm wavelength (λ) (Seinfeld and Pandis, 1998) and an extinction efficiency of approximately $10 \text{ m}^2 \text{ g}^{-1}$ at 515 nm wavelength (Japar et al., 1986; Adams, 1990a). While BC is usually not a large part of the total aerosol mass, as shown in figure 1.14, it can be responsible for more than 25% of the total extinction in the U.S., shown in figure 1.15.



(a)



(b)

Figure 1.14 Annual mean BC (a) concentrations and (b) as percent of total aerosol mass (from Seinfeld and Pandis, 1998).

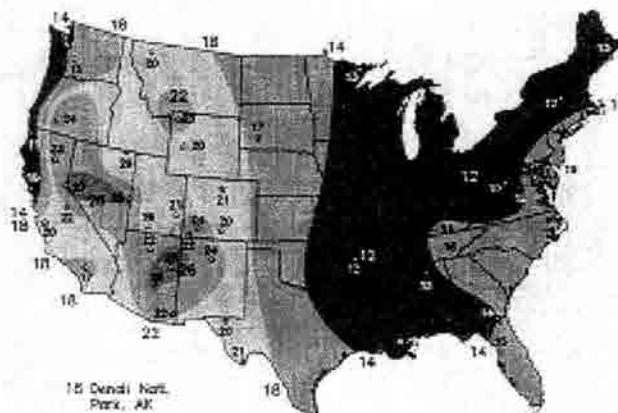


Figure 1.15 Percent contribution of BC toward light extinction in the U.S. (from Malm, 1994).

1.14 Project Objectives and Layout

The focus of this report is on the characterization of both the organic and black carbon aerosol fractions from BRAVO. Specific objectives of this work are to:

- Characterize the molecular composition of the organic aerosol present during BRAVO.
- Determine the importance of anthropogenic versus biogenic influence on BRAVO organic aerosol.
- Examine the relative importance of primary vs. secondary organic aerosol formation on BRAVO aerosol composition
- Use molecular markers to estimate the contributions of individual source types (motor vehicles, wood burning, and meat cooking) to BRAVO organic aerosol concentrations
- Characterize the concentrations and size distribution of black carbon during BRAVO

Study methodology will be discussed in Chapter 2. This includes the sampling of particles, extraction techniques and analysis methods. Gas Chromatography – Mass Spectroscopy theory and calculations of source contributions and secondary OC are also discussed further in Chapter 2. Results from the study, including results of applying the approaches to data analysis described above, are presented and discussed in Chapter 3. Conclusions and recommendations for future work are presented in Chapters 4 and 5.

2 Methodology

2.1 Collection Setup

Particles were collected using a modified Desert Research Institute (DRI) Fine Particulate/Semi-Volatile Organic Compound (FPSVOC) system (DRI Standard Operating Procedure, Number 1-601.2) at the K-Bar site in Big Bend National Park. The sampler collected aerosol on pre-fired quartz fiber filters. Air was drawn through a cyclone separator with a nominal cutoff aerodynamic diameter of 2.5 μm for a flow rate of 112 L/min. After air has been filtered and leaves the sampling channel, the air flow is pulled through the “flow determination tube” that leads to the pump. During this stretch, the air flow goes through a volumetric flow meter and a valve. The flow meter is used along with an elapsed time meter to determine the total volume of air pulled through each filter. The valve is used to adjust the flow. Flow meter readings were calibrated by comparison against a certified rotometer. Ambient flow rates during the study ranged from 80.6 L/min to 125.6 L/min, averaging 111.2 L/min. Changes in actual flow from the nominal 112 L/min flow for the cyclone probably altered the size cut from the nominal value of 2.5 μm . Twenty-four hour samples were collected; filters were changed at ~0800 CST each day (see appendix for daily sampling times and flow rates). Every Tuesday, a filter blank was collected by loading and unloading a new filter from the sampler.

2.2 Filter Preparation, Loading, Unloading and Storage

Prior to sampling, quartz fiber filters were wrapped in aluminum foil and baked at 500 °C for at least 12 hours to reduce the residual carbon levels found on new filters. The filters were stored in aluminum foil to keep them clean until they were loaded into the organics sampler. Filters were always handled using stainless steel forceps cleaned with isopropanol, as contact with hands or gloves could deposit unwanted organics onto the filter. After being unloaded from the organics sampler, they were folded using clean metal forceps and placed in a cleaned, baked glass jar with a Teflon-lined lid, which was subsequently labeled with the sample name and stored in a freezer at below 0 °C.

2.3 Establishment of BRAVO Groups

2.3.1 Organic Carbon Concentrations During BRAVO

Concentrations of organic carbon for daily BRAVO samples collected by the Interagency Monitoring of PROtected Visual Environments (IMPROVE) network were obtained from the University of California, Davis. Analyses were completed by the Desert Research Institute using their thermal/optical reflectance (TOR) combustion analysis method (Chow et al, 1993) to obtain organic carbon (OC) and elemental carbon (EC) concentrations. This analysis method is discussed further in section 2.3.2. The total mass of organic aerosol (OCM) is typically estimated by multiplying the OC mass by a factor of 1.4 (White et al., 1977; Japar et al., 1984; IMPROVE data guide, 1995; Turpin et al., 2001). This factor is chosen to account for typical additional organic molecule masses associated with non-carbon components (e.g., H, N, and O). Daily average OC concentrations in ng/m^3 were used to compute the mass of organic carbon collected by Colorado State University (CSU) on each filter. The conversion was done by multiplying the

daily average OC concentration by the total volume (m^3) collected by the CSU organic sampler using the following equation:

$$\text{OC daily concentration (ng/m}^3\text{)} * \text{Daily Volume Sampled (m}^3\text{)} / 1000 = \text{OC Collected (}\mu\text{g)} \quad (2.1)$$

It had been estimated that 400 μg of organic carbon is needed for detailed analysis and tracer quantification by Gas Chromatography – Mass Spectroscopy. Daily amounts of organic carbon collected during the study were mostly below 400 μg .

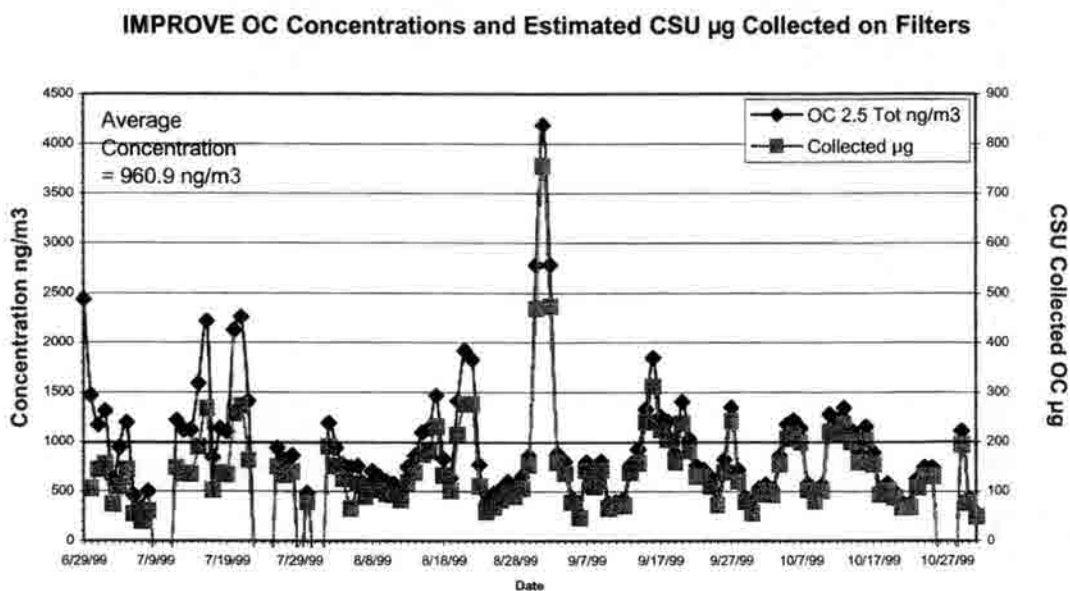


Figure 2.1 Daily IMPROVE OC concentrations and estimated CSU μg OC collected

The average daily concentration of organic carbon during BRAVO was 960.9 ng/m^3 (see figure 2.1). An average of $147.3 \mu\text{g}$ of organic carbon was estimated to be collected on each CSU filter. Due to previous preliminary analyses, some filters were not available in their entirety. Amounts of organic carbon available on each daily filter are shown in the figure 2.2. A twelfth of each

filter was kept for possible future organic and elemental carbon analysis; the computed available OC treats this part as unavailable.

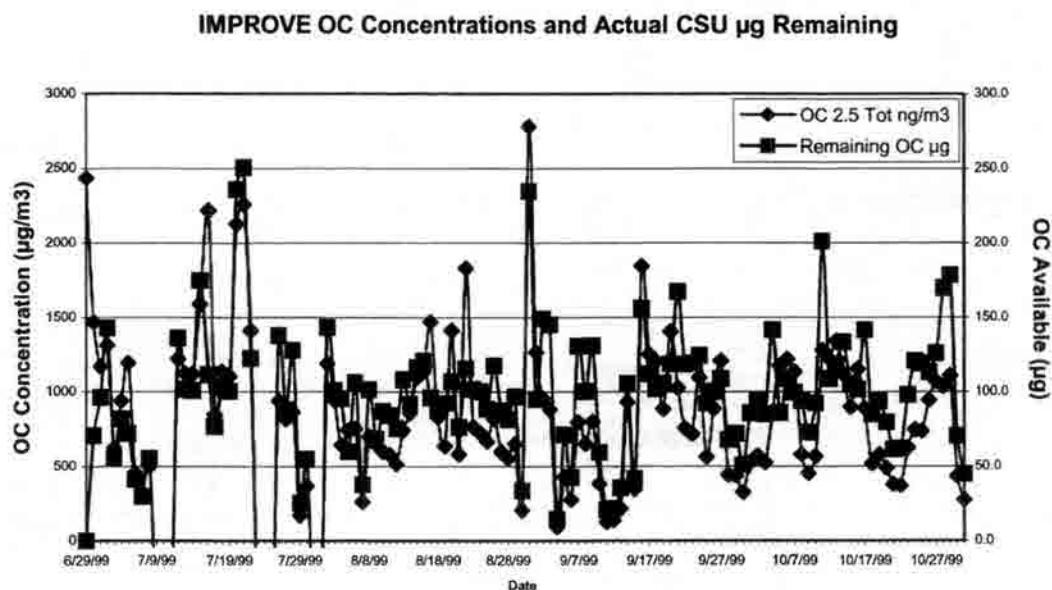


Figure 2.2 Daily IMPROVE OC concentrations and daily CSU OC (μg) remaining for analysis

As seen in Figure 2.2, none of the days have the minimum amount of OC assumed necessary for meaningful analysis. In order to provide at least 400 μg organic carbon for each extraction, daily filters were grouped. The groupings were established based on similarity in air mass back-trajectories, determined from the NOAA Hysplit model, and proximity in time. Details of this process can be found in chapter 2.3.3.

2.3.2 TOR Combustion Analysis

The thermal/optical reflectance (TOR) combustion analysis was used to determine organic and elemental carbon concentrations by the Desert Research Institute (DRI) (Chow et al., 1993); this method is the one also used by IMPROVE. Daily fine aerosol samples, with an aerodynamic diameter cutoff of ~2.5 μm achieved with a cyclone, were collected on pre-fired

quartz-fiber filters during BRAVO by IMPROVE, using the IMPROVE sampling system. For further details on IMPROVE sampling, see Malm et al. 1994 or

<http://vista.cira.colostate.edu/improve/Publications/otherDocs/IMPROVEDataGuide/IMPROVEDataGuide.htm>.

The TOR analysis consists of four steps (Chow et al., 1993): 1) volatilizing carbonaceous aerosol under varying temperature and oxidation environments; 2) passing the volatilized compounds through an oxidizer (MnO_2 at 912°C) to convert them into carbon dioxide; 3) reducing this CO_2 to methane by passing the flow through a methanator (firebrick with nickel catalyst at 550°C in a hydrogen stream); and finally, 4) quantifying the methane by flame ionization detection (FID).

For analysis, a 0.5 cm^2 circular punch was removed from the filter and placed vertically into a quartz boat, which is inserted into the oven area with a thermocouple pushrod. Figure 2.3 shows the configuration of the volatilization/ combustion area where the sample is analyzed.

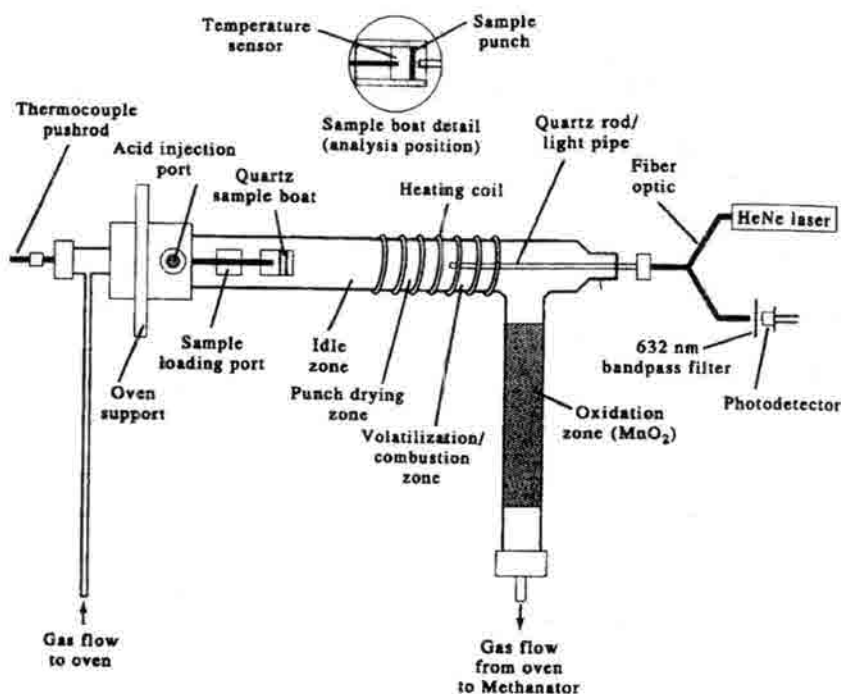


Figure 2.3 Volatilization/combustion area of DRI TOR carbon analyzer (from Chow et al., 1993)

Seven fractions, as a function of both temperature and oxidation environment, are used to quantify the amount of organic and elemental carbon. For the first fraction, the temperature is quickly ramped in a helium atmosphere from 25 to 120⁰ C, giving the OC1 fraction. This volatilizes a fraction of the organic carbon off the quartz sample filter in the form of CO₂, which is then converted to methane with the methanator. The amount of methane corresponds to the amount of OC volatilized, and is analyzed by FID. When the FID response returns to baseline, the carbon in that fraction has all been volatilized, and the next temperature/environmental regime is initiated. For the next three fractions, the temperature is ramped from 120 to 250⁰ C (OC2), 250 to 450⁰ C (OC3), and 450 to 550⁰ C (OC4). This process takes between 80 and 580 seconds for each segment. After the OC4 section is complete, a 2% O₂ / 98% He atmosphere is introduced to obtain EC1, and the temperature is then increased to 700⁰ C for EC2 and to 850⁰ C for EC3, again with the next fraction initiating when FID response goes back to baseline. Figure 2.4 shows an example of the resulting thermal/optical reflectance thermogram.

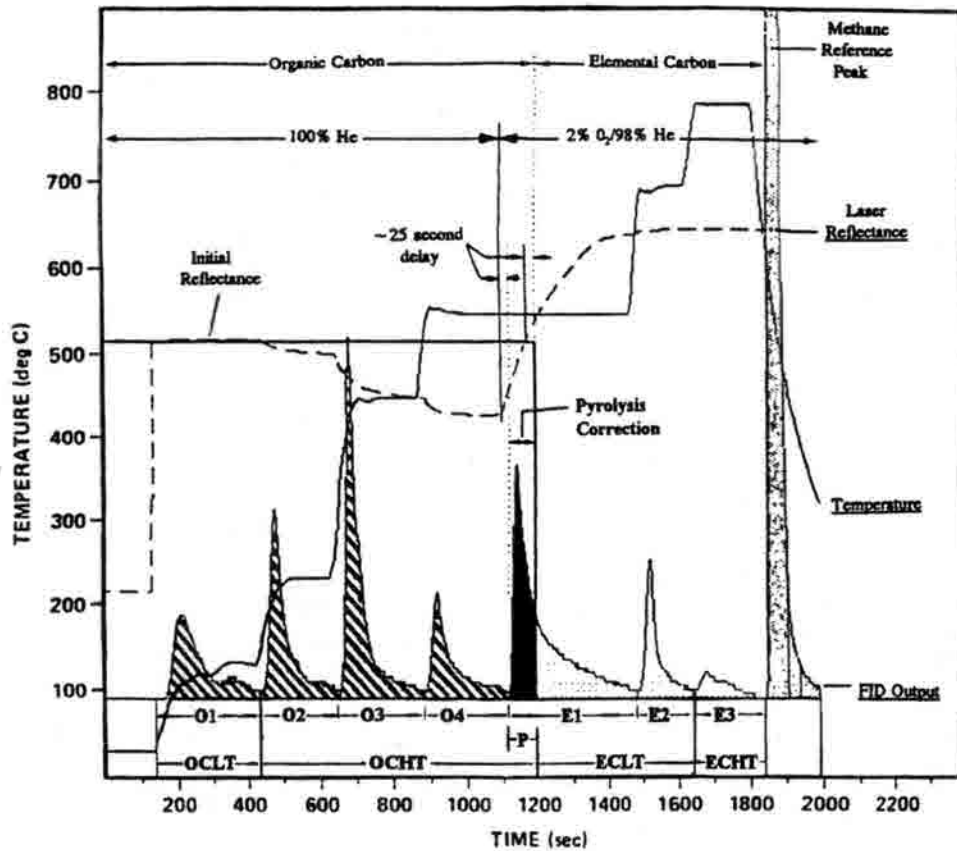


Figure 2.4 An example of a DRI thermal/optical reflectance carbon analyzer thermogram (from Chow et al., 1993)

Total organic carbon is defined as the sum of OC1 through OC4 plus OP:

$$\text{Total Organic Carbon} = \text{OC1} + \text{OC2} + \text{OC3} + \text{OC4} + \text{OP} \quad (2.2)$$

Total light absorbing carbon (assumed as elemental carbon) is defined as the sum of EC1 to EC3 minus OP:

$$\text{Total Elemental Carbon} = \text{EC1} + \text{EC2} + \text{EC3} - \text{OP} \quad (2.3)$$

The following equations were used to establish the estimates of uncertainty, obtained from Dr. Lowell Ashbaugh at UC Davis:

$$\sigma(EC) = \sqrt{(34)^2 + (0.067 * EC)^2} \text{ ng/m}^3 \quad (2.4)$$

$$\sigma(OC) = \sqrt{(120)^2 + (0.05 * OC)^2} \text{ ng/m}^3 \quad (2.5)$$

2.3.3 Use of the NOAA Hysplit Model

The NOAA Hysplit (HYbrid Single-Particle Lagrangian Integrated Trajectory) Model (Draxler, 1996) is a three-dimensional air mass trajectory model based on weather model data. This model, obtained from the NOAA web site at <http://www.arl.noaa.gov/ready/hysplit4.html>, was used to compute daily back trajectories for air masses coming into Big Bend. Back trajectories were run at 8 pm local time for each day with an ending height of 1000 meters, the estimated average height of the boundary layer. The final product (FNL) weather data of the Global Data Assimilation System (GDAS) that uses the Global spectral Medium Range Forecast model (MRF) was used. This data uses a 129x129 polar stereograph grid with approximately 190 km resolution, with 12 vertical layers and is run at 6 hour increments. It utilizes three-dimensional wind components, temperature, relative humidity, radiative and momentum fluxes. Additional information can be found at <http://www.arl.noaa.gov/ready-bin/fnl.pl>. A trajectory end time of 8 pm CST was selected because it is close to the middle of the daily sampling period, which ran from 8 am to 8 am CST. Trajectories were run for 240 hours prior to the end time of 8 pm.

A trajectory depicts the time integration of the position of a parcel of air as it is transported by the wind (Draxler, 1991). The parcel's passive transport by the wind is computed from the average of the three-dimensional velocity vectors at the particle's initial-position $P(t)$ and

its first-guess position $P'(t+dt)$. The velocity vectors, $v(P,t)$ and $v(P', t+dt)$, are interpolated in both space and time. The first guess position is determined using the equation

$$P'(t+dt) = P(t) + V(P,t) dt, \quad (2.6)$$

and the final position is found using the equation

$$P(t+dt) = P(t) + 0.5 [V(P,t) + V(P',t+dt)] dt. \quad (2.7)$$

These trajectories are only an approximation of where the air parcel has traveled. The exact latitude and longitude calculated by the back trajectory model does not mean that only those points affected the composition of the air parcels. The further away in distance and time from the origin, the more error is involved at each point. The area around each point plotted affects the air parcels, and with error increasing with time and distance, this area of effect also increases.

Absolute trajectory error is estimated to range between 20% to 30% of the travel distance (Draxler, 1991). This is not to discount the trajectories' utility, only to highlight that only general areas of influence can be established. Nonetheless, these are helpful guides that can assist us to determine what source regions likely affected the aerosol composition of the differing air masses sampled in Big Bend N.P.

2.3.4 Development of an IDL Code to Chart Multiple Trajectories

Daily trajectories were obtained using the NOAA Hysplit model in the form of a text file, which specifies hourly air mass height, latitude, and longitude measurements of the various air masses. A map of where each daily trajectory is coming from is also available on the web site. However, there is no simple way to chart a group of daily trajectories together, as is needed to establish groups for this organics study.

A code was written using Interactive Data Language (IDL) in order to chart multiple daily back-trajectories on the same map (see appendix for code). The code was developed with the purpose of reading off of a text file that lists the days in the group to be mapped. Then each

daily trajectory was charted individually on a map; different colors were used to distinguish each individual day, and annotations indicating the corresponding dates in the same color were added to the map. Trajectories were charted for only 72 hours, since the uncertainty in regards to the path of the trajectory increases greatly after that period of time. Additionally, major emitters of volatile organic compounds (VOC) and NO_x in the state of Texas, as listed on the EPA's Office of Air Quality Planning and Standards Web site (<http://www.epa.gov/air/data/netemis.html>), were denoted on the map. El Carbon Plants I and II, which are located in Mexico near Big Bend N.P., were also denoted. Major cities, including Dallas, Houston, Mexico City, and San Antonio were also placed on the map.

2.3.5 Composite Descriptions

Nineteen composites of filters of daily PM_{2.5} aerosol samples were established based on fine organic carbon concentration, date, and back trajectory similarities. Table 2.1 details the dates in each group as well as the OC concentrations and OC/EC ratios. Figures 2.5, 2.6 and 2.7 show each daily back trajectory, colored by group, where each point along a trajectory represents an hour. Back trajectories for each individual day can be found in the appendix. The groups range from 433 µg to 1350 µg total available organic carbon. The number of days in each group ranges from 3 to 10. Most trajectories follow along the Texas – Mexico border from the Gulf of Mexico into Big Bend. This was the dominant pattern July through August, with some variations when trajectories arrived mostly through Mexico or mostly through Texas and the southeastern U.S. Two groups in mid to late September featured advection from southwestern U.S. (Arizona and New Mexico), and two groups in October featured flow from the north through western Texas, New Mexico, Oklahoma and Colorado. Another group in October consists of air masses transported from the south-southeast in central Mexico.

Table 2.1 Trajectory Groupings: dates included, trajectory description, total OC (μg), and OC/EC; * denotes extracted and analyzed groups

Group Name	Dates Included	Trajectory Description	Total Extractable OC (μg)	OC/EC
BorderJuly	6/30-7/8	Fast moving along Tx/Mx Border	645	7.6
MidJuly*	7/12-7/17	Just South of Border	702	14.9
TxMxMidJuly*	7/18-7/20	ESE through Mx and Southern Tx	439	18.3
MxJuly*	7/21,7/22,7/26-7/28	SE through Mx south of border	726	7.8
BorderAugust*	8/2-8/8	Along Border, thru South Tx	708	7.7
SBorderAugust	8/9-8/15	South of Border	631	5.6
EtxMxAugust*	8/16-8/22	Almost due east through Tx	873	7.3
BorderLoop*	8/23,8/24,8/31,9/1	North Mx through Tx into SE US	823	7.7
Xborder*	8/25,8/29,9/6-9/8	SE along border, through South Tx	433	5.3
BorderSA*	8/26-8/28,8/30,9/2-9/5,9/9,9/10	Along Border in Aug and Sept	1349	3.5
EtxMxMidSept	9/13-9/17	Through North Mx into middle of Tx	659	6.9
SWSept1*	9/18,9/19,9/21,9/24,9/27	From SW US and NW Mx	570	5.6
SWSept2	9/20,9/22,9/23,9/25,9/26,9/29,9/30	From northern New Mexico, Ariz, N Tx	639	5.6
TxMxDip	9/28,10/1-10/6	South into Mx, then north/east to Tx	711	4.6
EtxMxMidOct*	10/11-10/14	Slow through North Mx into central/east Tx	562	5.4
CentralMx	10/7,10/18,10/25,10/29	From SW into central Mx	482	5.7
SSEOct*	10/15,10/16,10/26-10/28	From SSE into central/NE Mx	616	4.1
NtxOct1*	10/8-10/10,10/17,10/19	From North through Tx, OK, NewMexico, CO	495	7.7
NtxOct2	10/20-10/24,10/30,10/31	From North through Tx, OK, NewMexico, CO	537	5.8

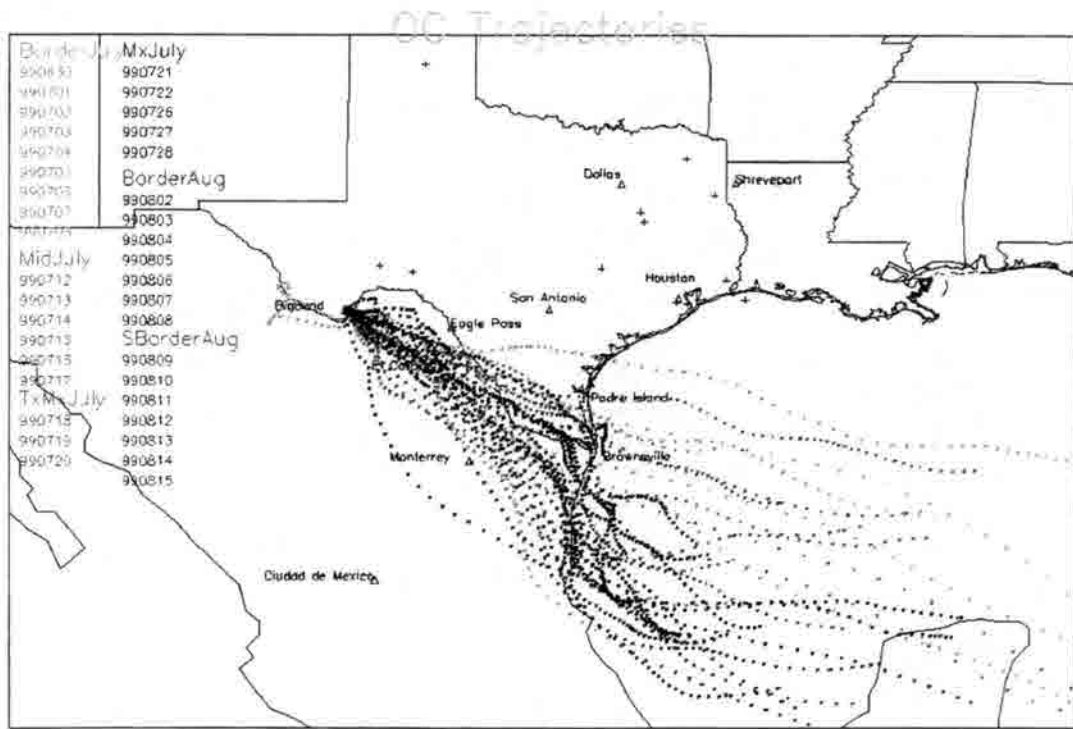


Figure 2.5 BRAVO groups' daily trajectories: Border July, Mid July, TxMxJuly, Mx July, Border Aug, SBorder Aug

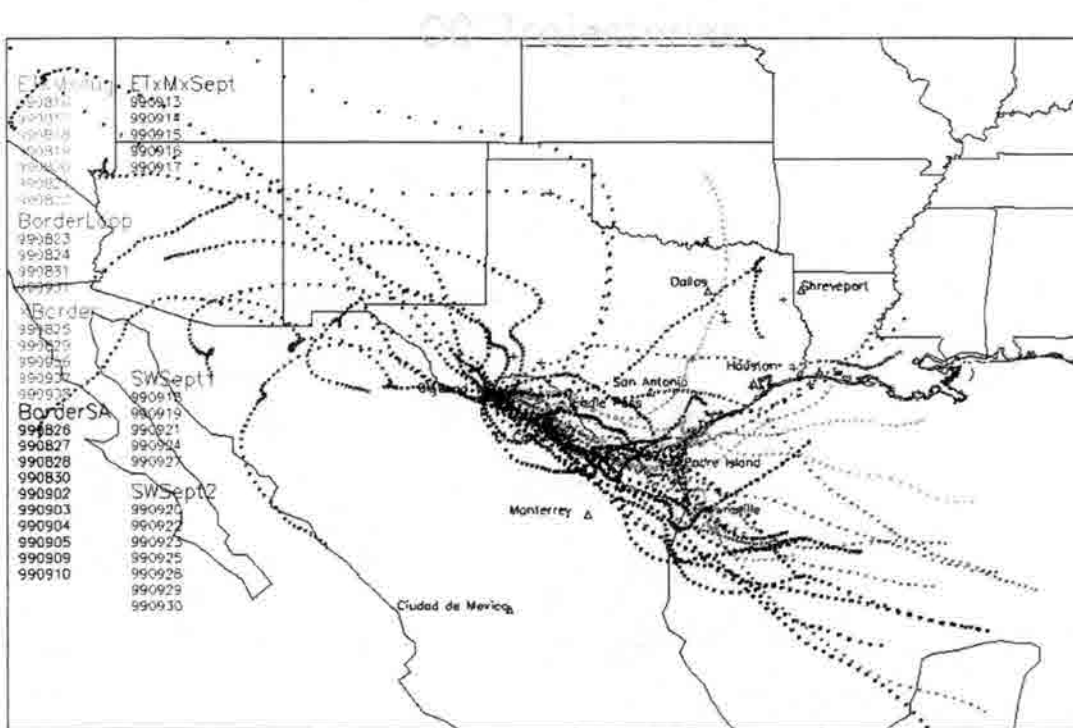


Figure 2.6 BRAVO groups' daily trajectories: ETxMxAug, Border Loop, XBorder, BorderSA, ETxMxSept, SW Sept1, SW Sept2

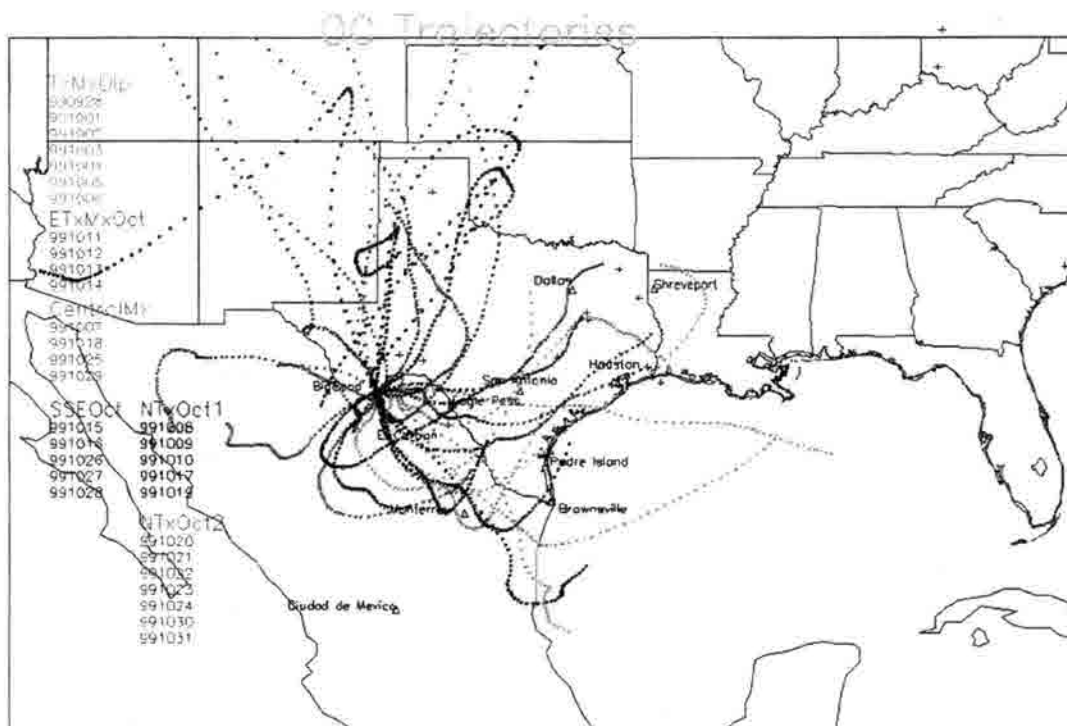


Figure 2.7 BRAVO groups' daily trajectories: TxMx Dip, ETxMx Oct, Central Mexico, SSE October, North Texas 1, North Texas 2

Group #1 : Fast Border July (Figure 2.5)

The first group consists of the trajectories from June 30th to July 8th, and contains 645 μg of organic carbon. Most of these days have low OC concentrations and move quickly along or near the border at the beginning of the study. The air mass from June 30th actually moves slowly around Big Bend and is somewhat stagnant, while the others are strongly influenced by strong onshore flow from the Gulf of Mexico. Southern Texas and Northern Mexico along the border are the primary sources of aerosol. No OC data were available for July 9th through 11th, so these days were omitted.

Group #2: Mid July (Figure 2.5)

The second group consists of the air masses from July 12th through July 17, and contains 702 μg total organic aerosol, making it the third largest group in terms of available organic carbon. All these days have trajectories that run just south of the border, originating from the Gulf of Mexico. These are generally fast moving, with July 13th and July 14th moving extremely fast. These days are also suspected Saharan dust episodes. Northern Mexico, including the Monterrey area and the power plants of El Carbon I and II, are potentially important influences in this group.

Group #3 : TxMx Mid July (Figure 2.5)

The days in this group, July 18th to July 20th, all have very similar trajectories. The total available organic carbon is 439 μg for this group. Air is transported from northern Mexico, passing over the El Carbon region and southern Texas. The 18th and 19th are about average for OC concentrations, while the 20th was the day with the seventh highest OC concentration (2128 ng/m^3).

Group #4 : Mx July (Figure 2.5)

This group includes July 21st – 22nd, and July 26th through July 28th, and contains a total available organic carbon loading of 727 μg . There were no IMPROVE OC data for July 23rd through July 25th, so these days were not included in the group. July 21st, with 2260 ng/m^3 , featured the fifth highest OC concentration during the study. The trajectories for the days in this group all pass south of the border from the Gulf, though there is likely some influence from southern Texas on the period between July 26 and July 28th, since these pass very close to the border. The trajectories from the 21st and 22nd are located farther into Mexico and pass near Monterrey. Northern Mexico may be a primary aerosol contributor to this group. These

trajectories are somewhat slower moving than those in previous July groups and may have more opportunity to form secondary aerosol and collect more organic aerosol via emissions in general.

Group #5 : Border August (Figure 2.5)

The filters from August 2nd through August 8th were combined in this group to total 708 μg available organic carbon. The trajectories all follow the Texas – Mexico border from the Gulf and are slower than previous groups of trajectories. These slow-moving air masses, under summer sunlight, have a good opportunity to form secondary aerosol. Southern Texas and northern Mexico are probably the main aerosol source regions. These days varied widely in organic aerosol concentration, with 1180 ng/m^3 on August 2nd and 564 ng/m^3 on August 7th.

Group #6 : South Border August (Figure 2.5)

These trajectories are faster moving than the previous August group. Dates included are August 9th through 15th, providing a total available organic carbon mass of 632 μg . The air mass trajectories all fall south of the border and are speeding in from the Southern Gulf near the Yucatan Peninsula. Northern and Northeastern Mexico are the primary areas of influence, though the air masses come very close to southern Texas.

Group #7 : ETxMx August (Figure 2.6)

This group has a total of 873 μg available organic carbon, and includes the filters from August 16th through August 22nd. Air masses during this period advect from the southeast into Big Bend. Southern Texas and northern Mexico appear to be the main potential source regions, with some urban impact from San Antonio. These days are mostly below average in organic carbon concentrations, with August 15th being the only day above average, at 1095 ng/m^3 .

Group #8 : Border Loop (Figure 2.6)

This group contains August 23rd, 24th, 31st, and September 1st, with 824 μg of available organic aerosol. August 31st features the third highest OC concentration with 2787 ng/m^3 , and September 1st has the highest OC concentration during the study at 4187 ng/m^3 . The trajectories on these days are nearly identical; both curve from the southeast and then from the northeast through southern Texas. The air masses on August 23rd and 24th advect west through central Texas into Big Bend. All four of these days seem to have significant influence from central and southern Texas, and may also have influences from Louisiana and the southeast US.

Group #9 : XBorder (Figure 2.6)

This group also contains air masses that travel along and cross the Texas-Mexico border. This group includes August 25th, August 29th, and September 6th through September 8th, with 433 μg of available organic carbon. These trajectories are all extremely close together, advecting from the south-southeast through northern Mexico and southern Texas, originating in the Gulf. They are somewhat faster moving than the previous group, BorderLoop, and all days have OC concentrations less than 800 ng/m^3 .

Group #10 : BorderSA (Figure 2.6)

This large group contains August 26th through 28th, August 30th, September 2nd through 5th, and September 9th and 10th. This group has the highest amount of OC available for extraction, with 1350 μg . These trajectories all follow the border, some slightly north and some slightly south, and all originate from the Gulf. Only September 2nd has above average OC concentrations, and at 2782 ng/m^3 is the second highest day in the study.

Group #11 : ETxMxMid September (Figure 2.6)

This group consists of the samples from September 13th through 17th and has a total of 659 μg available organic carbon. The trajectories suggest influences from southeastern Texas and northern Mexico. These trajectories are slower than most, indicating more stagnation. Most days had OC concentrations above average; September 16th featured the ninth highest organic carbon concentration with 1844 ng/m^3 . September 14th was the only day below average, though it was close to average with an organic carbon concentration of 925 ng/m^3 .

Group #12 : Southwest September 1 (Figure 2.6)

Representing a change from the usual southeasterly flow of the previous two months, this group features flow from the west-northwest, with influences from western Texas, southern New Mexico, Arizona, and northwestern Mexico. It includes September 18th, 19th, 21st, 24th, and 27th and a total available organic carbon mass of 570 μg . This group averaged an OC concentration of 1022 ng/m^3 , slightly more than average.

Group #13 : Southwest September 2 (Figure 2.6)

Similar to the previous group, the air masses in this group are from a more northerly to northwesterly direction, crossing North Texas, New Mexico and Arizona. This group includes September 20th, 22nd, 23rd, 25th, 26th, 29th and 30th and features an available organic carbon mass of 639 μg . The daily average OC concentrations in this group are generally below average, except for September 20th, with an OC concentration of 1405 ng/m^3 .

Group #14 : MxTxDip (Figure 2.7)

This group includes a variety of southeasterly to easterly trajectories, and appears to be mainly influenced by transport from northeastern Mexico and southern Texas, with some influence from central eastern Texas. Dates included are September 28th, and October 1st through

6th with 711 μg organic carbon available for extraction. Most days have below average OC concentrations, except for October 5th and 6th, which have 1173 ng/m^3 and 1219 ng/m^3 respectively.

Group #15 : ETxMx October (Figure 2.7)

These days are very similar and feature above average organic aerosol concentrations, ranging between 1118 ng/m^3 and 1342 ng/m^3 . Back trajectories in this group, comprised of samples from October 11th through 14th, come in from the east-northeast. A total of 562 μg of extractable organic carbon was estimated to be available. Transport during this period appears to be mainly from central Texas, but Northern Mexico also may influence the group's aerosol composition. This group is different than previous northern Mexico/southern Texas groups since there is more influence from Texas, and the trajectories do not originate in the Gulf. Rather, they originate from the southeastern U.S., which may have also contributed to the sampled aerosol.

Group #16 : Central Mexico (Figure 2.7)

The four days that make up this group have westerly to southerly trajectories that cross central and western northern Mexico, which distinguishes this group from the others. Dates included are October 7th, 18th, 25th, and 29th; total available organic carbon is 482 μg . There is a wide range of daily average organic carbon concentrations, with 1135 ng/m^3 on October 7th and only 518 ng/m^3 on October 18th.

Group #17 : SSE October (Figure 2.7)

This group is also distinctive since it consists of days that have slow trajectories from the south and southeast. With a total of 616 μg available organic carbon, this group contains the samples from October 15th, 16th, and 26th through 28th. The transport patterns suggest there may

be some influence from power plants in northern Mexico and/or from desert brush and other biogenic sources.

Group #18 : North Texas October 1 (Figure 2.7)

This group's predominant transport pattern is more northerly than the previous southwest US groups and primarily features fast transport through north Texas, eastern New Mexico and Oklahoma. Dates include October 8th through 10th, 17th and 19th, with 465 µg total available organic carbon. Organic carbon concentrations on these days are mostly well below average, probably due to fast advection over less populated areas.

Group #19 : North Texas October 2 (Figure 2.7)

This group of October 20th through 24th, 30th and 31st is very similar group #18 and features mainly fast moving air masses from North Texas and central New Mexico. Total available organic carbon mass is 537 µg, with only one day, October 24th, featuring more than 100 µg available OC mass, with 121 µg.

2.4 GC-MS Analytical Method

2.4.1 GC-MS Specifications

A HP 6890 Gas Chromatograph coupled with a HP 5973 Mass Selective Detector was used for organic analysis of the filter samples. Separation was completed using a 30m x 250 µm x 0.25 µm HP-5MS capillary column coated with 5% Phenyl Methyl Siloxane. The analysis run time was 53.5 minutes; an isothermal temperature of 65^o C was maintained for 10 minutes, then raised to 300^o C at a rate of 10^o C/min, then held at 300^o C for 20 minutes. Figure 2.8 graphically

represents the temperature scheme. A splitless inlet with helium gas was used, at a flow rate of 53.5 mL/min at 300⁰ C.

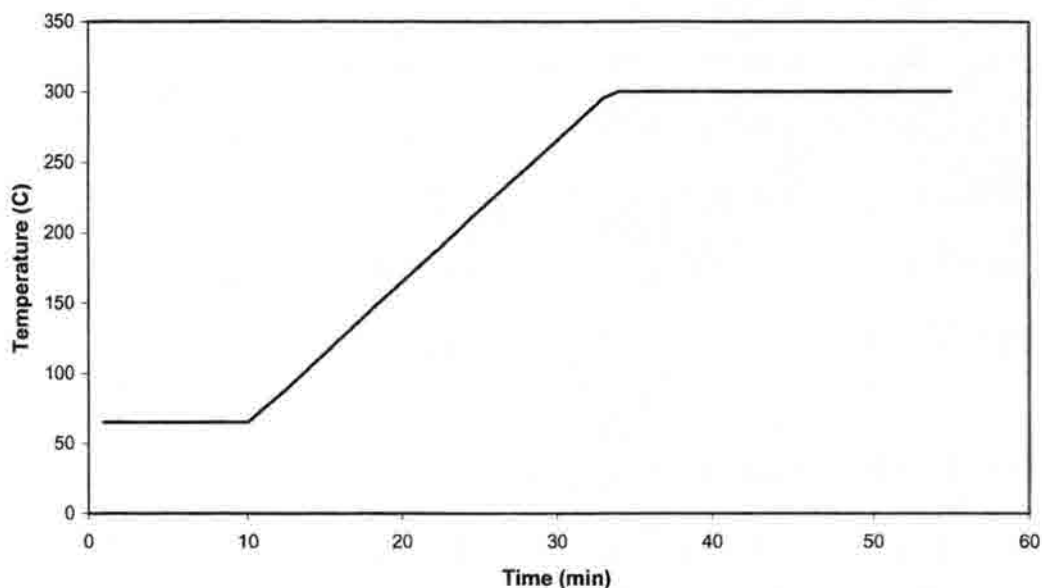


Figure 2.8 Graphical representation of the temperature scheme used for GC analysis

The mass spectrometer was operated in ion scan mode, starting at time 6.0 minutes. Mass to charge ratios of 50 to 500 were scanned at 2.94 scans/second. The ion source was set to 230⁰ C and the mass fragmenter set to 275⁰ C.

2.4.2 Gas Chromatography – Mass Spectroscopy Theory

Gas Chromatography (GC) is an analytical procedure used to separate individual compounds from a mixture of organic compounds for identification and quantification. The mixture is carried through the column by an inert gas (in our application this is helium) and the components of the mixture elute at different times depending on their structure, size, and interactions with the column. When compounds elute from the column, they are detected and

registered as peaks on a chromatogram. The area under each peak is proportional to the concentration of that compound. The time between when the sample is injected and when a compound elutes is called the retention time. This is a characteristic value for a specific compound, which can be used in conjunction with its mass spectrum to identify and quantify the concentration of the compound.

When the eluted components leave the GC, they are directed into the mass spectrometer (MS), where each eluted compound is bombarded with high energy electrons. The compound is first ionized and then is fragmented into charged fragments that are characteristic of the specific compound class. For example, large n-alkanes ($> C_{10}$) all fragment into the same mass-to-charge (m/z) fragments no matter the length of their carbon chain; m/z 71, 85 and 99 are the dominant fragments for all large n-alkanes. Fragments are then accelerated into a mass filter, which scans from m/z 50 to 500, counting the abundance of fragments possessing each mass/charge ratio. This occurs 2.94 times a second for sharp resolution. Thus, for every elution peak generated from the GC, a corresponding mass spectrum for that time is also found.

A series of standards of compounds of interest is prepared. Chromatograms of these standards are then obtained, with their characteristic retention times and mass spectra. Peak areas for each compound, divided by an internal standard area, are plotted as a function of concentration to obtain response factors. These plots should yield a straight line that passes through the origin. Quantification is therefore possible of a sample of unknown composition based on a compound's and internal standard's peak areas in that sample.

The internal standards used in this application are compounds with deuterium, a hydrogen isotope, substituted for hydrogen. This will usually give the same retention time as the non-deuterated analog, since the physical properties are still the same. Since deuterium has a different mass than hydrogen, the fragments of the internal standard will possess different m/z ratios and be readily identifiable. These deuterated compounds will not be found naturally in any sample, and therefore make excellent standards. The chosen internal standards are listed in table 2.2.

Internal standards are used to negate any differences in final volume or injected volume between samples. Any injection volume differences between samples will be reflected in the concentrations of the internal standards. This allows for comparison of compound concentrations between samples, even if there are injection volume differences or losses during sample preparation.

Table 2.2 Deuterated standards used for quantification: their concentrations and amounts added

Deuterated Standard	Concentration	Amount (μL)
Chrysene d-12	25 $\mu\text{g/mL}$	100
C28D58	250 $\mu\text{g/mL}$	50
Decanoic acid d-19	250 $\mu\text{g/mL}$	50
Benzaldehyde d-6	250 $\mu\text{g/mL}$	10

2.5 Extraction Methods

Dichloromethane was the solvent used to extract samples. It was found that there is little difference between extraction using dichloromethane and extraction with hexane and benzene/isopropanol (see section 2.5.2). Concentrated sample extracts were divided into three aliquots. One aliquot was methylated using diazomethane to methylate the carboxylic acids to methyl esters (see section 2.5.3). The second aliquot was silylated in order to silylate hydroxyl groups (such as on levoglucosan and cholesterol) into trimethylsilyl ester derivatives (see section 2.5.4). The third aliquot was used for direct injection without any derivatization, targeting compounds such as the alkanes and PAH. Sets of blank filters were also extracted. Deuterated internal standards were used for quantification.

2.5.1 DCM Extraction Method

An extraction method similar to previous studies (Zheng et al., 1997; Fang et al., 1999a; Oros et al., 1999a; Zheng et al., 2000; Didyk et al., 2000; Pio et al. 2001) was used to extract and analyze the groups of samples from BRAVO. The method is outlined in figure 2.9.

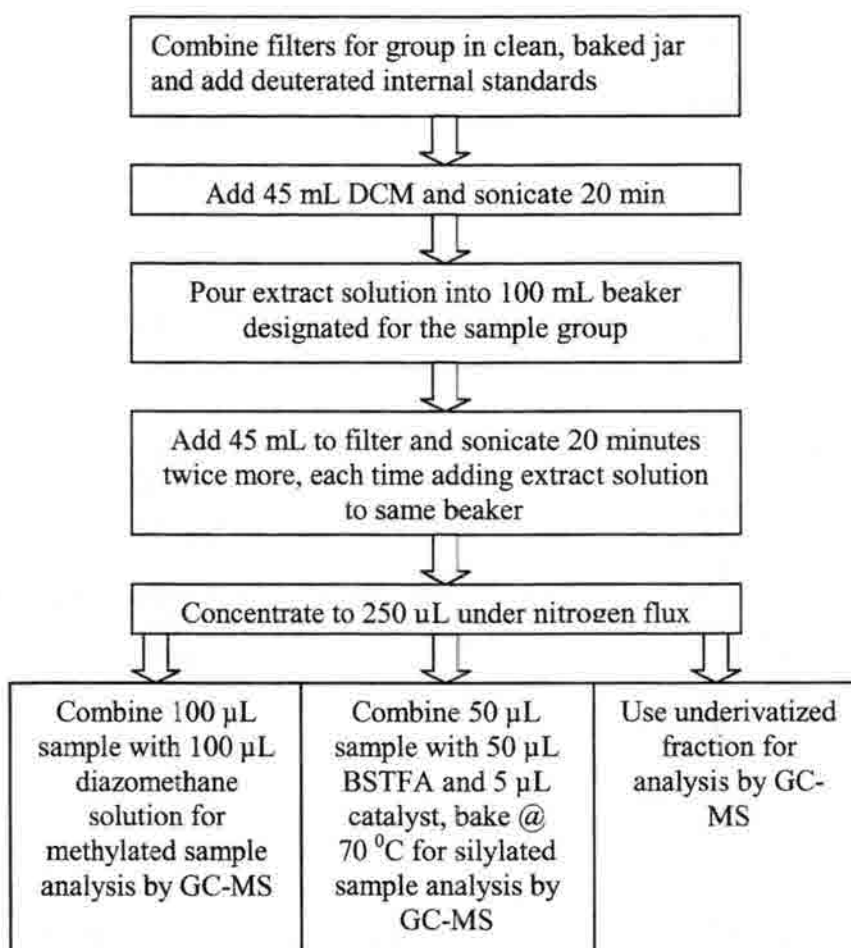


Figure 2.9 Flow chart of extraction and derivatization techniques

Daily filters were placed in clean, baked jars according to their group. Once each group was complete with the necessary filters, 45 mL dichloromethane (DCM) was added to each jar. Deuterated standards were then added for later quantification; table 2.2 gives the amount added and the concentrations of the deuterated standards used.

The jars with the grouped filters were then sonicated for 20 minutes. After sonication, the extract solution was carefully poured into a clean, baked 100 mL beaker. Next, 45 mL of DCM were added to the jar and sonicated again for 20 minutes, after which the extract solution was poured into the same corresponding beaker for the group. Then, the same process (45 mL DCM and 20 minutes sonication) was repeated once more, for a total of three times (3 x 45mL DCM).

Sample solutions were reduced in volume to approximately 4 mL via evaporation under nitrogen flux, using pre-purified nitrogen. Next, samples were filtered using an Osmonics MSI TefSep Teflon disc 0.2 μm filter to remove any quartz fiber filter residues from the extract solution. The filtered extract solution was then transferred to a 5 mL conical vial and concentrated to 250 μL via evaporation under nitrogen flux. DCM has a higher vapor pressure than the organic species of interest in the solution, and will therefore preferentially evaporate before the other species. The evaporation step increases the concentration of organic species significantly by decreasing the total solvent volume. Once the extract solution was concentrated to 250 μL , it was transferred to a 2 mL amber glass storage vial and kept in the freezer.

Samples were later derivatized. The methylation method was used to convert carboxylic acids to their analogous methyl esters, which are amenable to GC-MS quantification (Simoneit and Mazurek, 1982; Simoneit et al., 1988; Oros et al., 1999b; Simoneit, 1999). Diazomethane was generated and 100 μL added to a 100 μL aliquot of sample for methylation (see section 2.5.3). Silylation was used to silylate hydroxyl groups, such as those on levoglucosan and cholesterol, into their trimethylsilyl esters (see section 2.5.4). This also makes these species more amenable to analysis by GC-MS (Simoneit and Mazurek, 1982; Oros et al., 1999b; Simoneit, 1999). To silylate a sample, 50 μL of sample was combined with 50 μL of bis(trimethylsilyl)trifluoroacetamide (BSTFA) and 5 μL catalyst (cholortrimethylsilane) and heated for 2 hours at 70⁰C (Simoneit et al., 1988; Simoneit et al., 1993; Nolte et al., 1999).

Standards are derivatized in the same fashion so that the dilution from derivatization is factored into the calibration curves and remains consistent between standard and sample.

2.5.2 Comparison of DCM Extraction Method with Hexane/Benzene/IPA Extraction

Method

Hexane and a benzene/isopropanol solution (2:1 ratio) have been used for some previous organic aerosol extraction studies (Simoneit and Mazurek, 1982; Schauer et al., 1996). Benzene, however, when concentrated down as in this extraction technique, has been shown to contain significant concentrations of impurities. This is because these impurities have a lower vapor pressure than the benzene and will remain while the benzene is evaporated. Observed impurities include alkanes, PAH and alkanolic acids, all compounds of interest for aerosol analysis.

Dichloromethane is usually free of impurities such as those listed above and could be an excellent alternative solvent for extraction. However, the relative efficiencies of extraction by DCM and hexane/benzene/IPA were unknown.

To resolve this question, a comparison was conducted between these extraction methods. The extracted filters were samples of creosote wood smoke from Big Bend N.P., sampled by DRI. One set of filters was extracted with 3 x 25 mL DCM, and a corresponding set was extracted with 2 x 25 mL hexane and 3 x 25 mL benzene: IPA mixture (2:1 ratio). Three filters were quartered, and then each quarter was extracted. Two quarters from each filter were extracted separately using DCM, and two quarters from each filter were extracted separately with hexane plus benzene:IPA. This gives three sets of two quarter filters extracted in both DCM and hexane/benzene/IPA.

The extraction comparison was completed for alkanes, PAHs, and alkanolic acids. Concentrations of each species from these three categories were quantified against the standards. These results were then statistically evaluated for each group of compounds to test whether

differences in species concentrations obtained using the two extraction techniques are significantly different.

2.5.3 Calculations of Variances for Extraction Methods

For each compound, the average and standard deviation the concentrations extracted by the same technique from two filter quarters were determined, as illustrated in Table 2.3.

Table 2.3 Sample Method Comparison Table

Species	Concentration Quarter 1 (DCM) ng/m ³	Concentration Quarter 2 (DCM) ng/m ³	Average of both quarters ng/m ³	Standard deviation ng/m ³	Standard deviation / Average
Alkane 1	370	450	410	56.57	0.14
Alkane 2	505	420	462.5	60.10	0.13

The standard deviation is defined as

$$\text{standard deviation} = \sqrt{\frac{\sum_{i=1}^N (x_i - \bar{x})^2}{N - 1}} \quad (2.8)$$

where N is the number of replicates. For all of these cases, only two quarters can be averaged together, since for each extraction method, only 2 quarter filters are available from the same original sample filter. The N here is therefore 2, so the denominator is actually equal to one. To achieve a relative standard deviation that would not allow filters of higher loading to be weighed more than the lower filters, the standard deviations for each species were divided by that species' average concentration using the equation:

$$\text{Relative standard deviation} = \text{standard deviation} / \text{average} = \frac{\sqrt{\frac{\sum_{i=1}^N (x_i - \bar{x})^2}{N-1}}}{\bar{x}} \quad (2.9)$$

To combine these relative standard deviations in a useful manner, a pooled standard deviation was found for each family for both extraction methods. Normally, a pooled standard deviation (S_{pooled}) is computed as shown in the following equation:

$$S_{\text{pooled}} = \sqrt{\frac{\sum_{i=1}^{N_1} (x_i - \bar{x}_1)^2 + \sum_{j=1}^{N_2} (x_j - \bar{x}_2)^2 + \sum_{k=1}^{N_3} (x_k - \bar{x}_3)^2 + \dots}{N_1 + N_2 + N_3 + \dots - N_s}} \quad (2.10)$$

where N_1 is the number of data points in set 1, N_2 in set 2, etc... and N_s is the number of replicate sets included. For this study, the relative standard deviation for each category was used to find a pooled relative standard deviation. This transforms the previous equation into:

$$S_{\text{pooled}} = \sqrt{\frac{\sum_{i=1}^{N_1} \left(\frac{x_i - \bar{x}_1}{\bar{x}_1} \right)^2 + \sum_{j=1}^{N_2} \left(\frac{x_j - \bar{x}_2}{\bar{x}_2} \right)^2 + \sum_{k=1}^{N_3} \left(\frac{x_k - \bar{x}_3}{\bar{x}_3} \right)^2 + \dots}{N_1 + N_2 + N_3 + \dots - N_s}} \quad (2.11)$$

where N_1 is the number of data points in set 1, N_2 in set 2, etc., and N_s is the total number of replicate data sets being pooled.

The use of S_{pooled} is a tool that is used to estimate a standard deviation for a series of samples that will be superior to the standard deviation of a given subset (Skoog et al, 1992;

Devore, 1995). Sources of indeterminate error are assumed to be the same for each subset. Since the samples were obtained in similar fashion and extracted and analyzed via the same procedures, this is a reasonable assumption. It is also assumed that the error between measuring species in a family (alkanes, PAHs, acids) is similar, e.g. that the error in quantifying alkane 1 is similar to that of alkane 2.

A s_{pooled} of relative standard deviations was calculated for each family of species for the sets of filters extracted by hexane/benzene/IPA and by DCM. The number of replicate measurements for each family is equal to the number of filters included (3) times the number of quarters analyzed using the extraction method of interest (2) times the number of measured compounds in the chemical family (ten alkanes, 22 PAHs, or five alkanolic acids). N_s is equal to the number of replicate sets utilized, equal to the number of filters (3) times the number of species (10, 22, or 5). The denominator from equation 2.11, which represents the number of degrees of freedom in the calculation of s_{pooled} , is then equal to

$$\frac{[N \text{ filters (3)} * N \text{ quarters extracted (2)} * N \text{ species quantified (10, 22, or 5)}] - N \text{ quarterfilters (3)} * N \text{ species quantified (10, 22, or 5)}}{N_s}$$
(2.12)

This s_{pooled} of relative standard deviations was calculated for both methods (DCM and benzene/IPA).

Table 2.4 shows that there was little difference found between the extraction methods' reproducibility. For alkanes, a 34.6% standard deviation was found for the DCM extraction method and a 36.4% standard deviation was found for the hexane/benzene/IPA method. For PAHs, 14.1% was the standard deviation for the DCM method and 12.7% was the standard deviation for the hexane/benzene/IPA method. A 20.4% standard deviation for the DCM method and a 26.8% standard deviation for the hexane/benzene/IPA method were found for the alkanolic

acids. This shows that there is only a negligible difference between the two extraction methods' precision.

Table 2.4 Comparison of Extraction Methods for Alkanes, PAHs and Alkanoic Acids

Species	pooled relative standard deviation for DCM Extraction	pooled relative standard deviation for hexane/Bz/IPA Extraction
Alkanes	34.6%	36.4%
PAHs	14.1%	12.7%
Alkanoic Acids	20.4%	26.8%

2.5.4 Statistical Comparison between Extraction Methods

In addition to a variability analysis, a statistical test was applied to test whether differences in mean species' concentrations measured using the two extraction methods were significantly different. For this comparison, a null hypothesis was tested. The null hypothesis states that the extraction methods produce identical results and that observed differences in the concentrations ($x_{DCM} - x_{hex/bz/ipa}$) are the result of indeterminate errors. The absolute value of the concentration difference ($x_{DCM} - x_{hex/bz/ipa}$) is compared to a critical value. If the observed difference is less than the critical value, then the null hypothesis cannot be rejected and no significant difference between the extraction methods is demonstrated. A difference that is greater than the critical value indicates that there is a significant difference between the extraction methods. The equation for this comparison is:

$$\bar{x}_{DCM} - \bar{x}_{Hex/Bz/IPA} <?> \pm t s_{pooled} \sqrt{\frac{N_{DCM} + N_{Hex/Bz/IPA}}{N_{DCM} N_{Hex/Bz/IPA}}} \quad (2.13)$$

This analysis was done for each compound for each of the three samples. The s_{pooled} was calculated for each species class (alkanes, PAH, alkanolic acids) using the standard deviations of both the DCM and Hex/Bz/IPA samples as per equation 2.10. The denominator of equation 2.10 for each compound class is equal to the number of species evaluated for that class (10 alkanes, 22 PAH, 5 alkanolic acids), multiplied by the number of sets (2 for each sample), repeated six times (three DCM + three Hex/Bz/IPA), minus the number of replicate data sets ($3 \times 2 \times$ number of species). This number is also equal to the degree of freedom for each compound class, and is used to find t . Since the degree of freedom for each compound class is greater than 25, the t value used for the 95% confidence level is 1.96. The N 's in equation 2.13 are the number of replicate measurements. These are equal to 2 in all cases as each filter had two quarters analyzed utilizing each extraction method. The left side of equation 2.13 is simply the difference between the average concentrations for each quarter filter measured by the two extraction methods. This test is applied separately for each organic compound.

The results from the hypothesis tests are shown in tables 2.5 (alkanes), 2.6 (alkanoic acids) and 2.7 (PAH). Four out of twenty-six alkane comparisons (15%) were found to be significantly different between the DCM and Hx/Bz/IPA extraction methods. There were significant differences found for five out of 60 PAH comparisons (8.3%), and for two out of fifteen alkanolic acid comparisons (13%).

Overall, the two extraction methods appear to be similar, but since the DCM method yields cleaner blanks than the Hx/Bz/IPA method, the DCM method will be the preferred extraction method for this research.

Table 2.5 Differences between average concentrations measured by the DCM and Hx/Bz/IPA extraction methods for alkanes; values above the critical value of 835 at 95% confidence level (and therefore showing a significant difference between the methods) are denoted in bold

Alkane Species	Sample 112	Sample 113	Sample 114
n-C15	1782	110	-
n-C16	1199	171	-
n-C17	1368	678	-
n-C18	1633	191	-
n-C19	360	142	453
n-C20	103	200	19
n-C21	55	160	377
n-C22	144	144	341
n-C23	197	29	224
n-C24	53	44	283

Table 2.6 Differences between the DCM and Hx/Bz/IPA extraction methods for alkanic acids; values above the critical value of 1172 at 95% confidence level (and therefore showing a significant difference between the methods) are denoted in bold

Alkanoic Acid Species	Sample 112	Sample 113	Sample 114
n-C14	45	533	271
n-C15	8	193	150
n-C16	35	2292	222
n-C17	11	124	366
n-C18	192	3729	288

Table 2.7 Differences between the average concentrations measured by the DCM and Hx/Bz/IPA extraction methods for PAH; values above the critical value of 41969 at 95% confidence level (and therefore showing a significant difference between the methods) are denoted in bold

PAH Species	Sample 112	Sample 113	Sample 114
fluorenone	2905	2199	75557
phenanthrene	3192	291	43297
anthracene	527	1016	75594
3-Me phenanthrene	454	372	16795
2-Me phenanthrene	728	479	17422
2-Me anthracene	223	327	6569
9-Me phenanthrene	460	328	9949
1-Me phenanthrene	465	312	12123
9,10 Anthracenedione	19874	286766	163085
fluoranthene	149	14331	29941
Acephenanthrylene	497	513	3711
Pyrene	2060	10330	26988
Benzo[c]phenanthrene	577	339	9068
Benzo[ghi]fluoranthene	248	238	6640
Benz[a]anthracene	437	221	17459
Benzo[k]fluoranthene	1187	2801	16216
Benzo[b]fluoranthene	4779	1650	23008
Benzo[j]fluoranthene	102	840	2484
Benzo[e]pyrene	991	694	11255
Benzo[a]pyrene	345	1943	8543
Perylene	56	348	2877

2.5.5 Methylation for Acid Analysis

Due to the large polarity of the acids and the low polarity of the selected column, acids will not completely elute from the column. To remedy this, the samples are subjected to a derivatization for the analysis of acids. Carboxylic acids in the sample are derivatized to their corresponding methyl esters, which are amenable to analysis by GC-MS.

To form these methyl esters, a solution of diazomethane, CH_2N_2 , is prepared as follows. A methylation setup with an inner and outer tube is used, where gaseous transfer is allowed

between the two tubes from a hole in the side of the inner tube near the top. The outer tube has no contact with the air, as the top of it is completely blocked by the inner tube. The inner tube is open on the top, but will be sealed so that it is an internal system. This diazomethane generation system is shown in figure 2.10.

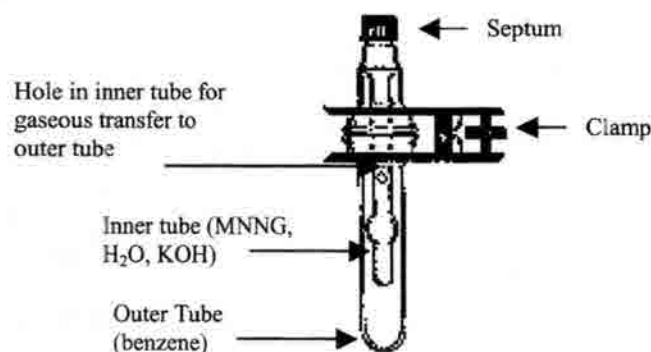
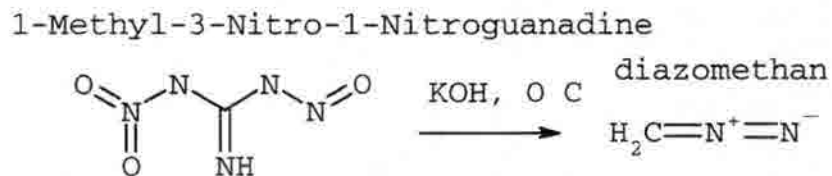


Figure 2.10 Diagram of diazomethane generating system, from Kimble Glassware Catalogue, part #767200

In a large beaker filled with ice water, the outer tube is placed in a ring clamp. The reaction should be done at 0 °C since the resulting product, diazomethane, is very reactive. 2 mL of benzene is added into the outer tube. The inner tube is then placed in the outer tube, with the hole in the back, and sealed together with a clamp. Next, 100 mg of 1-Methyl-3-Nitro-1-Nitroguanadine (MNNG) is weighed and added into the inner tube so that it rests in the bottom. *MNNG is very toxic and must be handled with extreme care.* 500 μ L of deionized water is then added to the inner tube by running it down the front of the tube, avoiding the hole. A septum is then screwed on to seal the inner tube. Next, 600 μ L of 5 M KOH solution is added via syringe through the septum into the inner tube, again running the liquid down the front of the tube to avoid the hole. The syringe is then quickly withdrawn.

A reaction then takes place, which generates diazomethane gas. This yellow gas goes through the hole in the inner tube, and then is absorbed into the benzene in the outer tube. This

reaction is complete after half an hour, and the benzene is turned to a yellow color. The reaction is as follows:



This diazomethane solution is then used to methylate a sample. By taking 100 μL of the diazomethane solution and 100 μL of sample solution and combining them in a 2 mL sample vial, acids in the sample solution are converted to methyl esters. This is done immediately after producing the diazomethane solution. The reaction to form the methyl esters is as follows:

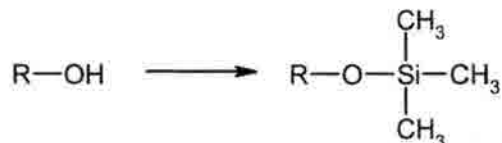


2.5.6 Silylation for Sugars and Alcohols

Other species such as sugars (like levoglucosan) and alcohols (such as cholesterol) are also too polar to completely elute from the GC column. Sample extracts are therefore subjected to silylation, where hydroxyl groups on these compounds are altered to trimethylsilyl ester groups. These derivatives are generally less polar, more volatile and more thermally stable, and can be detected and quantified using GC-MS.

To silylate a sample, 50 μL of concentrated sample extract is placed in a silylation vial that can be sealed by melting the glass top. Then 50 μL of bis(trimethylsilyl)trifluoroacetamide (BSTFA) is added to the silylation vial. Finally, 5 μL of a catalyst, chlorotrimethylsilane, is added. The vial is then sealed over a burner and heated in an oven for three hours at 70^o C. After

baking, the vials are broken open and the solution transferred to standard 2 mL sample vials. The silylation converts all hydroxyl groups to their corresponding trimethylsilyl ester groups. The reaction can be generalized to the following:



A different column must be used for runs of silylated samples to avoid cross contamination. This is because compounds such as levoglucosan, in their unsilylated form, stick in and contaminate the column from previous unsilylated runs that contained levoglucosan. Then, when a new sample with a silylating agent is introduced, these compounds become silylated and exit the column with the new sample, thus skewing the results of that sample. A different column is used for silylated runs to avoid this problem.

2.5.7 Extraction of Blank Filters

Blank filters were collected during the study every Tuesday (see section 2.1). These blank filters were grouped by month and extracted (section 2.5.1), so that a “blank” composite for each month was established. These monthly blanks were derivatized (sections 2.5.3, 2.5.4), and analyzed by GC-MS for alkanes, alkanolic acids, PAH, molecular markers, and other compounds.

Only alkanes and alkanolic acids were detected in the blank composites. The concentrations of species found in the blank composites are detailed in the appendix. These amounts (in ng) were used as a blank correction for the ambient BRAVO sample composites. The amount of a species found in a sample (in ng) was reduced by the amount found in the blank for the corresponding month. In groups that spanned two months, the average amount of a species in the blanks from the corresponding months was used. Using C16 alkane as an example, the equation used is as follows:

amount C16 alkane (ng) in sample group – amount C16 alkane (ng) in blank = actual C16

$$\text{alkane in sample group (ng)} \quad (2.13)$$

A concentration for this species in the sample group is then found by dividing the ng in the sample group by the total volume sampled for that group. Again using C16 alkane as an example, the equation is:

$$\text{concentration of C16 alkane (ng/m}^3\text{)} = \text{actual C16 alkane in sample group (ng)} / \text{total volume sampled for this group (m}^3\text{)} \quad (2.14)$$

2.6 Calculations of Source Influences from Tracer

Concentrations

As described in sections 1.8 and 1.9, certain organic tracers are unique to specific sources. These include hopanes for vehicular exhaust, cholesterol for meat cooking, and levoglucosan for wood smoke. A ratio between the concentration of these tracers and the total OC emitted from a source can be found from individual source profiles (Rogge et al., 1991, 1993a; Schauer et al., 1999a,b, 2001; Fine et al., 2001). This ratio, with the tracer's concentration in a sample, can then be used to estimate the amount of OC that a source contributed to the total OC in that sample. For this study, source profiles were taken from the literature. Resources were not available to generate new organic source profiles that might be more representative for emissions from sources in areas influencing Big Bend N.P.

2.6.1 Contributions from Vehicular Exhaust Calculations

For vehicular exhaust, a ratio between the amount of 17 α 21 β -hopane and the total organic carbon emitted from vehicle exhaust was assumed based on the emission source profiles shown in table 2.8.

Table 2.8 Source Profile for Vehicular Fine Particle Emissions (adapted from Rogge et al., 1993a; diesel from Schauer et al., 1999)

Type	Source Profile 17 α 21 β Hopane	Source Profile OC	Hopane/OC Ratio	OC/Hopane Ratio
Catalyst Equipped Auto	0.009 mg/km	9.015 mg/km	9.98×10^{-4}	1002
Non-Catalyst Equipped Auto	0.0182 mg/km	38.91 mg/km	4.68×10^{-4}	2137
Diesel Truck (Rogge 1993)	0.0942 mg/km	108.46 mg/km	8.69×10^{-4}	1151
Diesel Truck (Schauer 1999)	0.0114 mg/km	36.45 mg/km	3.95×10^{-4}	2531
Average Diesel				1841

This ratio can be used to estimate the contribution to primary fine aerosol OC mass contributed by vehicles by multiplying the hopane concentration by the OC/Hopane emission ratio, shown in equation 2.15:

$$\text{Sample Hopane } (\mu\text{g}) * \text{OC/Hopane} = \text{OC from Vehicular Exhaust } (\mu\text{g}) \quad (2.15)$$

The ratios vary for non-catalyst and catalyst autos and diesel trucks. Hopanes come from all three sources, but probably not in a 1:1:1 ratio, since there are far more catalyst-equipped cars on the road in the U.S. (and presumably also in northern Mexico) than non-catalyst or diesel trucks. A baseline ratio of 80:10:10 for catalyst:non-catalyst:diesel was assumed in this work to estimate the influence from vehicular exhaust. The average of the diesel profiles in Table 2.8 was used for this calculation. The primary OC fine aerosol from vehicular exhaust can be computed using equation 2.16:

$$\frac{\{[(.8*\text{Hopane } (\mu\text{g})*1002)+(.1* \text{Hopane } (\mu\text{g})*2137)+(.1* \text{Hopane } (\mu\text{g})*1841)] / \text{Sample OC } (\mu\text{g})\} * 100\% = \% \text{ OC from Vehicular Exhaust}}{(2.16)}$$

2.6.2 Contributions from Meat Smoke Calculations

Meat smoke influence can be estimated using cholesterol as a tracer. Though this has been found to be an excellent, unique tracer by Rogge et al. (1991), in ambient urban samples quantification of it is not always possible (Schauer et al., 1996). Cholesterol/OC emission ratios vary with the cooking method (e.g., charbroiling vs. frying). A ratio of 50:50 for charbroiling and frying of hamburger was used for baseline source contribution estimates in this study, utilizing the source profiles from Rogge et al. (1991) for charbroiling and frying and Schauer et al. (1999) for charbroiling; these values are detailed in table 2.9.

Table 2.9 Source Profile for Meat Cooking Emissions (adapted from Rogge et al., 1991 and Schauer et al., 1999)

Type	Source Profile Cholesterol	Source Profile OC	Cholesterol /OC Ratio	OC/ Cholesterol Ratio
Charbroiled Hamburger (Rogge)	15.3 kg/day	4900 kg/day	0.003	320
Charbroiled Hamburger (Schauer)	.004 g/kg	6.35 g/kg	6.25×10^{-4}	1599
Average Charbroiled				960
Fried Hamburger (Rogge)	15.1 kg/day	1400 kg/day	0.0108	93

The Schauer et al. (1999) profile has a much lower emission rate due to the smaller amount of time, 5 minutes, the meat spent on the grill compared to the 8 minutes from Rogge et al. (1991). The average of the two charbroiled hamburger profiles was used. To estimate the percentage of OC from meat smoke, equation 2.17 is used:

$$\{[(.5 * \text{Cholesterol } (\mu\text{g}) * 960) + (.5 * \text{Cholesterol } (\mu\text{g}) * 93)] / \text{Sample OC } (\mu\text{g})\} *$$

$$100\% = \% \text{ OC from Meat Cooking} \tag{2.17}$$

2.6.3 Contributions from Wood Smoke Calculations

Levoglucosan was used as a primary wood smoke tracer in this study, making use of source profiles published by Schauer et al. (2001), who found ratios of levoglucosan to total OC for pine and oak smoke, and Fine et al. (2001), who found ratios for a number of woods grown in

the northeastern U.S. (see Table 1.7). Additionally, source samples from burning of vegetation found in the Big Bend region, huisache and tamarisk, were collected by DRI and extracted, as described in section 2.6.4. Their levoglucosan profiles are also included in table 2.10.

Table 2.10 Source Profile for Wood Burning Emissions (adapted from Schauer et al., 2001, Fine et al., 2001, and source extracts)

Type	Source Profile Levoglucosan	Source Profile OC	Levoglucosan/ OC Ratio	OC/Levoglucosan Ratio
Pine Wood (Schauer)	1.375 g/kg wood	5.32 g/kg wood	0.258	3.88
Oak Wood (Schauer)	0.403 g/kg wood	3.01 g/kg wood	0.134	7.46
Red maple (Fine)	0.305 g/kg wood	2.82 g/kg wood	0.109	9.17
Northern Red Oak (Fine)	0.84 g/kg wood	4.99 g/kg wood	0.168	5.95
Paper Birch (Fine)	0.26 g/kg wood	2.34 g/kg wood	0.110	9.09
Eastern White Pine (Fine)	0.42 g/kg wood	8.37 g/kg wood	0.05	20
Eastern Hemlock (Fine)	0.35 g/kg wood	3.7 g/kg wood	0.095	10.5
Balsam Fir (Fine)	0.39 g/kg wood	4.8 g/kg wood	0.081	12.3
Huisache (source sample)	16.0 $\mu\text{g}/\text{m}^3$	4075 $\mu\text{g}/\text{m}^3$	0.004	255
Tamarisk (source sample)	11.4 $\mu\text{g}/\text{m}^3$	2152 $\mu\text{g}/\text{m}^3$	0.005	189

A ratio of 50:50 of pine:oak was assumed for this work, where the contribution of wood smoke to primary fine aerosol OC was calculated using the equation 2.18:

$$\frac{\{[.5 * \text{Levoglucosan } (\mu\text{g}) * 3.876] + (.5 * \text{Levoglucosan } (\mu\text{g}) * 7.463)\}}{\text{Sample OC}} (\mu\text{g}) * 100\% = \% \text{ OC from Wood Smoke} \quad (2.18)$$

This assumed ratio between pine and oak may not be a completely accurate representation of the composition of wood burned in the area, but changing the profile will not change the overall conclusions, detailed in section 3.5.2.

2.6.4 Extraction of Source Samples

Source samples of coal power plant, roadside, cement plant, wood and brush burning emissions were taken on pre-fired quartz fiber filters by DRI from August through December 1999. The main focus of DRI's experiments was to collect source samples suitable for measurement of trace metal concentrations. They kindly offered, however, to add another quartz filter to collect an additional sample that might be useful for constructing organic source profiles.

These samples were extracted using the Hexane/Bz/IPA method, and the samples of huisache and tamarisk, types of brush near Big Bend N. P., were analyzed for levoglucosan content. Levoglucosan concentrations were found to be lower than other wood smoke source profiles (see table 2.11). This may be due to the fact that huisache and tamarisk are not trees, such as pine or oak. Huisache is a flowering daisy (*Amblyolepis setigera*) found predominately in Texas. Tamarisk (*Tamarix aphylla*, *Tamarix gallica*, and *Tamarix parviflora*) is another flowering plant, of the dicot family, found throughout the U.S. Southwest.

Samples of emissions from a coal power plant, a cement plant, and roadside aerosol were extracted also. In general, the filters were too lightly loaded with aerosol to be useful for organic

source profile characterization. The results of these extractions are detailed in the appendix. Additionally, samples of creosote wood were used for the comparison study between the extraction methods in sections 2.5.3 and 2.5.4.

2.7 Estimations of Secondary OC

As discussed in section 1.12, the amount of secondary OC can be estimated from the amount of EC in a sample and an OC/EC_{minimum} ratio. The assumptions that are necessary for this equation to give reasonable estimates are: 1) the minimum OC/EC ratio must be derived from samples where secondary OC is negligible; 2) there is a low contribution of semi-volatile organic compounds in comparison with non-volatile; 3) the composition of primary carbonaceous aerosol sources and the relative contribution of each source must be spatially and temporally constant; and 4) the contribution of non-combustion primary particulate OC is small or constant.

If the minimum OC/EC was obtained from BRAVO samples, the first assumption may be invalidated, since it is expected that there will be significant transport ($> 1-2$ days) from emission sources to Big Bend, giving ample opportunity for secondary organic compound formation, especially in summer. Use of minimum OC/EC ratios from other locations is also problematic as source emissions may differ strongly between locations.

If the amount of semi-volatiles constitute a large fraction of the organic aerosol, the concentration would depend on many factors, including temperature variations. Additionally, with changing advection patterns and speeds, as well as summer versus autumn emissions during BRAVO, assumption three (3) may be questionable as well. If there is a large contribution from plant emissions or aerosol from leaf detritus, assumption four (4) may also be in question.

Overall, these assumptions may not always hold during BRAVO, but the calculation can still be an interesting comparative estimate of secondary organic carbon between BRAVO groups. The average OC/EC ratio during December-February 1988-1998 at Big Bend National

Park, obtained from IMPROVE data, was found to be 1.97. This value is used in the secondary OC calculations as an upper limit of the primary OC/EC ratio at Big Bend N.P. It is assumed that secondary organic aerosol formation in the region is reduced, but not eliminated, during the winter months. OC/EC minimum ratios of 1.1 (urban) and 1.5 (rural) were obtained from Castro et al. (1999) to be used as additional constraints in the calculations of secondary organic concentrations for BRAVO samples. Both of these ratios were used to calculate a range of secondary OC during BRAVO. The increase between urban and rural locations was attributed to a constant presence of long-range transported aerosol containing some secondary OC (Castro et al., 1999) and gas phase organics condensing into the particulate phase, which would raise the OC/EC ratio.

2.8 Aethalometer Sampling of Black Carbon

2.8.1 Aethalometer Setup

A Magee Scientific aethalometer, model AE-14U, was used to measure black carbon concentrations at 5 minute intervals during the study. It was run continuously through the study at a flow rate of 5 standard liters per minute. Sampling was done on a quartz fiber filter, which automatically advanced when the loading attenuates 75% of the incident light (for further details on the working of the aethalometer, see section 2.8.2) (Hansen, 1996). A cyclone was used to obtain a cutoff aerodynamic diameter of $\sim 1 \mu\text{m}$. This cyclone was in use for an hour, every other hour, so that sampling switched between the fine ($< 1 \mu\text{m}$) and total fraction every hour. The upper limit to the size of particles effectively transmitted through the sampling inlet to the aethalometer, in the sample train without the cyclone, is unknown. Data were recorded by the instrument on a 3.5 inch disk and by a data acquisition computer.

2.8.2 Aethalometer Sampling Principles

The aethalometer is a self contained instrument that determines the amount of black carbon in collected aerosol from the amount of optical attenuation through a quartz fiber filter tape on which aerosol is continuously collected. A source of white light from an incandescent lamp (wavelength range of ~ 500 to 1000 nm) shines down on the filter (Hansen, 1996). Every 5 minutes, the amount of light transmitted through a 0.95 cm² spot on the filter where aerosol is collected is measured. A beam also measures the transmission through a portion of the filter where aerosol is not collected, in order to correct variations in lamp brightness and changes in the electronic response of the sensor. The attenuation (ATN) of light through the collecting part of the filter is defined as:

$$ATN = 100 * \ln (I_0 / I) \quad (2.19)$$

where I_0 is the intensity through the part of the filter not collecting aerosol, and I is the intensity through the collecting part of the filter. Therefore, a value of 1 would be from a blank, while a value of 100 would be extremely dark. To obtain the attenuation for the 5 minute interval, the attenuation of a reading is subtracted from the previous reading, yielding the amount of attenuation due to the increase in aerosol deposited in the last 5 minute sampling period:

$$\begin{aligned} \text{Attenuation due to last 5 minute sampling period} &= \text{current attenuation} - \\ &\text{previous attenuation} \end{aligned} \quad (2.20)$$

From this attenuation value, the aethalometer can calculate the amount of black carbon present based on the manufacturer's calibration curves relating black carbon concentration and optical attenuation. This assumes that all absorption is due to black carbon. Since most aerosol species have a very small absorbing component in their refractive indices, as shown in table 2.11,

this is usually a valid assumption. One possibility for error is from a large amount of soil, which has a significant absorbing component, and as such may skew the amounts of black carbon calculated.

Table 2.11 Refractive indices of some atmospheric substances at $\lambda = 589$ nm unless otherwise noted (adapted from Seinfeld and Pandis, 1998; and Finlayson-Pitts and Pitts, 1999)

Species	Refractive index ($m = n - ik$)
Air	1.00029
Water Vapor	1.00025
H ₂ SO ₄	1.426
NH ₄ HSO ₄	1.473
(NH ₄) ₂ SO ₄	1.521
Benzene	1.501
Black Carbon	1.96 - 0.66 i ($\lambda = 550\text{nm}$)
Mineral Dust	1.56 - 0.006 i ($\lambda = 550\text{nm}$)

2.8.3 Aethalometer Data Assimilation

The aethalometer recorded black carbon concentrations every 5 minutes during the study. To make these measurements comparable to others done during the study, these must be averaged into daily concentrations for both the fine (less than 1 μm) and total black carbon.

Daily concentrations were computed using data from 8 am CST to 8am the next day, the same as other species' daily concentrations were sampled. Data for each fraction, fine and total black carbon, were then averaged to a daily concentration using an IDL code (see appendix for code).

3 Results and Discussion

3.1 General Characterization of Organic Aerosol During BRAVO

Organic carbon was found to comprise approximately 20% of the total fine aerosol mass during BRAVO, as seen in Figure 3.1 (received from Dr. Bill Malm, CIRA, personal communication, 2001). A similar contribution was estimated from fine soil, while sulfates contributed nearly half of the aerosol fine mass on average.

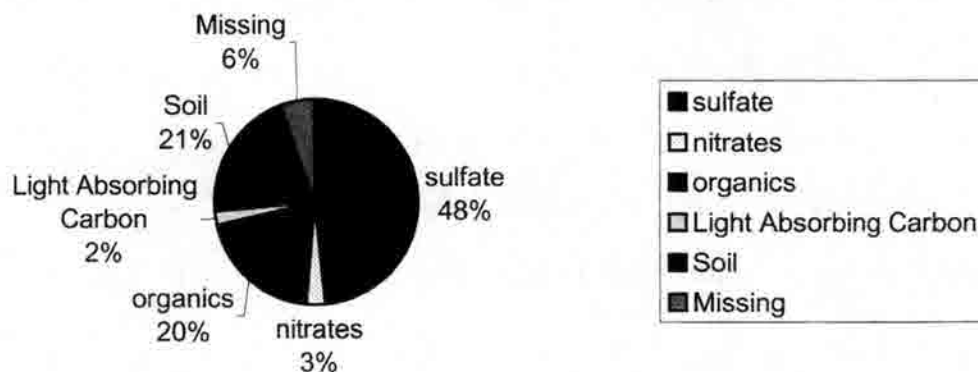


Figure 3.1 Mass budget of PM_{2.5} aerosol during BRAVO

Samples were analyzed for a wide range of organic compounds by GC-MS. Compounds studied include the n-alkane series, n-alkanoic acid series, four alkanolic diacids (succinic, adipic, malonic and azelaic acid), 28 polycyclic aromatic hydrocarbons (PAH), 28 wood smoke markers (levoglucosan, etc.), vehicle markers (hopanes and cholestanes) and meat smoke (cholesterol) markers.

3.1.1 Characterization of Compound Classes

As seen in figure 3.2, the relative abundance of acidic compounds is similar to a study at the Grand Canyon (Mazurek et al., 1997), which found that about half of elutable organics were acidic. This fraction can be of great significance since acidic hydrogen atoms may interact via hydrogen bonding with atmospheric water vapor. This can enhance condensation of atmospheric water vapor that could lead to particle growth, increased light scattering and decreased visibility. Additionally, the large amount of alkanolic acids may indicate marine influence on the aerosol composition.

Alkane, PAH, Alkanoic Acids and Total % of OC Identified

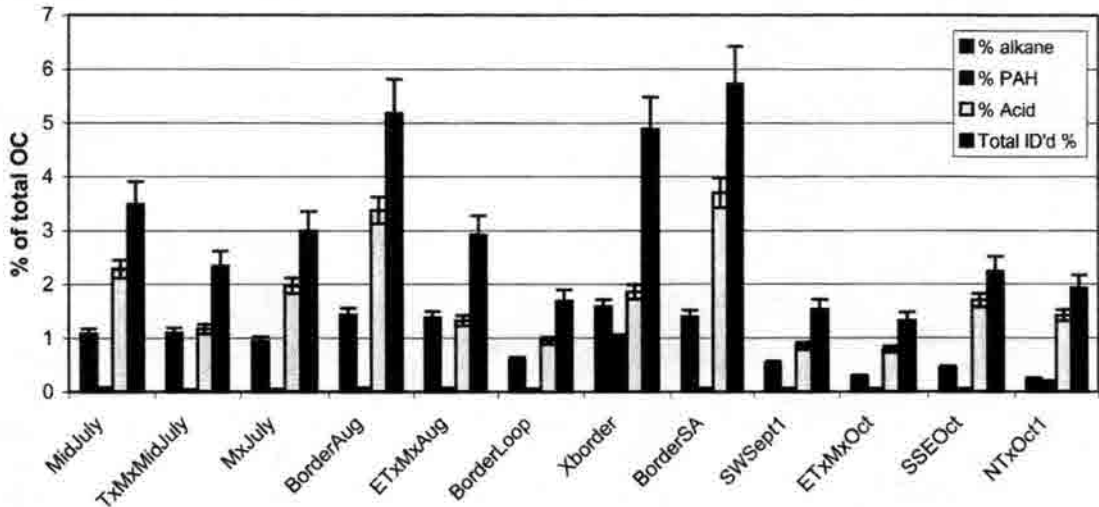


Figure 3.2 Percent of total OCM identified as alkanes, PAH and alkanic acids and total identified compounds percentage; error bars represent a 8.6% error for alkanes, 4.6% error for PAH and 7.3% error for alkanic acids, and 12.2% error for total identified compounds, all of which are one standard deviation

The fraction of $PM_{2.5}$ OCM ($OCM = 1.4 * OC$) identified as specific compounds ranged from 2% to 6% in the various sample groups. This is similar to other ambient aerosol studies in rural atmospheres (Schauer et al., 2000; Pio et al., 2001), though somewhat lower than urban studies, as detailed in table 3.1.

The groups with the highest percentage of identified compounds include periods that feature advection from the southeast along the Texas – Mexico border, especially during August and September. The group with the highest percentage of identified compounds, BorderSA, also has the highest amount of total OC (1349 μg). The large amount of identified compounds in XBorder is due to the detected presence of PAH. There are other groups during this time period that have similar advection patterns and have few PAH detected, resulting in a lower percentage of identified compounds. Groups with advection from the south and north have low amounts of identified compounds, but also feature low OC concentrations.

Table 3.1 Percentage of total OCM that has been identified as specific compounds in previous source sample and ambient studies and this BRAVO study (range of percent identified in parentheses)

Sample	Source Sample or Ambient	% of total OC that was identified	Reference
Wood Smoke (pine and oak)	Source Samples	21.3%	Rogge et al. (1998)
Car and Diesel Truck Exhaust	Source Samples	6.8%	Rogge et al. (1993), Schauer et al. (1999a)
Meat Charbroiling	Source Samples	10.5%	Rogge et al. (1991) Schauer et al. (1999b)
Los Angeles	Ambient (Urban)	11.3%	Rogge et al. (1993b)
Santiago, Chile	Ambient (Urban)	28.0%	Didyk et al. (2000)
Bakersfield, CA	Ambient (Urban)	12.0%	Schauer et al. (2000)
Kern Wildlife Refuge, CA	Ambient (Rural)	1.7%	Schauer et al. (2000)
Giesta, Portugal	Ambient (Rural)	3.8%	Pio et al. (2001)
Big Bend, Tx	Ambient (Rural)	3.1% (2%-6%)	This study

3.1.2 Typical Distributions of Alkanes and Alkanoic Acids

Alkane distributions predominately had peaks (C_{max}) of C23, C24 and C25 during the first three months of the study. With changing advection patterns in October, this C_{max} shifted to C29, perhaps reflecting an increased plant wax influence. Alkane distributions for three groups, MxJuly, BorderSA and SSEOct are shown in figure 3.3. Complete alkane distributions for each group can be found in the appendix. Error bars represent one standard deviation for the DCM extraction of alkanes, equal to 30%.

Alkane Concentrations for MxJuly, BorderSA and SSEOct

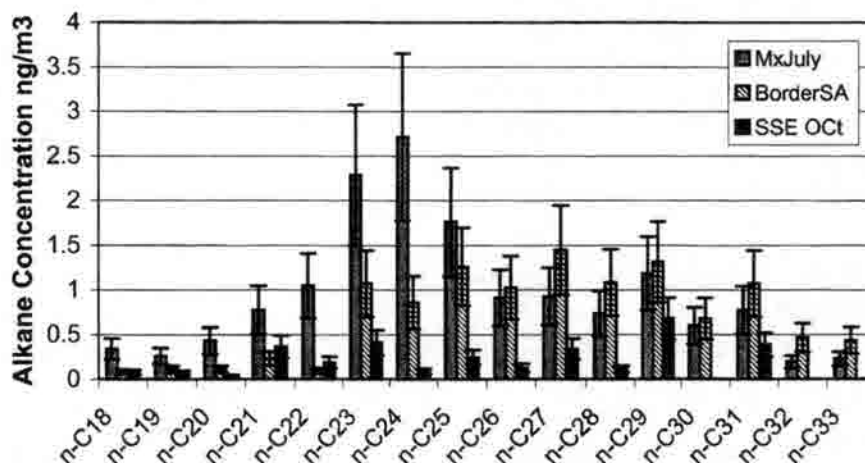


Figure 3.3 Alkane Concentrations for MxJuly, BorderSA and SSEOct; error bars represent a 34.6% (one standard deviation) error for alkanes for the DCM extraction method

Alkanoic acids were the most prevalent class of organic compound found during BRAVO (see figure 3.2). There is a large amount of C9 acid present, which will be discussed further in section 3.4. A C_{max} of C16 is found for most groups; C9 concentrations exceed C16 in four groups, possibly reflecting degradation of unsaturated acids. C16 is the secondary C_{max} for these four groups, so without the suspected secondary production of C9, C16 would be the highest in each group. Concentrations of alkanolic acids for three composite groups, MxJuly, BorderSA and SSEOct, are shown as examples in figure 3.4. Error bars represent one standard deviation for the DCM extraction of alkanolic acids, equal to 28%.

Concentrations of Alkanoic Acids for MxJuly, BorderSA and SSEOct

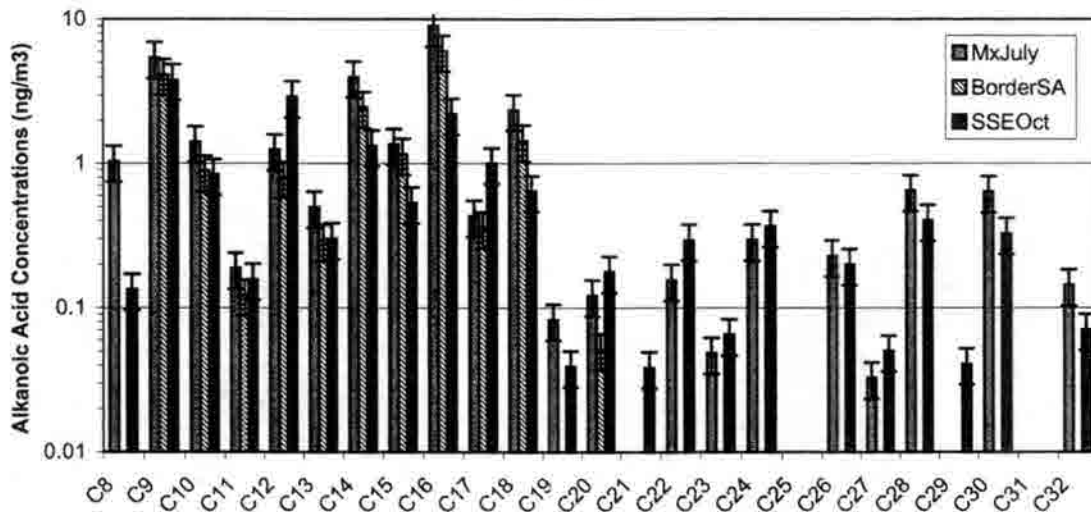


Figure 3.4 Concentrations of alkanoic acids in the sample groups MxJuly, BorderSA and SSEOct; error bars represent a 20.4% error (one standard deviation) for quantifying alkanoic acids with the DCM extraction method

3.2 Carbon Preference Indices

Alkane CPIs during BRAVO were generally below 2 and sometimes close to 1 (see Figure 3.5). During October, two sample groups featured CPIs that are significantly different than the previous ten samples at a 95% confidence level (ratios differ by more than the critical value of 1.35). The CPI values are 3.0 and 4.0 for these two samples, which suggests more biogenic influence during these periods. These groups also have much higher values for the plant wax (C26-C34) CPI. This may be due in part to seasonality with autumn foliage, but the main reason may be that the trajectories for the two October groups with higher CPIs are different from other groups. One group features advection from the north (NorthTexas1) and one group has air advecting from the south (SSEOct). These regions are not as populated or developed as those in southern Texas, which may lead to a larger relative biogenic contribution to the alkane concentrations in these October groups.

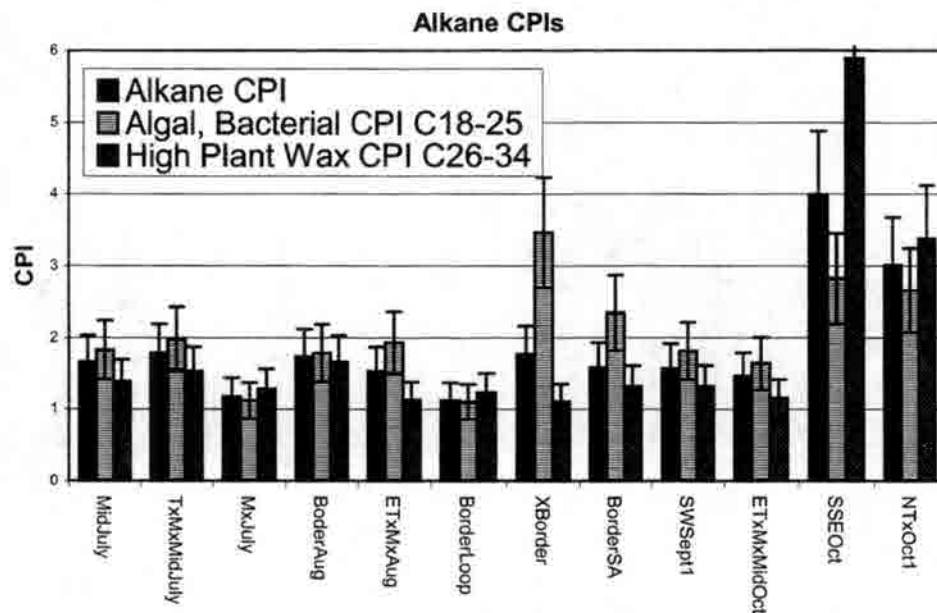


Figure 3.5 BRAVO groups' alkane CPIs; error bars represent one standard deviation, an average error in the alkane CPI calculation of 22.2%

Groups containing days with the highest OC concentrations, namely MxJuly (7/19, 7/20) and BorderLoop (8/31, 9/1), have the lowest alkane CPIs among all analyzed groups, suggesting that these days of high OC concentration are primarily influenced by anthropogenic sources. Interestingly, September 1st is also the day with the highest sulfate concentration, while August 31st is only the thirteenth highest and July 19 and 20 have lower than average sulfate concentrations.

The alkanolic acid CPIs appear to be more difficult to interpret. There are higher CPIs during the first and middle parts of the study, when the alkanes yielded low CPIs, as shown in figure 3.6.

Alkanoic Acid CPIs

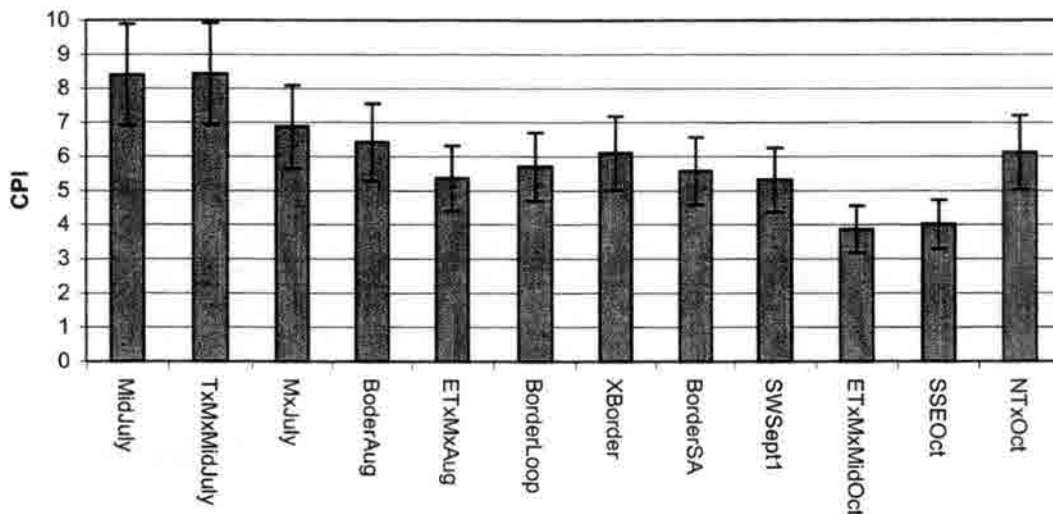


Figure 3.6 BRAVO groups' alkanoic acid CPIs; error bars represent a 17.7% error (one standard deviation) in calculating alkanoic acid CPIs with the DCM extraction method

Overall, the strong even:odd preference suggests that the alkanoic acids are mainly biogenic in origin, which is similar to other studies. As seen in table 1.1, previous studies found that in both urban and rural atmospheres, the alkanoic acids exhibit a strong biogenic influence (Mazurek and Simoneit, 1982; Simoneit, 1989), so this result is consistent with previous studies. Additionally, the alkanoic acids can be secondary products, which can further complicate interpretation of their CPI.

3.2.1 Plant Wax Influences on the n-Alkanes and n-Alkanoic Acids

Using equations formulated in section 1.5, the amount of odd number alkanes derived from plant wax was calculated for each BRAVO group. Contributions to the odd numbered alkanes (C25-C33) from plant wax ranged from 26% to 78%, as shown in figure 3.7. The two groups in October with advection from the north and from the south have the highest plant wax contributions, at 66% and 78%. The high plant wax influence during these periods is consistent

with the high alkane CPI results. These values were not found to be significantly different at a 95% confidence level, but were found to be different than previous samples at between 80%-90% confidence level (critical value of 37.4%). Groups with transport from eastern Texas and northeastern Mexico had smaller amounts of odd alkanes contributed from plant wax, which agrees well with the low CPIs found for these groups. Overall, the easterly to southeasterly advection patterns have a small contribution (< 50%) of plant wax influence, while air masses from the north, northwest and south-southeast have a higher proportion of plant wax influence.

Average % of odd n-alkanes C25-C33 derived from plant wax

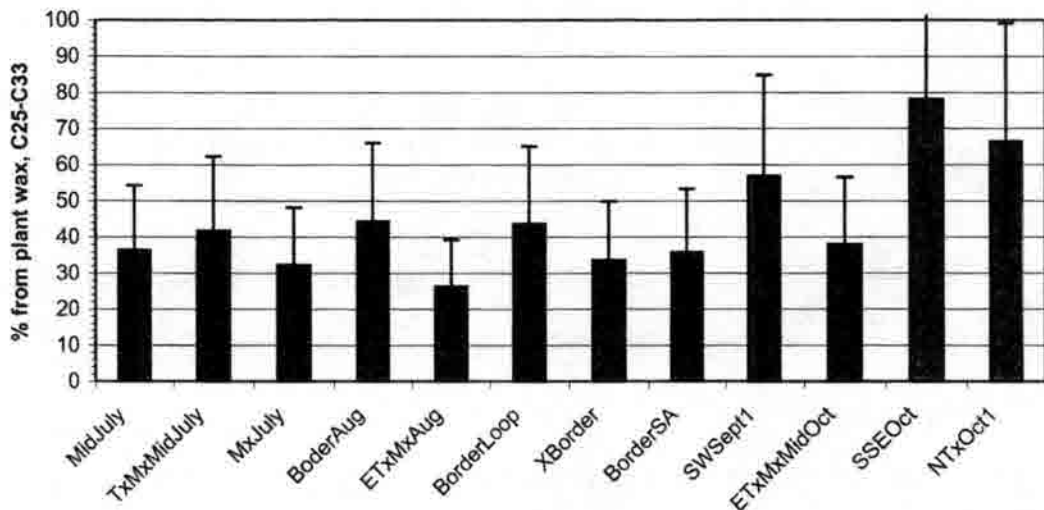


Figure 3.7 Average percentage contributions of odd n-alkanes (C25-C33) derived from plant wax; error bars represent an average 49.2% error (one standard deviation) for the plant wax percentage calculation

Contributions from plant wax emissions to the even numbered alkanolic acid concentrations, calculated similar to the alkanes, were high, ranging from 73% to 89%, detailed in figure 3.8. This suggests that plant wax emissions are the main contributor to the alkanolic acid concentrations, which agrees well with the high alkanolic acid CPIs. Both of these calculations suggest a large biogenic influence on the alkanolic acids found during BRAVO. However, since

alkanoic acids may also be secondary products, the plant wax influence calculated here might be an overestimation.

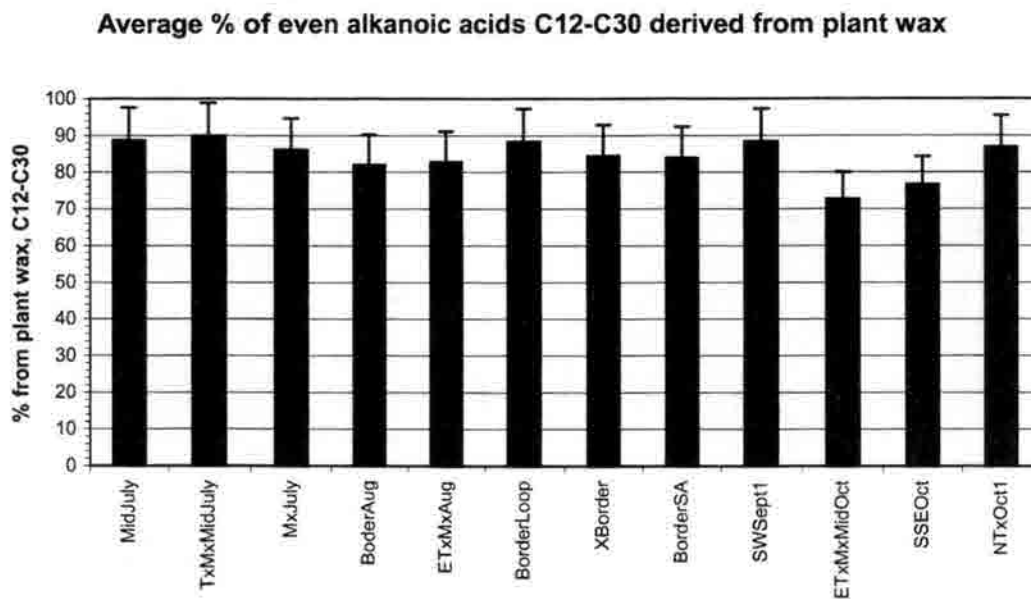


Figure 3.8 Average influence (%) of plant wax on even alkanolic acids (C12-C30) for BRAVO groups; error bars represent a 29.0% error (one standard deviation) for calculating alkanolic acid CPIs

3.3 PAH

In general, PAH were not found in abundance in BRAVO aerosol samples. Figure 3.9 shows the concentrations of PAH masses for each group (method described in section 1.7). Error bars represent one standard deviation of the DCM extraction method, equal to 15%. The lack of PAH may indicate that primary combustion emissions are not a significant contributor to the organic aerosol. However, the absence of benzo(a)pyrene (mass 252) indicates that the aerosol is somewhat aged. PAH may have been present at one time in the air masses, but atmospheric

processes during transport may have altered them to secondary products. The fact that PAH of m/z 202 is present in nearly every sample suggests that these may be longer lived than other PAH and that PAH from combustion was present at one time, but most species were altered or removed during transport.

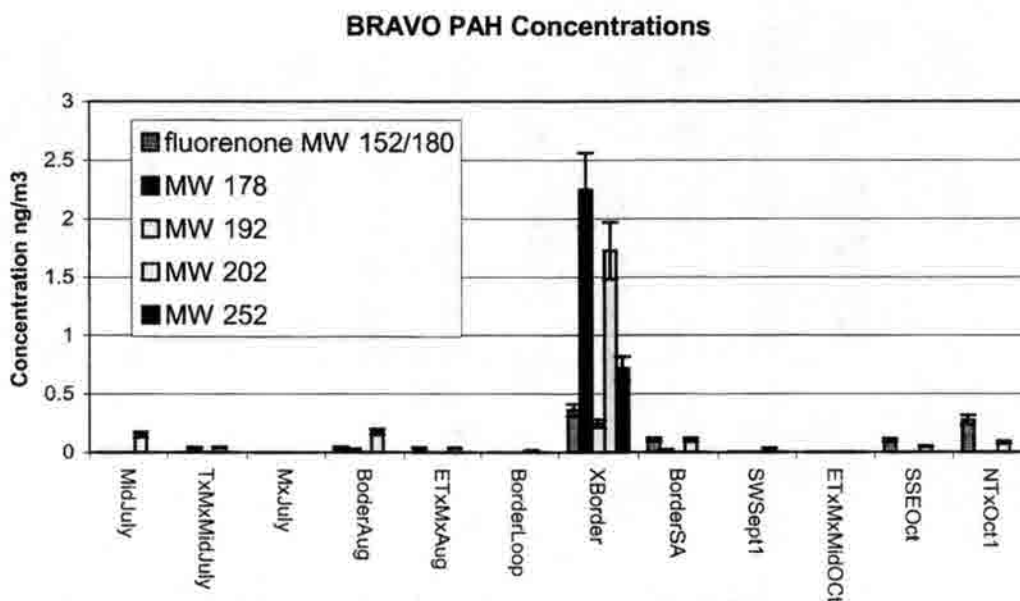


Figure 3.9 BRAVO groups' PAH concentrations, grouped by compound mass; error bars signify a 14.1% error (one standard deviation) in quantifying PAH with the DCM extraction method

One group, XBorder, consisting of samples from 8/25, 8/29, and 9/6-9/8, features higher PAH concentrations. This suggests that for this group, combustion emissions were present and relatively fresh. Interestingly, this group of trajectories is not unique for the time period, advecting along the Texas-Mexico border and not significantly faster than other groups. Levoglucosan is also present in this group (discussed further in sections 3.5 and 3.6), but not in others, suggesting that this group may have included aerosol from biomass burning. This could be the source of the PAH, though anthropogenic sources may have contributed as well.

3.4 n-Alkanoic Diacids and C18 Ratio

Alkanoic diacids were found during BRAVO, but not in abundance, with concentrations averaging 1 ng/m³; figure 3.10 displays these results. Since low PAH concentrations suggest primary combustion emissions are only minor contributors to the observed PM_{2.5} OC, one might expect secondary organic aerosol species, including diacids, to be relatively important contributors. Although the low concentrations of diacids observed runs contrary to this hypothesis, this may reflect removal of these soluble species by precipitation upwind of the park. The low concentrations of diacids are similar to results from a rural study in Crete (Gogou et al., 1996), where concentrations were less than 6 ng/m³, again suggesting that diacids may be effectively removed during transport.

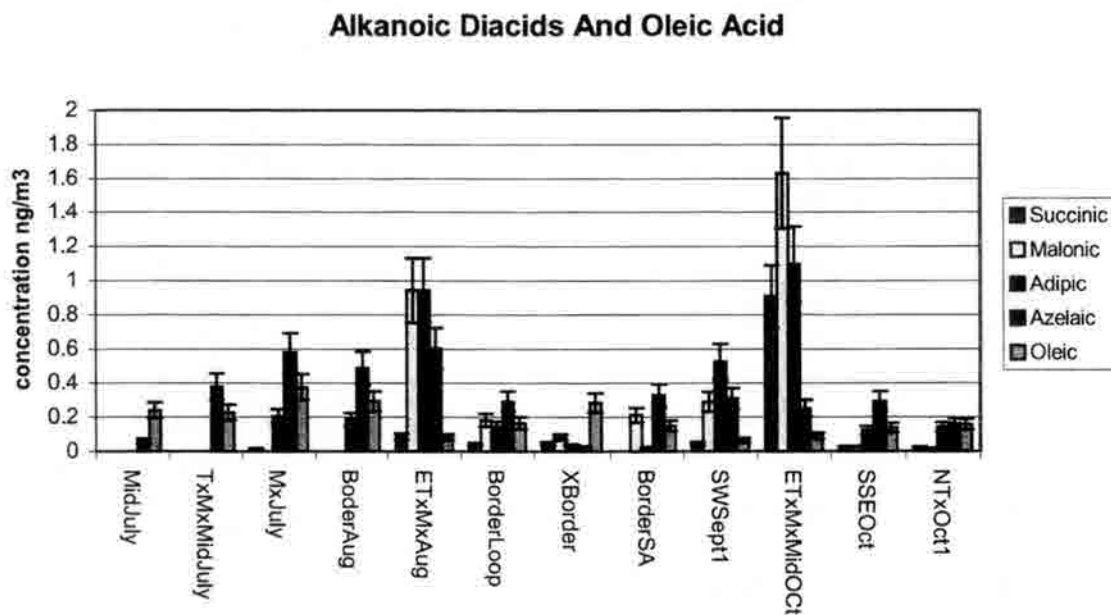


Figure 3.10 BRAVO groups' concentrations of alkanolic diacids and oleic acid; error bars represent a 20.4% error (one standard deviation) for alkanolic acids with the DCM extraction method

The ratio between the saturated C18 acid and the mono-unsaturated C18 acid (oleic acid) can be used to gauge the age of aerosol. Figure 3.11 shows that during BRAVO, the average ratio was 6.6, varying between 5 and 11.

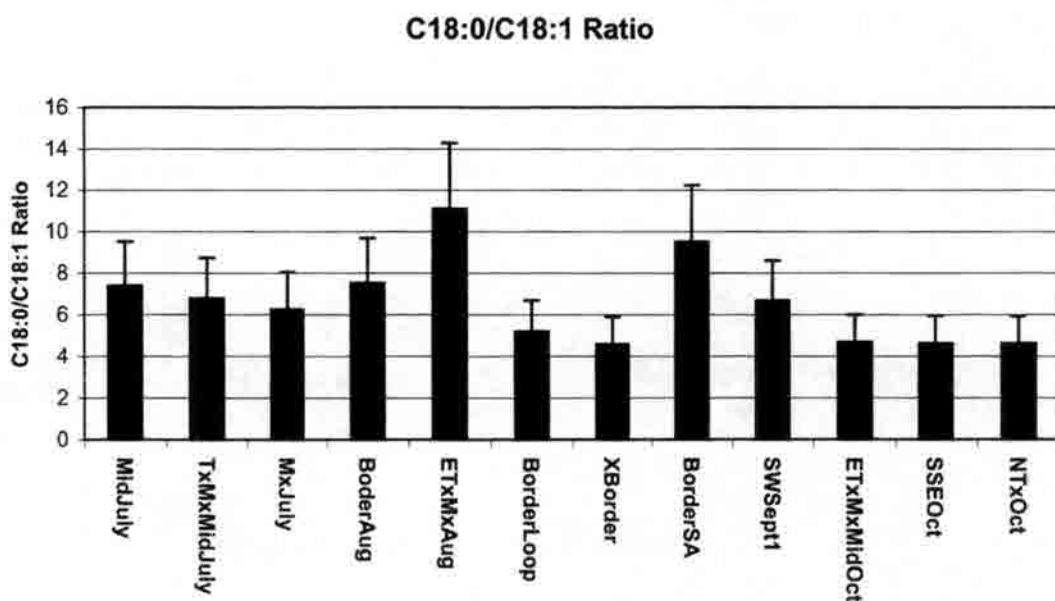


Figure 3.11 BRAVO groups' C18:0 / C18:1 ratios; error bars represent a 28.8% error (one standard deviation) in calculating this ratio

Overall, this ratio indicates that the aerosol during BRAVO was aged and subject to more decomposition than found in urban environments (see table 1.4). The BRAVO ratios are similar to those found in the rural mountains of California. These high, rural-like ratios may reflect a combination of local rural biogenic emissions and aged aerosol that advected from an urban area. The two groups with highest ratios (9.5 and 11) are not clearly explained based on their air mass patterns. Neither of these groups are unique in trajectory direction or speed, but they do have high average temperatures (third highest and highest overall), which may have accelerated the reaction. Figure 3.12 shows there is a modest correlation ($r^2=.54$) between the C18 ratio and the average temperature, with the higher ratios found during periods with higher temperatures. This

may indicate that days of higher temperature had aerosol that was more “aged” and altered than lower temperature days, perhaps reflecting faster decomposition during warmer periods.

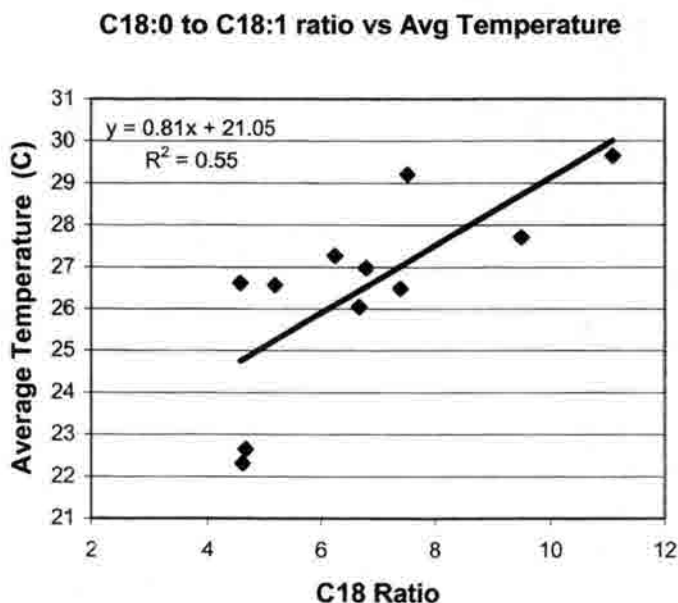


Figure 3.12 Graph of average temperature and C18 ratio for BRAVO groups

Additionally, there is a large amount of C9 acid in every sample, with an average of 22% of the total acid being C9 (see figure 3.13). While there is no strong correlation ($r^2=0.06$) between the C18 ratio and C9 acid concentration (see figure 3.14) the large amounts of C9 acid may reflect breakdown of the oleic acid, again indicating that the aerosol was subject to atmospheric aging processes.

% C9 of total alkanolic acid

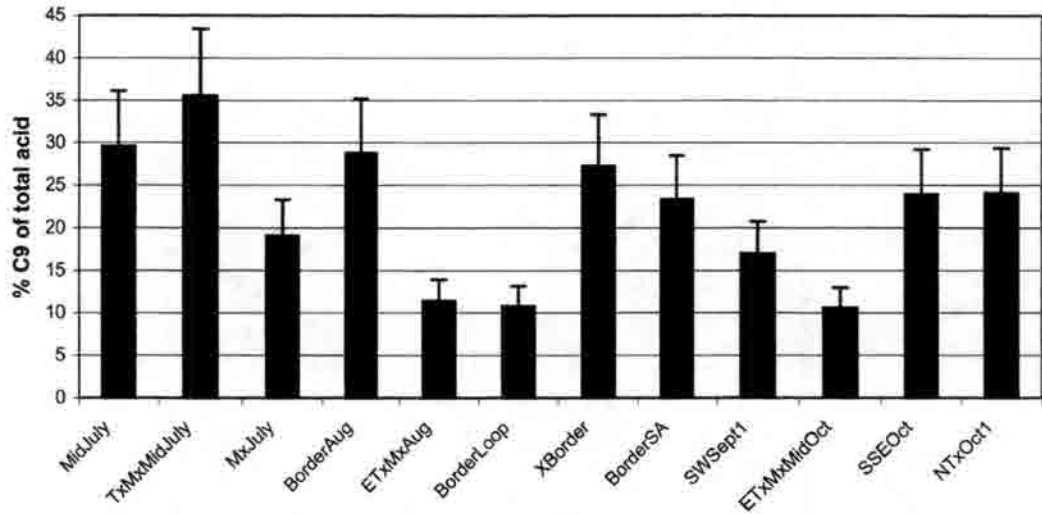


Figure 3.13 Percentage of total alkanolic acid that is C9 acid; error bars represent a 22.2% error (one standard deviation) in calculating this ratio.

C18 ratio vs C9 acid concentration

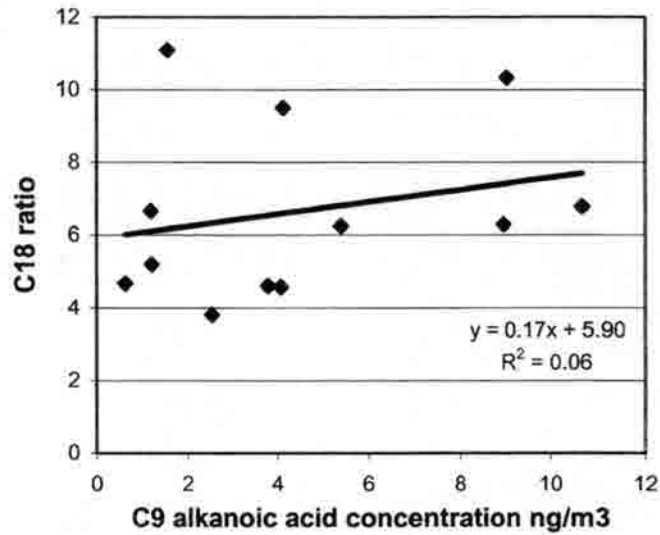


Figure 3.14 C18 ratio vs. C9 alkanolic acid concentration (ng/m³).

3.5 Tracers: Maximum Influences of Sources

3.5.1 Source contribution estimates from tracer concentrations

The composites of samples collected during BRAVO generally contained concentrations of molecular tracers at or below their detection limits, precluding a quantitative source apportionment. Maximum source contributions were estimated by assuming a source tracer concentration equal to the detection limit of the species.

Figure 3.15 presents maximum influences calculated for vehicles, meat cooking and wood smoke. Levoglucosan, the main molecular marker used for wood smoke, was detected in only one sample, XBorder. Other sugar anhydrides, galactosan and mannosan, were also found in this group. Since this is also the only group with many PAH present, the combination of all these factors indicates wood smoke was present in this group. Using equations provided earlier in sections 1.8 and 1.9, it was estimated from the levoglucosan concentration that wood smoke contributed 1% of the total OC present in this group. The detection limit for levoglucosan was used as the maximum possible concentration of levoglucosan for the other groups. Using this detection limit, maximum wood smoke contributions to OC were estimated to range from 0.06% to 0.12 %. Overall, primary fine aerosol emissions from wood smoke do not appear to be a significant contributor to BRAVO PM_{2.5} OC.

Hopanes and cholestanes were not found in any group, so maximum influences for vehicular exhaust were determined using the detection limits. Maximum OC contributions, based on the detection limit for 17 α 21 β -hopane and equations discussed in sections 2.6, were found to be between 0.7% and 4.3%, with an average of 1.8%. This minimal amount of vehicle exhaust influence is similar to results from the Grand Canyon, where little evidence of vehicle exhaust was found (Mazurek et al., 1997).

Cholesterol, the meat smoke tracer, was not found in any BRAVO samples. The detection limit was used to estimate maximum possible meat cooking contributions to observed

OC concentrations. The ratio of OC/cholesterol is similar to that of OC/hopanes, yet calculated meat smoke contributions are much higher than vehicular exhaust. This is because the detection limit for cholesterol is higher than detection limits for other species, resulting in much larger upper bound contribution estimates. Maximum possible contributions from meat smoke were estimated to range from 4.8% to 19.9%, with an average maximum contribution of 12.9%.

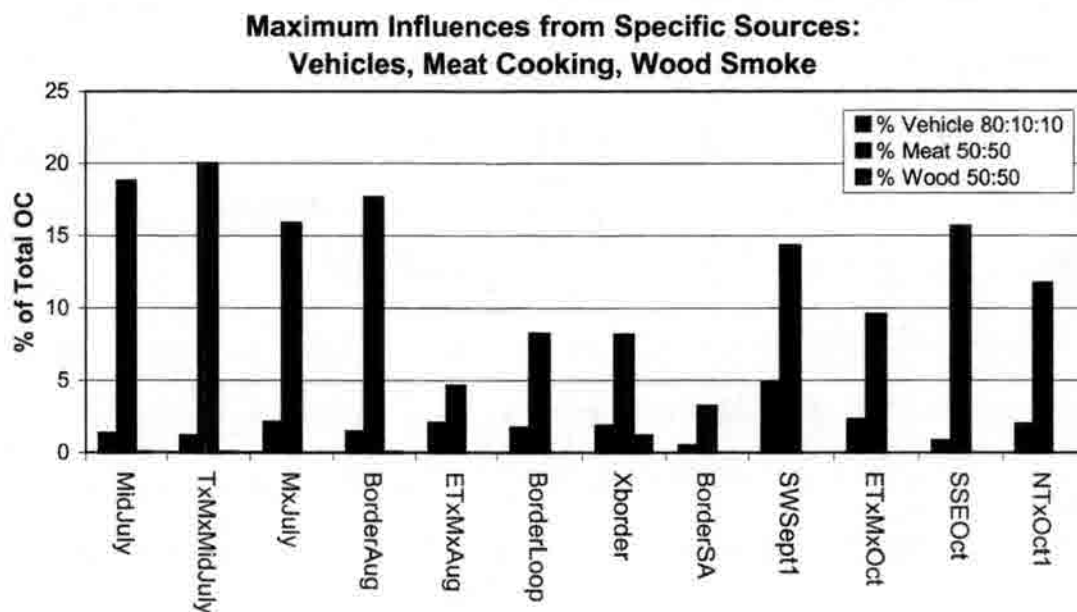


Figure 3.15 Maximum estimated influences for BRAVO groups for vehicular exhaust, meat cooking and wood smoke: using Rogge (1993) for autos and Schauer (1999) for diesel, Rogge (1991) for meat cooking, and Nolte (2001) for wood smoke.

3.5.2 Sensitivity Analysis of Source Influences

In atmospheric aerosol the ratio of source type contributions, such as the catalyst to noncatalyst to diesel ratio for vehicular exhaust, is not known. A sensitivity analysis was carried out for vehicular exhaust, meat smoke, and wood smoke to explore the impact that changing the ratios between different sources of these emissions would have.

Using hopane concentrations, maximum contributions from vehicular exhaust were calculated using a variety of ratios between catalyst, non-catalyst autos and diesel truck emissions, based on the source profiles from Rogge et al. (1993). Varying between ratios (catalyst:non-catalyst:diesel) of 80:10:10, 70:20:10, 70:10:20, 70:15:15, and 50:25:25, it was found that there is only a 14.5% difference in source contribution estimates between the lowest value (at 80:10:10) and the highest value (at 50:25:25). This translates to a range of 0.4% to 4.4% influence of vehicular exhaust on OC for the 80:10:10 ratio to a range of 0.5% to 5.1% for the 50:25:25 ratio. Results are shown in figure 3.16.

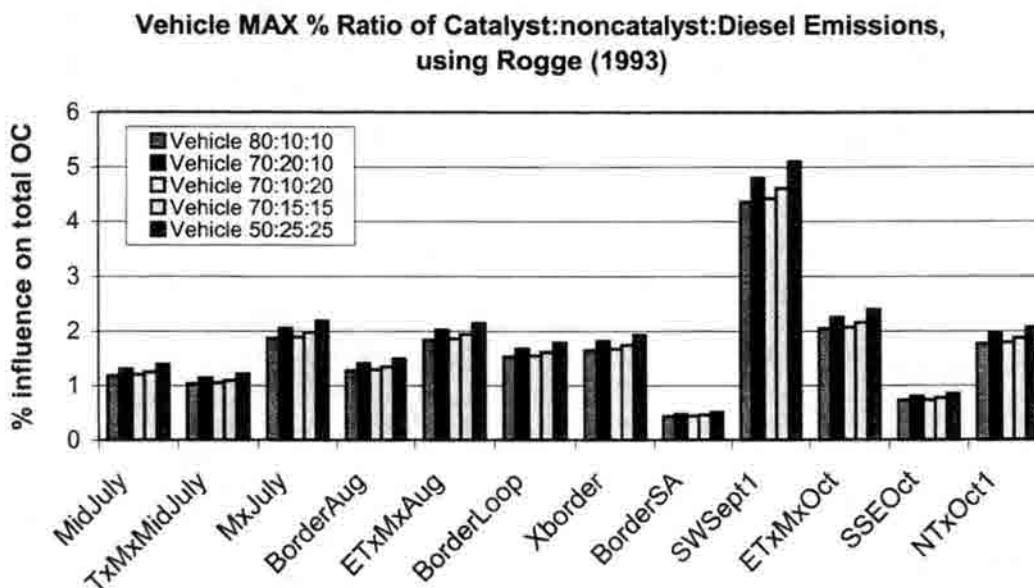


Figure 3.16 Sensitivity study using for vehicular exhaust using Rogge et al. (1993): varying the ratio between catalyst, non-catalyst and diesel emissions

There is also another source profile for diesel trucks from Schauer et al. (1999) that can be used in conjunction with the Rogge et al. (1993) profiles for catalyst and non-catalyst autos. When using this profile for the diesel truck influence, in conjunction with Rogge et al. (1993) for catalyst and non-catalyst autos, there is an increase of 14.8% from the Rogge et al. source profile calculations. This translates to values of 0.5% to 4.9% for maximum vehicle influence on total

OC (for 80:10:10) to 0.6% to 6.4% (for 50:25:25), where the difference between these fleet compositions is now 23.9%. The results of using the Schauer et al. (1999) diesel profile are shown in figure 3.17.

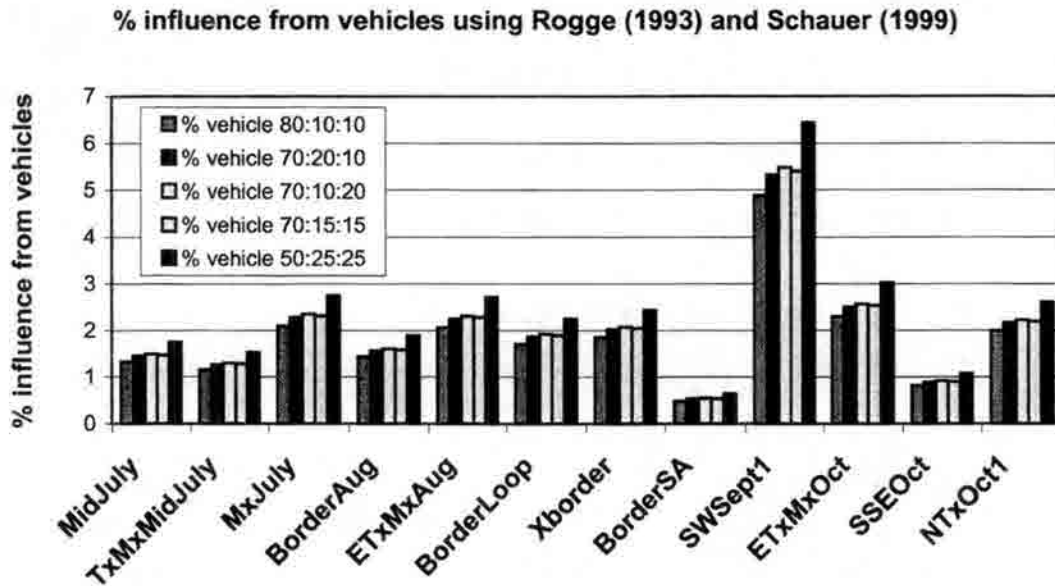


Figure 3.17 Sensitivity analysis of vehicular exhaust influence using Rogge et al. (1993) for auto and Schauer et al. (1999) for diesel emissions

Similar to the vehicles, a sensitivity analysis for meat cooking was done, varying the ratio between charbroiling and frying meat, from 75:25 to 25:75. Here there is a greater variation between these ratios, with a difference of 43% between them. The ratio with 75:25 charbroiling:frying gave the highest contribution limits. Overall, higher amounts of charbroiling increase the calculated meat smoke upper contribution limits. These results are presented in figure 3.18.

Comparison of Ratios for Meat Cooking using Rogge (1991)

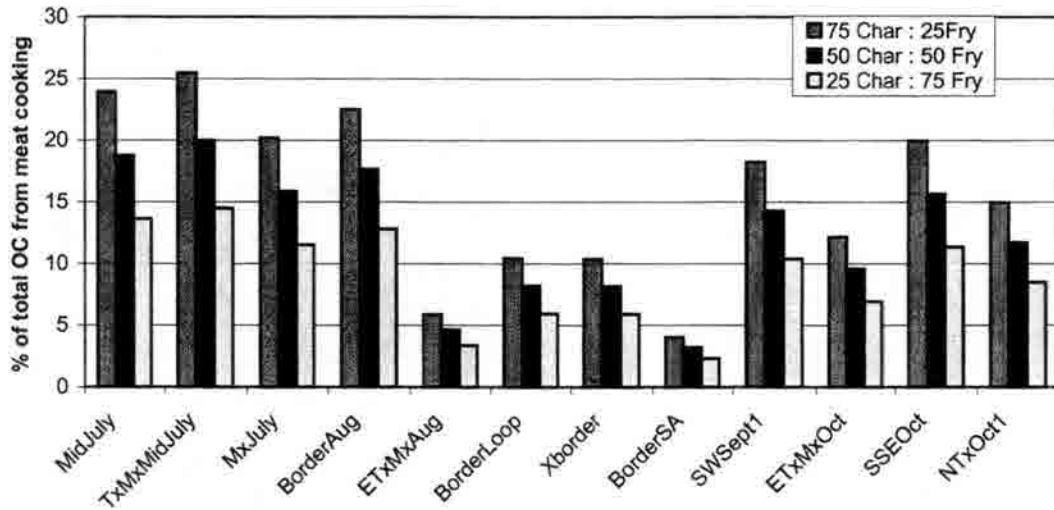


Figure 3.18 Sensitivity analysis for meat cooking: varying the ratio of charbroiling:frying meat

Wood smoke ratios were also analyzed for sensitivity between pine and oak smoke using source profiles from Nolte et al. (2001). It was found that there is a difference of 27% in contribution estimates between the ratios of 75:25 (pine:oak) and 25:75 (pine:oak). However, the wood smoke influence based on levoglucosan was less than 1.5% regardless of the ratio used. The results are shown in figure 3.19.

Wood Smoke Influence based on Levoglucosan

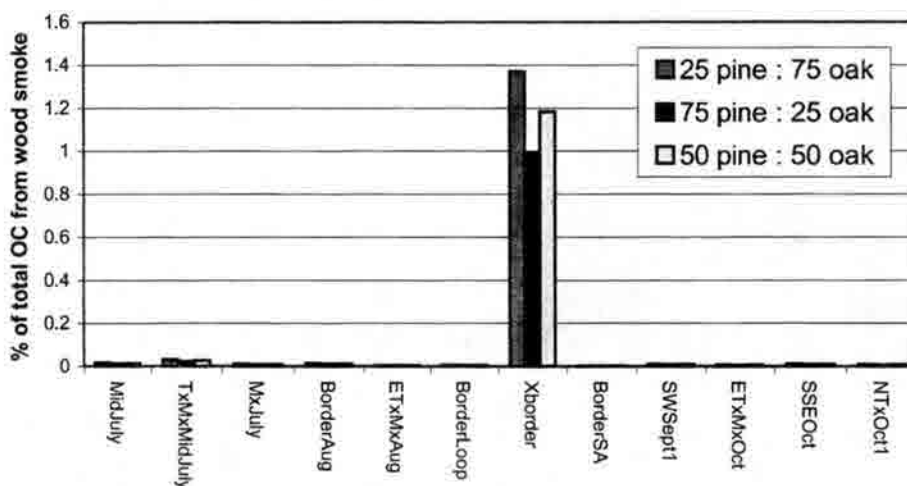


Figure 3.19 Sensitivity analysis for wood smoke: varying the ratio between pine and oak smoke

3.6 Tracers: Other Wood Smoke Markers

Despite finding levoglucosan in only one sample, other wood smoke markers were evident in many samples. Figure 3.20 presents the concentrations of the various wood smoke markers found in each BRAVO group.

4-Ethylguaiacol was found in every sample and vanillin was found in almost every sample, while neither was evident in the blank filter extracts. 4-Ethylguaiacol is emitted from both softwood and hardwood combustion, while vanillin comes mainly from softwood combustion (Hawthorne et al., 1988, 1989, 1992; Edye and Richards, 1991; Sagebiel and Seiber, 1993; Simoneit et al., 1993; Rogge et al., 1998; Oros et al., 1999b; McDonald et al., 2000; Nolte et al., 2001; Schauer et al., 2001; Fine et al., 2001). Retene, another softwood combustion product (Ramdahl, 1983; Oros et al., 1999b), is found only in three BRAVO groups.

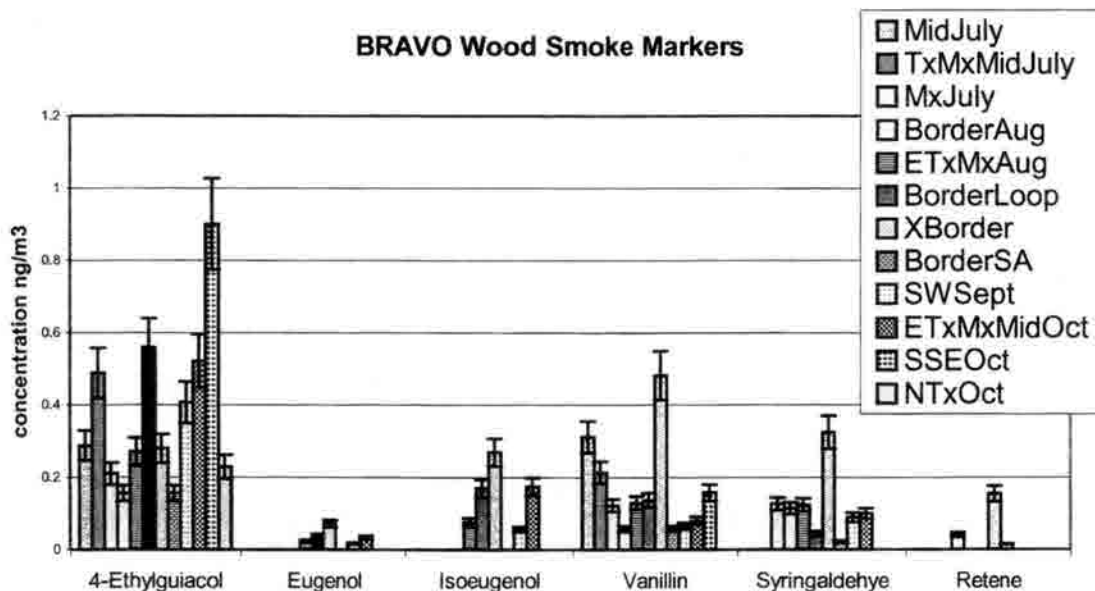


Figure 3.20 BRAVO groups' concentrations of wood smoke markers; error bars represent a 14.1% error (one standard deviation) in quantifying PAH

The presence of other wood smoke markers without levoglucosan, as found in samples other than XBorder, is peculiar, since levoglucosan is proposed as a long-lived compound and therefore the best tracer for wood smoke (Fraser and Lakshmanan, 2000). It is also emitted at much higher concentrations than other wood smoke tracers detected in many BRAVO sample groups (Fine et al., 2001; Schauer et al., 2001). Other compounds emitted in wood smoke have been suggested as tracers, though long-term stability for these compounds is still undetermined. These include retene (Ramdahl, 1983) and phenolic lignin derivatives like guiacols (4-ethylguaiacol, eugenol, vanillin) for softwood combustion, and syringols (syringaldehyde) for hardwood combustion (Nolte et al., 2001). Using alternative tracers for both wood smoke and vehicular exhaust is explored further in section 3.7.

Acid-catalyzed hydrolysis (Kops and Spanggaard, 1972; Penczek et al., 1985) in acidic cloud drops (Fraser and Lakshmanan, 2000) has been proposed as a selective removal mechanism for levoglucosan (see figure 3.21). This reaction may not affect many other wood smoke tracers and could explain the lack of levoglucosan in most sample groups. Separate CSU studies of

BRAVO fine aerosol composition revealed the presence of considerable aerosol acidity along with excess gaseous nitric acid, both factors that could strongly acidify clouds formed in the region, creating conditions conducive to possible destruction of levoglucosan.

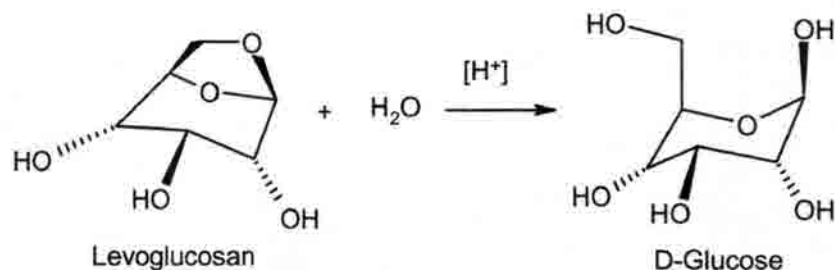


Figure 3.21 Acid-catalyzed hydrolysis of levoglucosan in acidic cloud drops

3.7 Estimated Source Contributions from Consideration of Alternative Tracers

3.7.1 Calculations Using Vanillin as a Source Tracer for Wood Smoke

The commonly used source specific tracers, such as hopanes, cholesterol and levoglucosan, were generally not found in the BRAVO group samples (sections 3.5 and 3.6). This may be due to many reasons, including degradation or loss by precipitation and cloud scavenging in transport. Vanillin is an emission product of wood combustion, and though it is found in greater concentrations from softwood combustion (Rogge et al., 1998; Nolte et al., 2001), it is also found in hardwood combustion aerosol. Vanillin was detected in eleven of twelve BRAVO groups. This raises the possibility of using vanillin as a molecular tracer for wood smoke. Additionally, elemental carbon comes only from combustion (discussed in section 1.13), and can be used to estimate a maximum influence from vehicles, similar to the use of hopanes.

Similar to finding the percentage influence from wood smoke using levoglucosan as a molecular tracer (section 1.9), vanillin was used to calculate the contribution to total OC from wood smoke. Data published by Schauer et al. (2001) were used as the source profile for pine and oak wood smoke, and ratios between the concentration of vanillin and total OC from these source samples were found. Figure 3.22 shows the calculated OC contribution from wood smoke, using vanillin as a tracer, for each BRAVO group. In all samples but NTxOct1, the actual vanillin concentration was used; in this last group, the detection limit of vanillin was used.

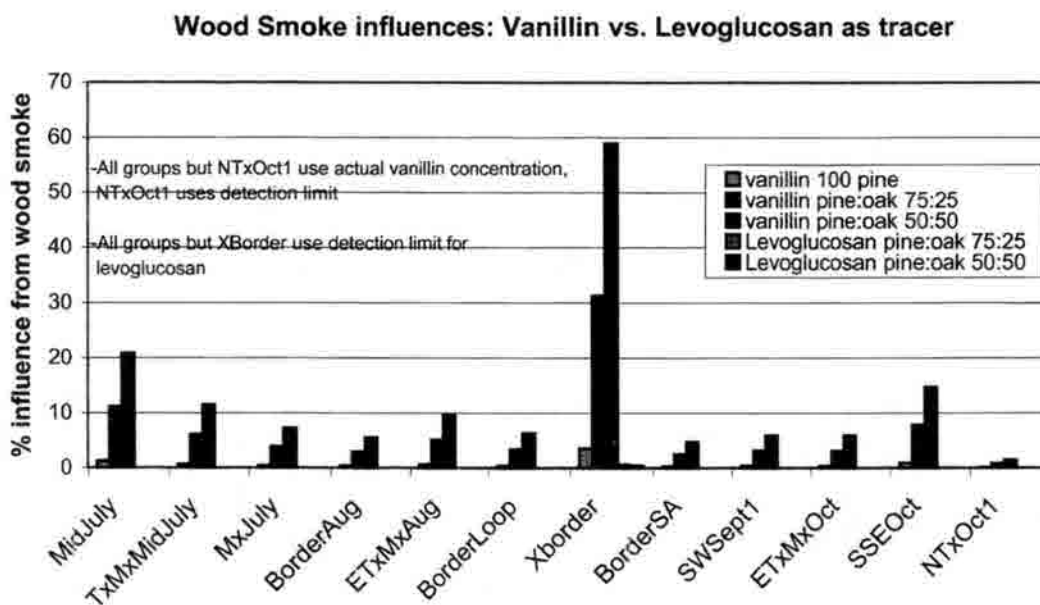


Figure 3.22 Influence of wood smoke (%) on total OC: comparison of using vanillin versus levoglucosan as tracer using source profiles from Schauer et al. (2001)

Using vanillin as the tracer for wood smoke apportionment, possible wood smoke influence increases by up to three orders of magnitude, ranging from 1.4% to 59%. Wood smoke influence is very sensitive to the assumed wood mix; an increase in oak from 25% to 50% nearly doubles the estimation of wood smoke contributions. With such a wide range of influence calculated from levoglucosan and vanillin, it is difficult to identify which is the most accurate.

3.7.2 Calculations of Vehicle Influence Using EC as a Source Tracer

Since elemental carbon is generated only from combustion, it can be used as a crude combustion tracer. If all EC is assumed to come from vehicle exhaust, then the maximum possible impact of vehicular exhaust on the BRAVO samples can be estimated. This is done by using the OC/EC ratios of the BRAVO samples, and the OC/EC ratios from catalyst equipped automobiles, non-catalyst equipped automobiles, and diesel trucks, using the source profiles from Rogge et al. (1993a) and Schauer et al. (1999). For an 80:10:10 ratio, the maximum vehicular influence would be:

$$\text{Max vehicle influence \%} = 100 * [(.8 * \text{OC/EC}_{\text{source-catalyst}} * \text{EC}_{\text{sample}}) + (.1 * \text{OC/EC}_{\text{source-noncatalyst}} * \text{EC}_{\text{sample}}) + (.1 * \text{OC/EC}_{\text{source-diesel}} * \text{EC}_{\text{sample}})] / \text{OC}_{\text{sample}} \quad (3.1)$$

Figure 3.23 shows the calculated maximum influence from vehicular exhaust using EC, with amounts of each of the three sources (catalyst, non-catalyst, diesel) varied. Using EC as a tracer for vehicular emissions, calculated influence on the OC from vehicles ranges from 18% to 76%, using a ratio of 80:10:10 (catalyst:noncatalyst:diesel). There is some sensitivity of these percentages to the chosen ratio, mainly influenced by the amount of noncatalyst-equipped autos in the ratio. A 26% increase in values from the 80:10:10 ratio to the 50:25:25 ratio is found using EC.

% Vehicular Influence, derived from EC, using Rogge et al (1993)
 OC/EC for autos, Schauer et al (1999) for deisel
 (Ratio of catalyst equipped auto:noncatalyst auto:deisel)

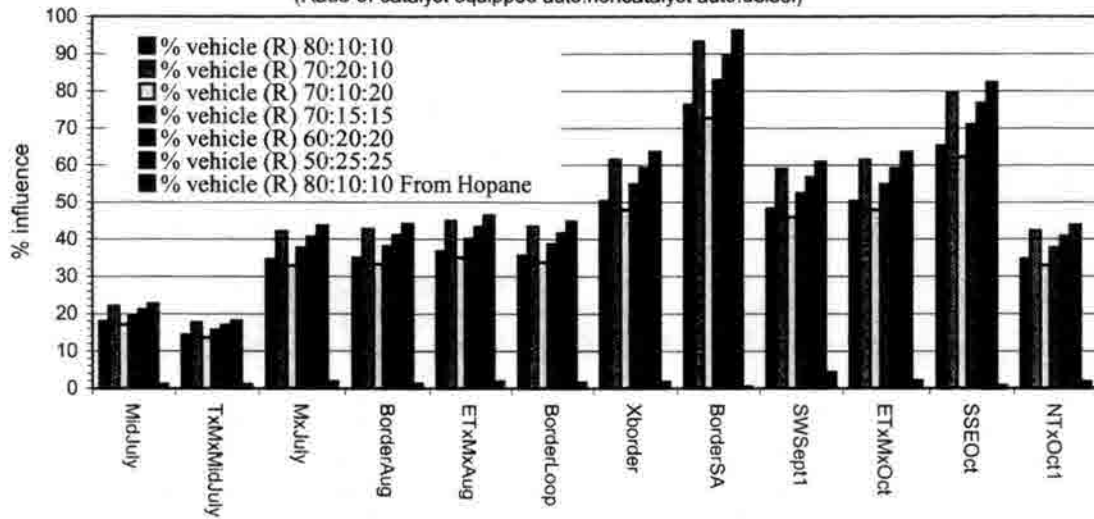


Figure 3.23 Maximum influence on the BRAVO OC from vehicles, based on EC

The values generated using EC as a vehicle emission tracer are an order of magnitude higher than the values found using hopanes as the source tracer. Atmospheric processes may alter hopanes during transport from source regions, and therefore its concentrations may decrease between to detection limit levels by the time it reaches Big Bend. The estimate assuming all EC is from vehicles gives an alternative upper bound to possible vehicle contributions to the OC, although the upper bound may be far too high if other combustion sources are significant contributors to the observed EC.

3.8 Tracers: Other Compounds

3.8.1 Secondary Biogenic Aerosol

6,10,14-trimethylpentadecan-2-one was ubiquitous during the study, as seen in figures 3.24 and 3.25, and could provide further insight into the biogenic impact on PM_{2.5} OC during BRAVO.

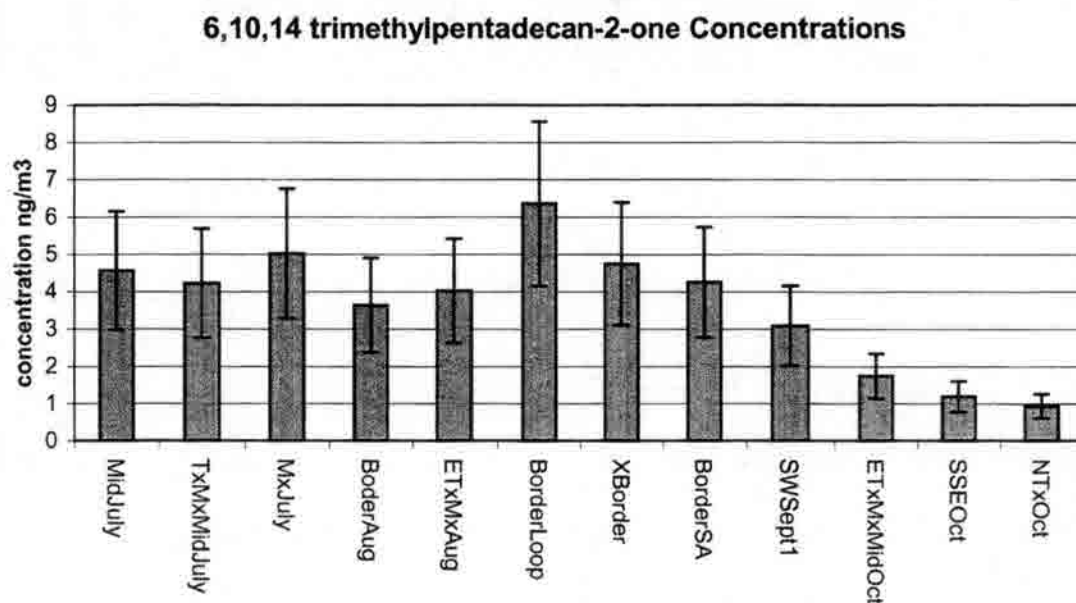


Figure 3.24 BRAVO groups' 6,10,14-trimethylpentadecan-2-one concentrations; error bars represent a 34.6% error (one standard deviation) in quantifying alkanes with the DCM method

Variation in the concentration of 6,10,14 trimethylpentadecan-2-one indicates secondary aerosol from biomass degradation is present in different amounts throughout the study. The concentration decrease in October suggests secondary biogenic particles are becoming less significant in these two samples, perhaps reflecting a seasonal change or a different composition with advection from the north and south during these sample periods. These two October samples also have much higher alkane CPIs, which may indicate that an increase in primary biogenic emissions may be related to a decrease in secondary biogenics, though this needs to be

studied further. These last two samples were found to be statistically different at an 80% or higher confidence level (critical value of 2.62) from all but ETxMxOct, which also had a low concentration of this species.

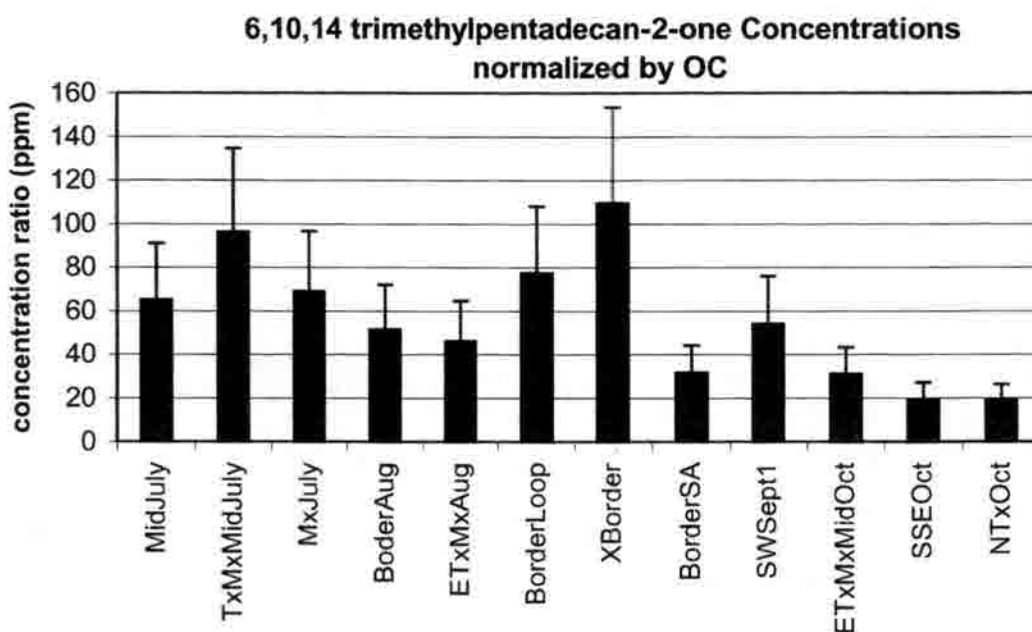


Figure 3.25 BRAVO groups' concentrations of 6,10,14 trimethylpentadecan-2-one normalized by OC in ppm; error bars represent a 40% error in this calculation (one standard deviation)

Concentrations of 6,10,14 trimethylpentadecan-2-one normalized by the total OC for each sample are shown in figure 3.25. There is much more variation between samples compared to the non-normalized graph, though the later samples still have the lowest concentration ratios (ppm). This increased variation suggests caution in reaching conclusions based on figure 3.24.

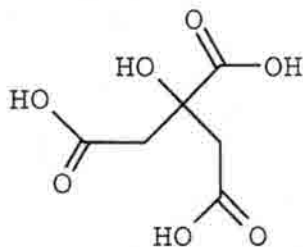
3.8.2 Coal and Fossil Fuel Markers

Pristane and phytane, tracers of petroleum and fossil fuel combustion (such as coal) were not found in the BRAVO aerosol. Picenes, proposed coal use tracers, were not found either. The lack of these tracers indicates that primary emissions of fossil fuel combustion were not a significant fraction of the organic aerosol. This seems to be consistent with the lack of hopanes,

which can be emitted from both vehicles and coal utilization. It is possible, however, that these compounds were altered into secondary products by reaction during transport.

3.8.3 Citric Acid

Citric acid was ubiquitous during the study. Its structure is shown in figure 3.26, and concentrations for each BRAVO composite in figure 3.27. The origin of this compound is unknown, as there is not a large presence of citrus fruit trees in Texas (Wiedmeyer, 1999, personal communication, 2001) from which the citric acid could originate. It may be a primary emission from local sources in or near Big Bend N. P., or could possibly be a secondary oxidative product from higher compounds. This latter possibility is intriguing since there were low concentrations of diacids, yet this triacid is present, perhaps as a further degradation product from higher order compounds. Another distinct possibility is from contamination from work in the vicinity of the quartz fiber filters with ammonia denuders, where citric acid is used as a coating solution, though the absence of it in field blanks casts uncertainty on this.



citric acid

Figure 3.26 Structure of citric acid

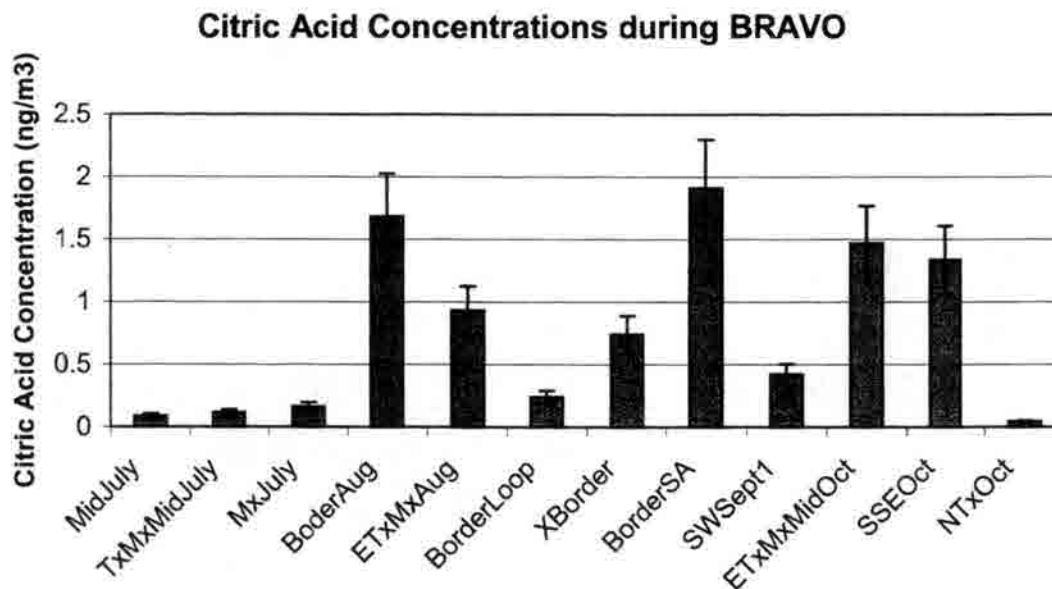


Figure 3.27 Citric acid concentrations during BRAVO; error bars represent a 20.4% error (one standard deviation) in quantifying acids with the DCM extraction method

3.9 Secondary Organic Aerosol Estimations

Amounts of secondary organic aerosol have been calculated in previous studies based on a minimum OC/EC ratio (see table 3.2). Secondary organic carbon, as a percentage of total OC, was calculated for the BRAVO sample groups, using equations presented in section 1.12. The OC/EC ratio used for this estimation (1.95) was the average ratio during winter (IMPROVE December through February data in 1988-1998) at Big Bend N. P. Using this baseline OC/EC ratio, secondary organic carbon was calculated to contribute between 45% and 90% of the total OC during the study, as shown in figure 3.28. While there is a relatively wide range of values, none of these values are significantly different from each other at a 95% confidence level (critical value of 91%).

Secondary OC %, OC/EC min = 1.95
 (average of OC/EC during Dec-Feb 1988-1998, BBNP)

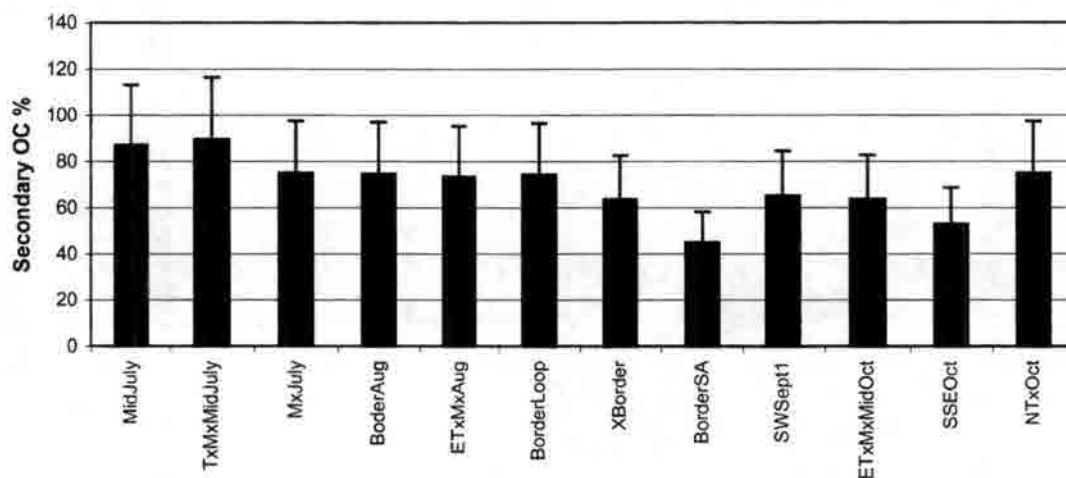


Figure 3.28 Percentage of OC that is secondary during BRAVO, assuming an $OC/EC_{min} = 1.95$ (average winter (Dec-Feb, 1988-1998) ratio at BBNP); error bars represent a 30.5% error (one standard deviation) for this calculation

The high percentage of secondary OC is larger than typically found in urban environments (Turpin et al., 1991a; Castro et al., 1999; Lin et al., 2001), but similar to observations in rural areas, especially in the summer (Castro et al., 1999). Table 3.2 lists the estimated secondary organic carbon percentages from previous studies, and the correlation of these values with EC concentration where reported. Higher percentages of secondary OC at rural sites are attributed to more photochemical oxidation during transport to rural sites. Overall, the large amount of estimated secondary organic carbon during BRAVO agrees with other qualitative secondary OC indicators that suggest a large amount of secondary aerosol formation.

Table 3.2 Listing of Secondary OC % and correlation between EC concentration and Secondary OC

Location	Secondary OC %	r ² between EC and OC _{sec}	Reference
Los Angeles (summer)	40%-80%	N/A	Turpin et al. 1991a
Birmingham, UK (urban winter)	17%	0.11	Castro et al. 1999
Taiwan (urban winter)	40%	N/A	Lin et al. 2001
Oporto, Portugal (urban summer)	47%	0.38	Castro et al. 1999
Areao, Portugal (rural winter)	45%	0.83	Castro et al. 1999
Areao, Portugal (rural summer)	78%	0.96	Castro et al. 1999

There is a fairly high correlation between the percentage of secondary organic carbon and both the OC/EC ratios and EC concentration (ng/m³) during BRAVO. This is shown in figures 3.29 and 3.30.

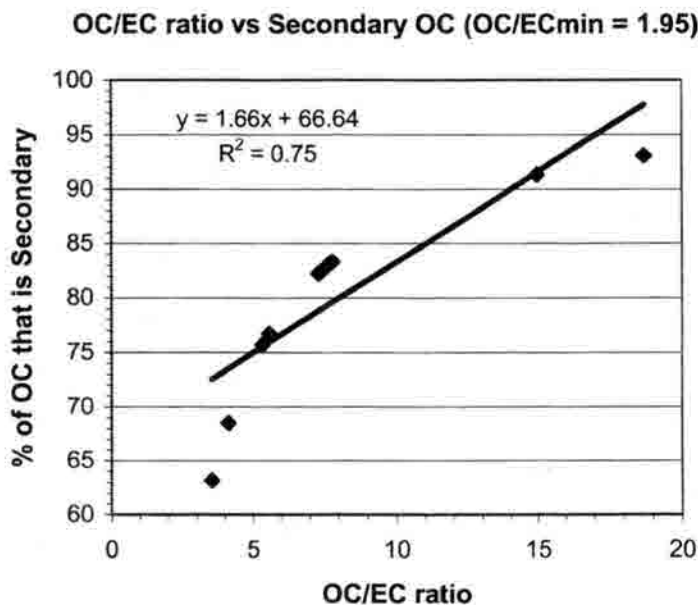


Figure 3.29 Secondary OC Percentage vs. OC/EC ratio for BRAVO groups, assuming a primary OC/EC ratio of 1.95 (average winter ratio at BBNP)

EC Concentration vs Secondary OC (OC/Ecmin = 1.95)

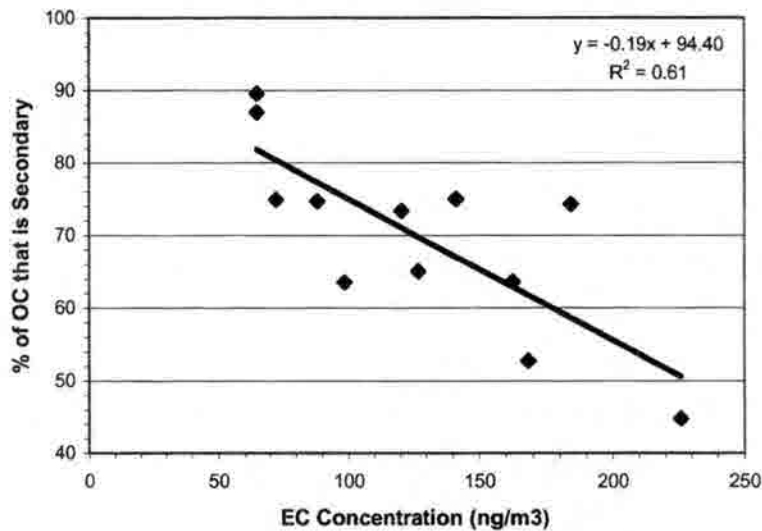


Figure 3.30 EC concentration vs. secondary OC percentage, using an OC/EC ratio of 1.95 (average winter ratio at BBNP)

The correlations between secondary OC and both EC concentration ($r^2=0.61$) and OC/EC ratios ($r^2=0.75$) are similar to the high correlations found in rural areas in European atmospheres (Castro et al., 1999). The urban sites in Castro et al. (1999) have lower secondary organic carbon percentages, as well as a low correlation between secondary OC and EC concentration. The high correlations in rural areas are attributed to increased gas/particle conversion from volatile organic compounds (VOC) and photochemical oxidation over a long transport period (Castro et al., 1999). Similar processes are probably also important during BRAVO.

There is no strong correlation between the percentage of estimated secondary organic carbon and other possible secondary OC indicators, such as the C18 ratio or normalized 6,10,14-trimethyl pentadecan-2-one concentrations. Figures 3.31 and 3.32 compare these values with the secondary organic aerosol percentages for BRAVO; 6,10,14-trimethylpentadecan-2-one is plotted as its concentration divided by the total OC.

% of Secondary OC (oc/ec=1.95) vs 6,10,14trimethyl pentadecan-2-one/OC

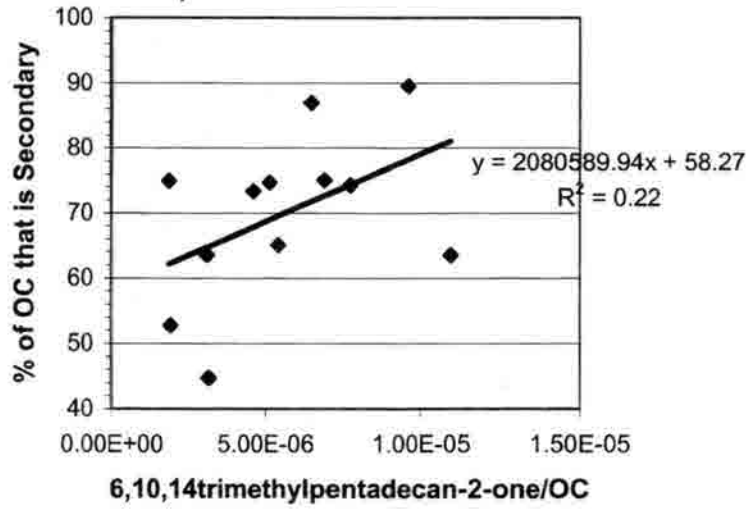


Figure 3.31 Graph of Estimated Secondary OC % (OC/EC=1.95) vs. 6,10,14trimethylpentadecan-2-one divided by total OC

Secondary OC % (oc/ec=1.95) vs C18 ratio

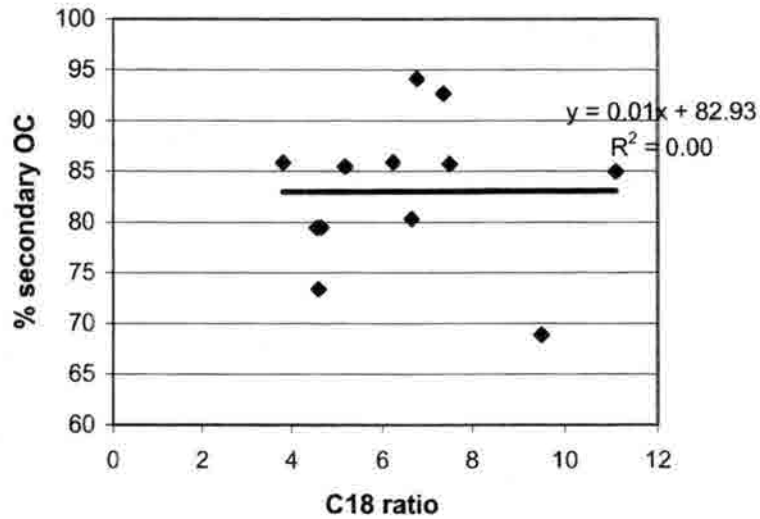


Figure 3.32 Graph of Estimated Secondary OC % (OC/EC=1.95) vs. C18 Ratio

Though there is a lack of strong correlation between the calculated secondary OC and these secondary aerosol indicators, this may be due to an oversimplification in the calculation and the assumptions therein, described in section 1.12. Also, with the differing air advection patterns observed during BRAVO, the ratio of primary OC/EC may not remain constant, invalidating another assumption.

3.10 Black Carbon

Black carbon, reported as Light Absorbing Carbon (LAC) in figure 3.1, was found to comprise 2% of the total fine aerosol mass during BRAVO. Black carbon concentrations sampled by the aethalometer (see figure 3.30) ranged from 25 ng/m³ to 267 ng/m³, with an average of 128 ng/m³. The fine fraction, with a cut of 1 µm aerodynamic diameter, averaged 115 ng/m³ (88% of total BC), ranging between 23 ng/m³ and 242 ng/m³. The detection limit, equal to the average blank concentration plus three standard deviations, was found to be 71 ng/m³. A discussion on the calculations is presented in section 3.10.1. Black carbon in the coarse fraction (greater than 1 µm aerodynamic diameter) was found by subtracting the fine black carbon fraction from the total black carbon concentration:

$$\text{Coarse BC} = \text{Total BC} - \text{Fine (1 } \mu\text{m aerodynamic diameter cutoff) BC} \quad (3.2)$$

This coarse fraction ranged between 1 ng/m³ and 46 ng/m³, with an average daily concentration of 17.7 ng/m³, averaging 12% of the total BC. Figure 3.33 shows the daily black carbon concentrations for these fractions.

**CSU Aethalometer Daily BC Concentrations : Total, Fine (1 μm cut),
and Coarse ($>1 \mu\text{m}$)**

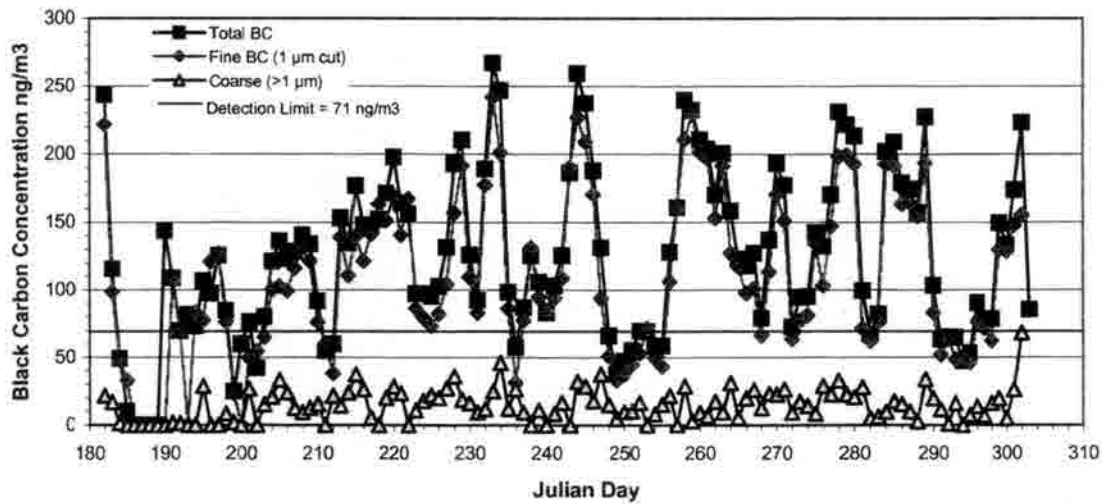


Figure 3.33 CSU Aethalometer Daily Black Carbon Concentrations (ng/m^3): Total BC, Fine BC (1 μm aerodynamic diameter cut), and Coarse BC (Total – Fine). The aethalometer detection limit, calculated based on the average blank plus three standard deviations, was estimated as 71 ng/m^3 .

3.10.1 Calculation of the Aethalometer Detection Limit

The detection limit for the aethalometer was found to be 71 ng/m^3 , based on the average blank concentration plus three standard deviations:

$$\text{Detection Limit} = \text{Average Blank Concentration} + 3 \text{ Standard Deviations} \quad (3.3)$$

Table 3.3 shows the blank concentrations for each blank run. The average plus three standard deviations was chosen as the detection limit because at this value there is a 99.75% probability that the measured value is significantly different from a blank.

Table 3.3 Aethalometer Blank Run Concentrations, Average Concentration, Standard Deviation, and Detection Limit (Avg + 3 SD)

Run #	Blank Concentration (ng/m ³)
1	45.583
2	37.583
3	47.333
4	22.455
5	38.417
6	54.033
7	26.167
8	24.545
9	37.583
10	16.054
Average	34.875
Standard Deviation	12.178
Detection Limit = Average + 3 SD	71.409

The average for these blank concentrations ($N_{\text{blanks}} = 10$) was 34.88 ng/m³, with a standard deviation of 12.18 ng/m³. The detection limit, as the sum of the average and three standard deviations, is 71.4 ng/m³.

3.10.2 Comparison of CSU Aethalometer BC with NPS Aethalometer BC and

IMPROVE EC

The National Park Service also conducted aethalometer measurements from July 1st through August 12th and October 12th through 31st. These measurements were made in 5 minute increments, with no size cut, and were averaged to daily concentrations in the same manner as the CSU aethalometer data, as shown in section 2.6.1. Figure 3.34 compares the two aethalometer data sets against each other.

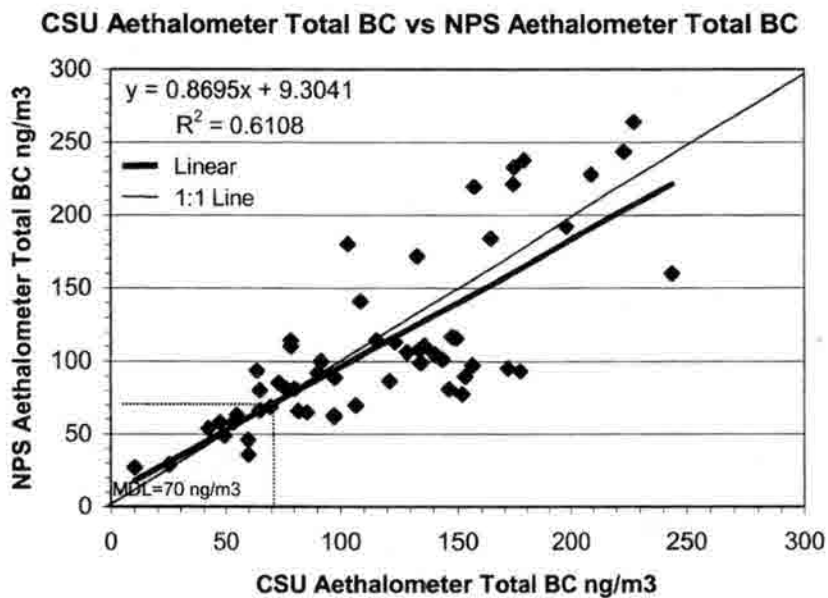


Figure 3.34 CSU Aethalometer Total BC (ng/m^3) versus NPS Aethalometer Total BC (ng/m^3)

A correlation of $r^2 = 0.6108$ was found between reported concentrations from the two instruments. This marginal correlation indicates there are some problems with reproducibility between the instruments. This is poorer than a previous study in Fort Collins, where collocated aethalometers were strongly correlated with $r^2 = 0.98$ (Calame, 1999).

Daily aerosol samples were also taken and evaluated by IMPROVE, as discussed in section 2.3.2. From the TOR combustion analysis, elemental carbon concentrations were found. Elemental carbon and black carbon concentrations are intended to be similar measures of carbonaceous aerosol with a large light absorbing component of its refractive index. The terms elemental and black carbon are used to differentiate between the two methods that quantify this species, TOR combustion (elemental carbon) and aethalometer (black carbon) sampling. However, other absorbing particles, such as soil or dust, will add to the light attenuation found by the aethalometer. If these are present, they will skew the aethalometer measurement of black carbon. Figure 3.35 is a graph that shows there is only a modest correlation between these two methods during this study.

CSU Aethalometer Fine (1 μm) BC vs. IMPROVE Fine (2.5 μm) EC

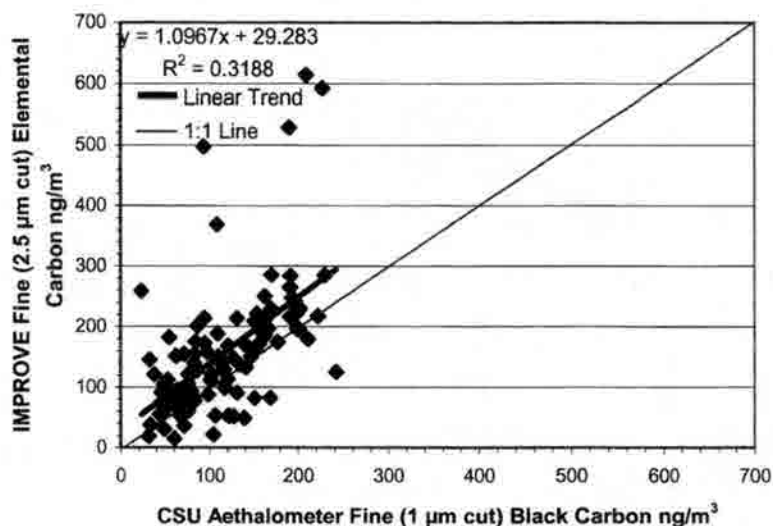


Figure 3.35 CSU Aethalometer Fine Black Carbon (1 μm aerodynamic diameter cut) versus IMPROVE fine EC from TOR analysis (2.5 μm aerodynamic diameter cut)

Chow et al. (1993) reported good correlation between IMPROVE EC and the Lawrence Berkeley Laboratory aethalometer (Hansen et al., 1982) in the Harvard Uniontown, PA, Acidic Aerosol Study (July-August 1990), with an r^2 of 0.86. During BRAVO, the correlation between the CSU aethalometer and IMPROVE EC was only $r^2=0.32$ ($n=99$). This poor correlation may reflect the different size cuts. As figure 3.35 shows, the IMPROVE fine EC concentrations are generally larger than the aethalometer concentrations. This is expected, since the IMPROVE fine EC, with a size cut of $2.5 \mu\text{m}$ aerodynamic diameter, includes a larger part of the fine aerosol fraction than the aethalometer with the $1 \mu\text{m}$ cut, and can therefore be expected to have higher concentrations.

The NPS aethalometer, measuring total black carbon, also has a poor correlation with the IMPROVE EC, as shown in Figure 3.36. This low correlation of $r^2=0.39$ again may be due at least partly to the comparison of a method with a size cut to one without. Lower correlations in BRAVO may also reflect difficulty accurately measuring the low EC/BC concentrations present.

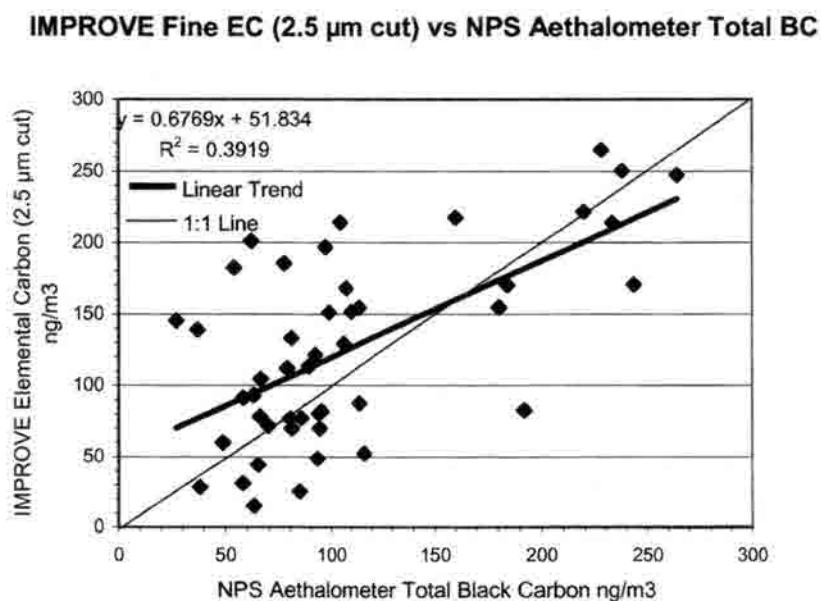


Figure 3.36 IMPROVE Fine Elemental Carbon ($2.5 \mu\text{m}$ aerodynamic diameter size cut) versus NPS Aethalometer Total Black Carbon

3.10.3 Aethalometer Black Carbon and Inorganic Species

The black carbon concentrations from the aethalometer were also compared with other inorganic species analyzed by CSU during the study. Sulfate constituted 48% of the fine aerosol during BRAVO (see figure 3.1), making it the most abundant species. Figure 3.37 shows that sulfate and black carbon concentrations show modest correlation, with an $r^2=0.68$.

CSU Aethalometer Fine (1 μm cut) BC vs CSU Fine (2.5 μm cut) SO₄ =

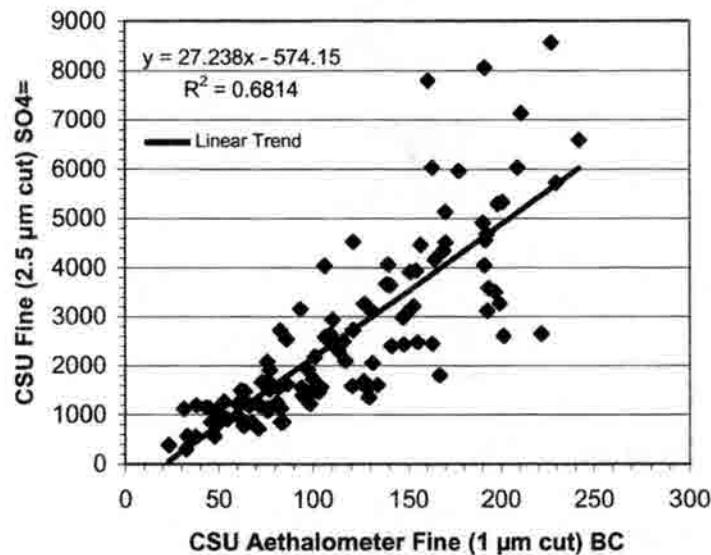


Figure 3.37 CSU Aethalometer Fine Black Carbon (1 μm size cut) versus CSU Fine (2.5 μm size cut) SO₄⁻²

The correlation between fine black carbon and fine sulfate indicates that these species generally track together, suggesting the possibly of similar source regions.

Nitrates only constituted 3% of the total fine aerosol during BRAVO (figure 3.1). Total reduced nitrogen, N[-III], is defined as the sum of the gaseous ammonia, NH_3 , and particulate ammonium, NH_4^+ :

$$\text{Total N[-III]} = \text{NH}_3 (\text{gaseous}) + \text{NH}_4^+ (\text{particulate}) \quad (3.4)$$

There is a correlation of $r^2=0.69$ between fine BC ($1 \mu\text{m}$ size cut) and fine ($2.5 \mu\text{m}$ size cut) total N[-III], shown in figure 3.38.

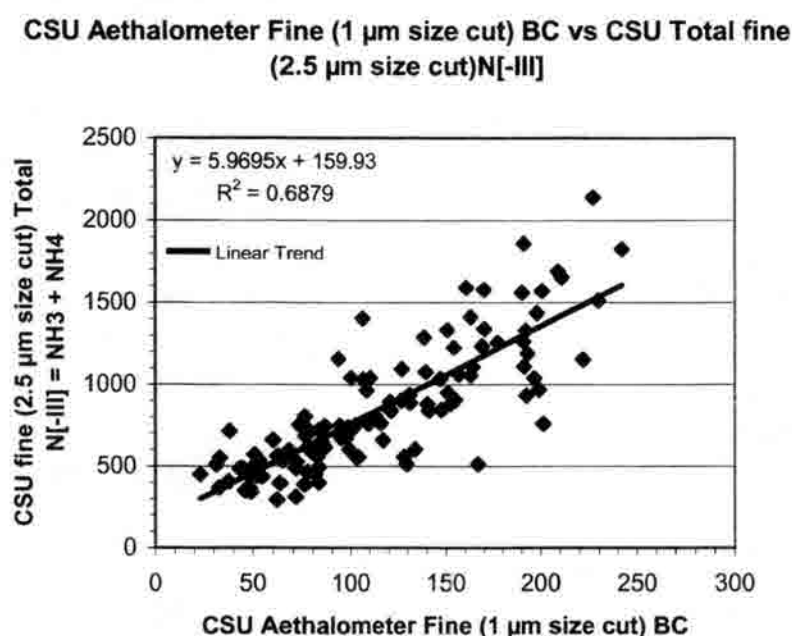


Figure 3.38 CSU Aethalometer Fine BC ($1 \mu\text{m}$ size cut) vs CSU total fine N[-III] ($2.5 \mu\text{m}$ size cut)

This correlation again suggests that the ammonia/ammonium and black carbon are frequently advected together into Big Bend.

Soluble potassium is sometimes used as a tracer for wood combustion, and a correlation with black carbon might suggest a large presence of wood smoke in the aerosol. As shown in figures 3.39 and 3.40, there is only a weak correlation between K^+ and black carbon concentrations.

CSU Aethalometer Fine (1 μm size cut) BC vs CSU Fine (2.5 μm size cut) K+

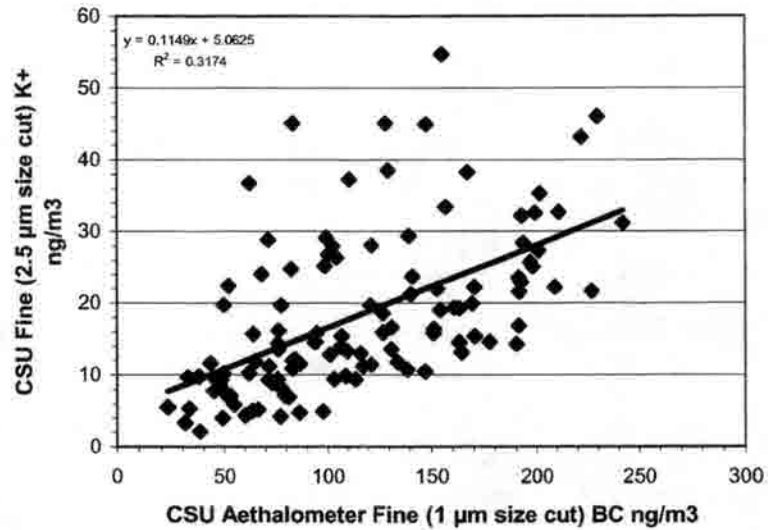


Figure 3.39 CSU Aethalometer Fine BC (1 μm size cut) vs. CSU Fine K⁺ (2.5 μm size cut)

CSU Aethalometer Total BC vs CSU Fine (2.5 μm size cut) K+

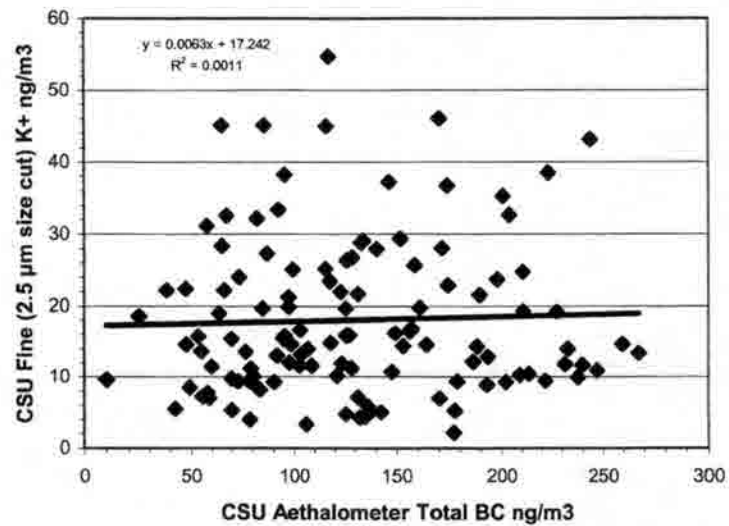


Figure 3.40 CSU Aethalometer Total BC vs. CSU Fine K⁺ (2.5 μm size cut)

The lack of strong correlation between potassium and black carbon suggests that there is not a large amount of wood smoke influencing the aerosol composition during BRAVO. This agrees with the absence of levoglucosan, and the small amounts of wood smoke markers found in the organic aerosol fraction (sections 3.5 and 3.6).

4 Conclusions

Molecular characterization of the organic carbon (OC) fraction of fine (<2.5 μm aerodynamic diameter) aerosol present during the Big Bend Regional Aerosol and Visibility Observational (BRAVO) study was performed utilizing Gas Chromatography – Mass Spectroscopy (GC-MS). Although OC was found to comprise an average of 20% of the $\text{PM}_{2.5}$ mass during BRAVO, OC concentrations on individual days were too low for a detailed analysis by GC-MS. Therefore, multi-day composite samples, selected based on common air mass trajectories and temporal proximity, were extracted and analyzed for numerous compounds including n-alkanes, PAH, alkanolic acids, and trace species previously demonstrated as useful signatures for various carbonaceous aerosol source types. An average of 3.5% of the $\text{PM}_{2.5}$ organic compound mass ($\text{OCM}=\text{OC}\times 1.4$) was identified as individual compounds. Alkanolic acids were the most abundant compound class, followed by the alkanes and PAH. Major conclusions reached are listed below.

- **Anthropogenic emissions appear to contribute more strongly than biogenic emissions to primary aerosol OC during the period July – September**

During the first three months of the study, where air masses advected to the park primarily along the Texas – Mexico border, alkane Carbon Preference Indices (CPI) were generally below two, indicating a strong influence from anthropogenic emissions. Days with the highest OC concentrations had the lowest CPI's, suggesting that anthropogenic emissions became more

important contributors as OC concentrations rose. Estimated plant wax contributions to alkanes during this period averaged only 35%.

- **Biogenic emissions became more important contributors to primary fine aerosol OC concentrations in October, when transport patterns also changed.**

In October, when air masses arrived from the north and south, OC concentrations fell and alkane CPIs increased, indicating a greater contribution from biogenic aerosol. Plant wax contributions to n-alkane concentrations during this period ranged between 66% and 78%

- **Vehicle emissions, wood smoke, and meat cooking emissions appear to be only minor contributors to observed OC concentrations.**

Concentrations of molecular tracers were generally at or below detection limits during BRAVO, so maximum source contributions were estimated by assuming source tracer concentrations were equal to detection limits. Levoglucosan, a widely accepted wood smoke tracer, was detected in only one sample, XBorder, yet the estimated wood smoke OC contribution for this group was only 1% of the total OC. Upper limits to wood smoke contributions, based on the levoglucosan detection limit, ranged from 0.06% to 0.12 % for the other composites. Despite a lack of levoglucosan, however, other wood smoke markers, such as vanillin, 4-ethylguaiacol and retene, were detected. The absence of levoglucosan may have resulted from acid-catalyzed hydrolysis of levoglucosan in acidic cloud drops or haze particles. Vanillin, which was detected in eleven out of twelve composites, was used to make an alternative estimate of wood smoke influence. Results indicated wood smoke could have contributed between 1% and 59% of the fine aerosol OC observed in different composite groups.

Hopanes, the molecular marker for vehicular exhaust, were not detected in any composite sample. Maximum vehicle emission OC contributions were estimated to be between 0.7% and 4.3%, with an average of 1.8%, based on the hopane detection limit. The lack of significant

vehicle exhaust influence is similar to previous results from the Grand Canyon. An alternative, but crude, upper bound to vehicular exhaust influence was also estimated assuming all elemental carbon (EC) present was emitted by vehicles. The vehicle OC contributions estimated using this assumption ranged from 18% to 76% for different groups.

The molecular marker for meat smoke, cholesterol, was not detected in any composite sample. Maximum possible OC contributions from meat smoke, estimated using the cholesterol detection limit, were estimated to range from 5% to 20%, with an average maximum contribution of 13%. Although these contributions appear high, they simply reflect a high cholesterol detection limit and do not necessarily imply meat smoke was an important source of observed OC.

- **Several findings suggest that a large fraction of the fine aerosol OC is secondary (formed in the atmosphere)**
 - Examination of ratios of aerosol organic carbon to elemental carbon indicates that secondary organic aerosol may have contributed between 45% and 90% of the total BRAVO aerosol organic carbon. These estimates are derived from examining the increase in the aerosol OC/EC ratio above average values observed at Big Bend National Park during winter months (December through February) in the years 1988-1998. Implicit in this analysis are assumptions that (i) winter OC concentrations are comprised solely of primary emissions (i.e. secondary OC formation does not occur in winter) and (ii) primary aerosol OC emission sources impacting Big Bend OC levels during BRAVO have the same OC/EC ratio as those impacting the park in an average winter period. Although these assumptions are clearly too simplistic, use of this approach should at least provide a reasonable estimate of the rough importance of secondary OC formation.

- The average ratio between saturated and unsaturated (oleic) C18 acid during BRAVO was 6.6, indicating that the aerosol during BRAVO was aged and subject to more decomposition than found in typical urban environments.
 - There is a large amount of C9 acid, averaging 22% of the total alkanolic acids present. This is a product of the chemical breakdown of oleic acid and again suggests that the aerosol was subject to significant chemical processing en route to the park.
 - An absence of benzo(a)pyrene suggests that the observed aerosol is somewhat aged. This observation is tempered, however, by the generally low PAH concentrations observed, which may indicate that combustion emissions upwind of the park were not significant contributors to observed OC concentrations. Secondary OC was estimated to range between 45% and 90% of the total OC during the study. This large amount of secondary OC is similar to rural areas, and supports the C18 ratio suggesting the aerosol advecting into Big Bend N. P. is generally aged and subject to degradation by atmospheric processes.
 - 6,10,14-trimethylpentadecan-2-one was ubiquitous during the study, and indicates secondary aerosol from biomass degradation is present throughout the study. The higher concentrations found in sample composites featuring summer advection along the Texas – Mexico border, along with low CPIs during the same period, indicate secondary aerosol formation from vegetation emissions was important during this period. A decrease in concentration in October, correlating with higher CPIs, indicates less significant secondary aerosol formation from biogenic precursor emissions late in the study.
- **Aerosol black carbon, mostly present in submicron particles, was observed at low concentrations throughout the study**

Black carbon (BC) concentrations measured with an aethalometer were found to comprise only ~ 2% of the total fine aerosol mass during BRAVO. Fine BC (1 μm cut) had an average concentration of 115 ng/m^3 and constituted 88% of the total BC. CSU aethalometer BC had a

marginal correlation with BC from a collocated NPS aethalometer, and a weak correlation with IMPROVE EC (2.5 μm cut). A high correlation was found between BC and SO_4^{-2} concentrations, suggesting these species have similar source regions.

Overall, aerosol from the primary advection pattern along the Texas – Mexico border appears to be influenced by anthropogenic sources, with much of it arriving at Big Bend N. P. as secondary products. Molecular markers for primary emissions of wood smoke, vehicle exhaust and meat cooking were seldom detected, which may be due to degradation via atmospheric processes or upwind loss by cloud scavenging and precipitation. When different advection patterns from the north and south appear in October, there appears to be a relatively stronger influence from primary biogenic emissions.

5 Future Work

Based on the work presented on the characterization of the carbonaceous aerosol present at Big Bend N. P. during the BRAVO study, some recommendations for future work have been formulated. These are:

- **Increase sampling volume and total aerosol mass loading in future studies**

The amount of OC collected on daily filters was not enough for a meaningful analysis by GC-MS, and the amount of OC that was characterized as individual compounds in composite samples was less than 7%. With an increase in sampling volume, daily filters could be analyzed, which would provide more accurate information about the changing composition of the organic aerosol. Also with this increase in aerosol loading, the amount of compounds identified may increase. Additionally, molecular markers such as levoglucosan and hopanes, which were generally at or below detection limits, may be detected.

- **Compare efficiencies between the Hx/Bz/IPA and DCM extraction methods for levoglucosan and other compounds in the silylated fraction**

The comparison between extraction methods was not done for compounds normally analyzed in the silylated fraction, such as levoglucosan and cholesterol. If the DCM extraction method was significantly different than the Hx/Bz/IPA method, this could explain the absence of levoglucosan in the extracted BRAVO samples, though with similar extraction efficiencies found for a wide range of compound types, this would be surprising.

- **Conduct study during times of different advection patterns and source influence**

The advection patterns for July, August and most of September were similar, along the Texas – Mexico border from the Gulf of Mexico. Only in late September and October was there a change in this pattern. It would be interesting to examine the organic content at Big Bend during other months, especially in the spring. May, June and April are the three months with the highest months aerosol OC concentrations, probably due to increased biomass burning.

- **Investigate the stability of the source tracers**

Air masses that were advected into Big Bend N. P. from sources (urban centers, biomass burning fields) generally had from one to several days of transport, where atmospheric processes could degrade and alter source tracers. There have not been extensive studies on this subject, and a stability analysis of levoglucosan, hopanes etc. under atmospheric conditions would be invaluable.

- **Characterize both the fine and coarse mode organic aerosol**

It was reported that the coarse fraction ($> 2.5 \mu\text{m}$) of aerosol during BRAVO was comprised of approximately 20% organic carbon. Since most emissions of organic compounds typically considered (e.g., combustion and plant wax emissions) are probably mainly contributing to the fine fraction, characterizing the composition of this coarse fraction would be very interesting. This coarse mode aerosol OC may originate from dust, sea salt, plant or tire abrasion, or other sources.

- **Sample sources and develop source profiles of regional emissions**

Source profiles of local anthropogenic emissions as well as biomass burning of local plants and trees would be useful in calculating more accurate source contributions specific to the area. These samples would need a significant amount of OC for meaningful analysis by GC-MS. Although the BRAVO source samples collected by DRI could have been quite useful for the carbonaceous aerosol source apportionment, the aerosol loadings on the filters were too low to permit trace organic species analysis.

- **Investigate the lack of consistency between methods of obtaining light absorbing carbon concentrations**

There was not a high correlation between the CSU and NPS co-located aethalometers or between either aethalometer BC and IMPROVE EC. This lack of high correlation between the methods should be investigated further to see whether this was an aberration or whether there are truly significant differences between methods of measuring light absorbing carbon.

References

- Abas, M. R., Simoneit, B. R. T., Elias, V., Cabral, J. A., Cardoso, J. N., (1995). "Composition of Higher Molecular Weight Organic Matter in Smoke Aerosol from Biomass Combustion in Amazonia." *Chemosphere* **30(5)**: 995-1015.
- Abas, M. R. B., and Simoneit, B. R. T. (1996). "Composition of Extractable Organic Matter of Air Particles from Malaysia: Initial Study." *Atmospheric Environment* **30(15)**: 2779-2793.
- Adams, K. M., Davis, L. I. Jr., Japar, S. M., Finley, D. R., Cary, R. A. (1990a). "Measurement of atmospheric elemental carbon: real-time data for Los Angeles during summer 1987." *Atmospheric Environment* **24A**: 597-604.
- Adams, K. M., Davis, L. I. Jr., Japar, S. M., Finley, D. R. (1990b). "Real-time *in situ* measurements of atmospheric optical absorption in the visible via photoacoustic spectroscopy IV. Visibility degradation and aerosol optical properties in Los Angeles." *Atmospheric Environment* **24A**: 605-610.
- Alves, C., Pio, C., and Duarte, A. (1999). "The organic composition of ait particulate matter from rural and urban Portuguese areas." *Physical and Chemistry of the Earth (B)* **24(6)**: 705-709.
- Appel, B. R., Wall, S. M., Knights, R. S., (1980). "Characterization of carbonaceous materials in atmospheric aerosols by high-resolution mass spectrometric thermal analysis." *Adv. Environmental Science and Technology* **9**: 353-365.
- Azevedo, D. A., Moreira, L. S., and de Siqueria, D. S. (1999). "Composition of extractable organic matter in aerosols from urban areas of Rio de Janeiro city, Brazil." *Atmospheric Environment* **33**: 4987-5001.
- Big Bend Air Quality Work Group (1999). "Report of the study conducted from Sept. 9 to October 13, 1996." Big Bend National Park Regional Visibility Preliminary Study. Prepared for the U.S. EPA, National Park Service, SEMARNAP, and PROFEPA.
- Bigg, E. K. (1986). "Discrepancy between observation and prediction of concentrations of cloud condensation nuclei." *Atmospheric Research* **20**: 82-86.
- Calame, L. (1999). Aerosol Black Carbon Measurements in Fort Collins, CO. Atmospheric Science Department, Fort Collins, Colorado State University.

- Castro, L. M., Pio, C. A., Harrison, R. M., and Smith, D. J. T. (1999). "Carbonaceous aerosol in urban and rural European atmospheres: estimation of secondary organic carbon concentrations." *Atmospheric Environment* **33**: 2771-2781.
- Chow, J. C., Watson, J. G., Pritchett, L. C., Pierson, W. R., Frazier, C. A., and Purcell, R. G. (1993). "The DRI Thermal/Optical Reflectance Carbon Analysis System: Description, Evaluation and Applications in U.S. Air Quality Studies." *Atmospheric Environment* **27A(8)**: 1185-1201.
- Devore, J. L. (1995). Probability and Statistics. Pacific Grove, Duxbury Press.
- Didyk, B. M., Simoneit, B. R. T., Pezoa, L. A., Riveros, M. L., Flores, A. A. (2000). "Urban aerosol particles of Santiago, Chile: organic content and molecular characterization." *Atmospheric Environment* **34**: 1167-1179.
- Draxler, R. R. (1991). "The accuracy of trajectories during ANATEX calculated using dynamic model analyses versus rawinsonde observations." *Journal of Applied Meteorology* **30**: 1446-1467.
- Draxler, R. R. (1996). "Trajectory optimization for balloon flight planning." *Weather and Forecasting* **11**: 111-114.
- Edye, L. A. a. R., G. N. (1991). "Analysis of Condensates from Wood Smoke : Components Derived from Polysaccharides and Lignins." *Environmental Science and Technology* **25(6)**: 1133-1137.
- Elias, V. O., Simoneit, B. R. T., Cordeiro, R. C., and Turco, B. (2001). "Evaluating levoglucosan as an indicator of biomass burning in Carajas, Amazonia: a comparison to the charcoal record." *Geochimica et Cosmochimica Acta* **65(2)**: 267-272.
- Eskinja, I., Soljic, Z., Svel-Cerovecki, S., Eskinja, M., Sojat, V. (1996). "Sources and fate of polycyclic aromatic hydrocarbons in ambient air of urban and rural Croatian sites." *International Journal of Environmental Analytical Chemistry* **63**: 251-268.
- Fang, M., Zheng, M., Wang, F., To, K. L., Jaafar, A. B., and Tong, S. L. (1999a). "The solvent-extractable organic compounds in the Indonesia biomass burning aerosols- characterization studies." *Atmospheric Environment* **33**: 783-795.
- Fang, M., Zheng, M., Wang, F., Chim, K/ S., and Kot, S. C. (1999b). "The long-range transport of aerosols from northern China to Hong Kong- a multi-technique study." *Atmospheric Environment* **33**: 1803-1817.
- Fine, P. M., Cass, G. R., Simoneit, B. R. T., (2001). "Chemical Characterization of Fine Particle Emissions from Fireplace Combustion of Woods Grown in the Northeastern United States." *Environmental Science and Technology* **35**: 2665-2675.
- Finlayson-Pitts, B. J., Pitts, J. N. (1999). Chemistry of the Upper and Lower Atmosphere. San Diego, Academic Press.
- Fraser, M. P. and Lakshmanan, K. (2000). "Using Levoglucosan as a Molecular Marker for the Long-Range Transport of Biomass Combustion Aerosols." *Environmental Science and Technology* **34**: 4560-4564.

Gebhart, K. A., and Malm, W. C. (2000). "A preliminary look at source-receptor relationships in the Texas-Mexico border area." *Journal of the Air and Waste Management Association* **50**: 858-868.

Gill, P. S., Graidel, T. E., and Weshler, C. J. (1983). "Organic films on atmospheric aerosol particles, fog droplets, cloud droplets, raindrops, and snowflakes." *Reviews of Geophysics* **21(4)**: 903-920.

Gogou, A., Stratigakis, N., Kanakidou, M., and Stphanou, E. G. (1996). "Organic aerosols in Eastern Mediterranean: components source reconciliation by using molecular markers and atmospheric back trajectories." *Organic Geochemistry* **25(1/2)**: 79-96.

Gray, H. A., Cass, G. R., Huntzicker, J. J., Heyerdahl, E. K., and Rau, J. A. (1986). "Characteristics of atmospheric organic and elemental carbon particle concentrations in Los Angeles." *Environmental Science and Technology* **20**: 580-589.

Hansen, A. D. A., Rosen, H., and Novakov, T. (1982). "Real-time measurement of the absorption coefficient of aerosol particles." *Applied Optics* **21**: 3060-6032.

Hansen, A. D. A. (1996). The Aethalometer, Magee Scientific Company.

Hatakeyama, S., Tanonaka, T., Weng, J., Bandow, H., Takagi, H., Akimoto, H., (1985). "Ozone-cyclohexene reaction in air: quantitative analysis of particulate products and the reaction mechanism." *Environmental Science and Technology* **19**: 935-942.

Hatakeyama, S., Ohno, M., Weng, J., Takagi, H., Akimoto, H. (1987). "Mechanism for the Formation of Gaseous and Particulate Products from Ozone-Cycloalkene Reactions in Air." *Environmental Science and Technology* **21**: 52-57.

Hawthorne, S. B., Kreiger, M. S., Miller, D. J., and Barkley, R. M., (1988). "Identification of methoxylated phenols as candidate tracers for atmospheric wood smoke pollution." *Environmental Science and Technology* **22**: 1191-1196.

Hawthorne, S. B., Kreiger, M. S., Miller, D. J., and Mathiason, M. B. (1989). "Collection and quantification of methoxylated phenol tracers for atmospheric pollution from residential wood stoves." *Environmental Science and Technology* **23(4)**: 470-475.

Hawthorne, S. B., Miller, D. J., Langenfeld, J. J., Krieger, M. S., (1992). "PM10 High-Volume Collection and Quantification of Semi- and Nonvolatile Phenols, Methoxylated Phenols, Alkanes, and Polycyclic Aromatic Hydrocarbons from Winter Urban Air and Their Relationship to Wood Smoke Emissions." *Environmental Science and Technology* **26(11)**: 2251-2262.

Hildemann, L. M., Klinedinst, D. B., Klouda, G. A., Currie, L. A., and Cass, G. R. (1994). "Sources of urban contemporary carbon aerosol." *Environmental Science and Technology* **28(9)**: 1585-1576.

<http://vista.cira.colostate.edu/improve/Publications/OtherDocs/IMPROVEDataGuide/IMPROVEDataGuide.htm> (1995). IMPROVE Data Guide: A guide to interpret data, UC Davis.

Jacobson, M. C., Hansson, H. C., Noone, K. J., Charlson, R. J., (2000). "Organic Atmospheric Aerosols: Review and State of the Science." *Reviews of Geophysics* **38**: 267-294.

- Japar, S. M., Szkarlat, A. C., Gorse, Jr., R. A., Heyerdahl, E. K., Johnson, R. L., Rau, J. A., and Huntzicker, J. J. (1984). "Comparison of solvent extraction and thermal optical carbon analysis methods: application to diesel vehicle exhaust aerosol." *Environmental Science and Technology* **18**: 231-234.
- Japar, S. M., Brachaczek, W. W., Gorse, R. A. Jr., Norbeck, J. M., and Pierson, W. R. (1986). "The contribution of elemental carbon to the optical properties of rural atmospheric aerosols." *Atmospheric Environment* **20**: 1281-1289.
- Kadowaki, S. (1994). "Characterization of carbonaceous aerosols in the Nagoya urban area 2. behavior and origin of particulate n-alkanes." *Environmental Science and Pollution Research* **28**: 129-135.
- Kavouras, I. G., Lawrence, J., Koutrakis, P., Stephanou, E. G., and Oyola, P. (1999). "Measurement of particulate aliphatic and polynuclear aromatic hydrocarbons in Santiago de Chile: source reconciliation and evaluation of sampling artifacts." *Atmospheric Environment* **33**: 4977-4986.
- Kawamura, K. and Gagosian, R. B. (1987a). "Implications of w-oxocarboxylic acids in the remote marine atmosphere for photo-oxidation of unsaturated fatty acids." *Nature* **325(22)**: 330-332.
- Kawamura, K. and Kaplan, I. R. (1987b). "Motor exhaust emissions as a primary source for dicarboxylic acids in Los Angeles ambient air." *Environmental Science and Technology* **21**: 105-110.
- Kawamura, K. and Ikushima, K. (1993). "Seasonal Change in the Distribution of Dicarboxylic Acids in the Urban Atmosphere." *Environmental Science and Technology* **27**: 2227-2235.
- Kawamura, K., Semere, R., Imai, Y., Fujii, Y., and Hayashi, M. (1996a). "Water soluble dicarboxylic acids and related compounds in Antarctic aerosols." *Journal of Geophysical Research* **101(D13)**: 18721-18728.
- Kawamura, K., Kasukabe, H., and Barrie, L. A. (1996b). "Source and reaction pathways of dicarboxylic acids, ketoacids and dicarbonyls in arctic aerosols: one year of observations." *Atmospheric Environment* **30(10/11)**: 1709-1722.
- Kawamura, K. and Sakaguchi, F. (1999). "Molecular distributions of water soluble dicarboxylic acids in marine aerosols over the Pacific Ocean including tropics." *Journal of Geophysical Research* **104(D3)**: 3501-3509.
- Kendall, M., Hamilton, R. S., Watt, J., and Williams, I. D. (2001). "Characterization of selected speciated organic compounds associated with particulate matter in London." *Atmospheric Environment* **35**: 2483-2495.
- Kubatova, A., Vermeylen, R., Claeys, M., Cafmeyer, J., Maenhaut, W., Roberts, G., and Artaxo, P. (2000). "Carbonaceous aerosol characterization in the Amazon basin, Brazil: novel dicarboxylic acids and related compounds." *Atmospheric Environment* **34**: 5037-5051.

- Kulmala, M., Korhonen, P., Vesala, T., Hansson, H. C., Noone, K., and Svenningsson, B. (1996). "The effect of hygroscopicity on cloud droplet formation." *Tellus, Series B* **48**: 347-360.
- Lawrence, J. and Koutrakis, P. (1996). "Measurement and speciation of gas and particulate phase organic acidity in an urban environment." *Journal of geophysical research* **101(C4)**: 9171-9184.
- Lee, W. G., and Huang, R. (1993). "Diurnal variation of organic aerosols in a severely polluted atmosphere." *Journal of Environmental Science and Health* **A28(7)**: 1565-1579.
- de Leeuw, J. W., Simoneit, B. R. T., Boon, J. J., Rijpstra, W. I. C., deLange, F., Leeden, and C. J. C. W., V. A., Burlingame, A. L., and Schenck, P. A (1977). "Phytol-derived compounds in the geosphere." *Advances in Organic Geochemistry*. Ed. Campos and Goni: 61-79.
- Legrand, M. and De Angelis, M. (1996). "Light carboxylic acids in Greenland ice: a record of past forest fires and vegetation emissions from the boreal zone." *Journal of Geophysical Research* **101**: 4129-4145.
- Limbeck, A., Puxbaum, H., Otter, L., Scholes, M. C. (2001). "Semivolatile behavior of dicarboxylic acids and other polar organic species at a rural background site." *Atmospheric Environment* **35**: 1853-1862.
- Limbeck, A. and Puxbaum, H. (1999). "Organic acids in continental background aerosols." *Atmospheric Environment* **33**: 1847-1852.
- Lin, J. J. and Tai, H.S. (2001). "Concentrations and distributions of carbonaceous species in ambient particles in Kaohsiung City, Taiwan." *Atmospheric Environment* **35**: 2627-2636.
- Malm, W. C. (1999). *Introduction to Visibility*. Fort Collins, CO, CIRA.
- Matsumoto, G. and Hanya, T. (1980). "Organic constituents in atmospheric fallout in the Tokyo area." *Atmospheric Environment* **14**: 1409-1419.
- Mayol-Bracero, O. L., Rosario, O., Corrigan, C. E., Morales, R., Torres, I., Perez, V. (2001). "Chemical Characterization of submicron organic aerosols in the tropical trade winds of the Caribbean using gas chromatography/mass spectroscopy." *Atmospheric Environment* **35**: 1735-1745.
- Mazurek, M., Masonjones, M. C., Masonjones, H. D., Salmon, L. G., Cass, G. R., Hallock, K. A., and Leach, M. (1997). "Visibility-reducing organic aerosols in the vicinity of Grand Canyon National Park: Properties observed by high resolution gas chromatography." *Journal of Geophysical Research* **102(D3)**: 3779-3793.
- McDonald, J. D., Zielinska, B., Fujita, E. M., Sagebiel, J. C., Chow, J. C., Watson, J. G. (2000). "Fine Particle and Gaseous Emission Rates from Residential Wood Combustion." *Environmental Science and Technology* **34**: 2080-2091.
- McDow, S. R. and Huntzicker, J. J. (1990). "Vapor adsorption artifact in the sampling of organic aerosol: face velocity effects." *Atmospheric Environment* **24A**: 2563-2571.
- Neilsen, T. (1984). "Reactivity of polycyclic aromatic hydrocarbons toward nitrating species." *Environmental Science and Pollution Research* **18**: 157-163.

- Nielsen, T., Seitz, B., and Ramdahl, T. (1984). "Occurance of nitro-PAH in the atmosphere in a rural area." *Atmospheric Environment* **18**(10): 2159-2165.
- Nolte, C. G., Schauer, J. J., Cass, G. R., Simoneit, B. R. T. (2001). "Highly Polar Organic Compounds Present in Wood Smoke and in the Ambient Atmosphere." *Environmental Science and Technology* **35**: 1912-1919.
- Novakov, T., Corrigan, C. E., Penner, J. E., Chuang, C. C., Rosario, O. and Mayol- and O. L. Bracero (1997). "Organic aerosol in the Caribbean trade winds: a natural source?" *Journal of Geophysical Research* **102**(D17): 21307-21313.
- Oros, D. R., Standley, L. J., Chen, X., Simoneit, B. R. T. (1999a). "Epicuticular wax compositions of predominant conifers of western North America." *Verlag der Zeitschrift fur Naturforschung C* **54c**: 17-24.
- Oros, D. R. and Simoneit, B.R.T. (1999b). "Identification of molecular tracers in organic aerosol from temperate climate vegetation subjected to biomass burning." *Aerosol Science and Technology* **31**: 433-445.
- Oros, D. R. and Simoneit, B.R.T. (2000). "Identification and emission rates of molecular tracers in coal smoke particulate matter." *Fuel* **79**: 515-536.
- Payne, K. (1982). "Chemistry and Toxicology of PCDDs." *Chemical Industry* **9**: 298-300.
- Penczek, S., Kubisa, P., Matyjaszewski, K. (1985). Cationic Ring-Opening Polymerization. 2: Synthetic Applications. Berlin, Springer-Verlag.
- Penner, J. E., Dickenson, R. E., and O'Neill, C. A. (1992). "Effects of aerosol from biomass burning on the global radiation budget." *Science* **256**: 1432-1434.
- Pio, C. A., Alves, C. A., and Duarte, A. C. (2001a). "Identification, abundance and origin of atmospheric organic particulate matter in a Portuguese rural area." *Atmospheric Environment* **35**: 1365-1375.
- Pio, C. A., Alves, C. A., and Duarte, A. C. (2001b). "Organic components of aerosols in a forested area of central Greece." *Atmospheric Environment* **35**: 389-401.
- Prescott, L. M., Harley, J. P., and Klein, D. A. (1999). Microbiology. Boston, WCB McGraw-Hill.
- Ramdahl, T. (1983). "Retene- a molecular marker of wood combustion in ambient air." *Nature* **306**: 580-582.
- Rogge, W. F., Hildemann, L. M., Mazurek, M. A., Cass, G. R. (1991). "Sources of Fine Organic Aerosol 1. Charbroilers and Meat Cooking Operations." *Environmental Science and Technology* **25**(6): 1112-1125.
- Rogge, W. F., Hildemann, L. M., Mazurek, M. A., Cass, G. R. (1993a). "Sources of Fine Organic Aerosol 2. Noncatalyst and Catalyst-Equipped Automobiles and Heavy-Duty Diesel Trucks." *Environmental Science and Technology* **27**: 636-650.

- Rogge, W. F., Mazurek, M. A., Hildemann, L. M., Cass, G. R. (1993b). "Quantification of Urban Organic Aerosols at a Molecular Level: Identification, Abundance and Seasonal Variation." *Atmospheric Environment* **27A(8)**: 1309-1330.
- Rogge, W. F., Hildemann, L. M., Mazurek, M. A., Cass, G. R. (1998). "Sources of Fine Organic Aerosol. 9. Pine, Oak, and Synthetic Log Combustion in Residential Fireplaces." *Environmental Science and Technology* **32**: 13-22.
- Sagebiel, J. C. a. S., J. N. (1993). "Studies on the occurrence and distribution of wood smoke marker compounds in foggy atmospheres." *Environmental Science and Technology* **12**: 813-822.
- Satsumabayashi, H., Kurita, H., and Yokouchi, Y., Ueda, H. (1990). "Photochemical formation of particulate dicarboxylic acids under long -range transport in central Japan." *Atmospheric Environment* **24A**: 1443-1450.
- Schauer, J. J., Rogge, W. F., Hildemann, L. M., Mazurek, M. A., Cass, G. R. (1996). "Source Apportionment of Airborne Particulate Matter Using Organic Compounds as Tracers." *Atmospheric Environment* **22**: 3837-3855.
- Schauer, J. J., Kleeman, M. J., Cass, G. R., Simoneit, B. R. T. (1999a). "Measurement of emissions from air pollution sources. 1. C1 through C29 organic compounds from meat charbroiling." *Environmental Science and Technology* **33**: 1566-1577.
- Schauer, J. J., Kleeman, M. J., Cass, G. R., Simoneit, B. R. T. (1999b). "Measurement of emissions from air pollutions sources 2. C1 through C30 organic compounds from medium duty diesel trucks." *Environmental Science and Technology* **33**: 1578-1587.
- Schauer, J. J., and Cass, G. R. (2000). "Source Apportionment of Wintertime Gas-Phase and Particle-Phase Air Pollutants Using Organic Compounds as Tracers." *Environmental Science and Technology* **34**: 1821-1832.
- Schauer, J. J., Kleeman, M. J., Cass, G. R., Simoneit, B. R. T. (2001). "Measurement of Emissions from Air Pollution Sources 3. C1-C29 Organic Compounds from Fireplace Combustion of Wood." *Environmental Science and Technology* **35**: 1716-1728.
- Schneider, J. K., Gagosian, R. B., Cochran, J. K., and Trull, T. W. (1983). "Particle size distributions of n-alkanes and 210Pb in aerosols off the coast of Peru." *Nature* **304**: 429-431.
- Seinfeld, J. H., and Pandis, S. N. (1998). *Atmospheric Chemistry and Physics*. New York, John Wiley and Son, Inc.
- Sempere, R. and Kawamura, K. (1994). "Comparative distributions of dicarboxylic acids and related polar compounds in snow, rain and aerosols from urban atmosphere." *Atmospheric Environment* **28**: 449-459.
- Sempere, R. and Kawamura, K. (1996). "Low molecular weight dicarboxylic acids and related polar compounds in the remote marine rain samples collected from western pacific." *Atmospheric Environment* **30**: 1609-1619.

Sicre, M. A., Marty, J. C., Saliot, A., Aparicio, X., Grimalt, J., and Albaiges, J. (1987). "Aliphatic and aromatic hydrocarbons in different sized aerosols over the Mediterranean sea: occurrence and origin." *Atmospheric Environment* **21(10)**: 2247-2259.

Sicre, M. A., Marty, J. C., Sallot, A. (1990). "n-Alkanes, fatty acid esters, and fatty acid salts in size fractionated aerosols collected over the Mediterranean Sea." *Journal of Geophysical Research* **95**: 3649-3657.

Simoneit, B. R. T. (1978). The organic Chemistry of Marine Sediments. Chemical Oceanography. J. P. R. a. R. Chester. New York, Academic Pre. **7**: 233-311.

Simoneit, B. R. T., and Mazurek, M. (1982). "Organic Matter of the Troposphere - II. Natural Background of Biogenic Lipid Matter in Aerosols over the Rural Western United States." *Atmospheric Environment* **16(9)**: 2139-2159.

Simoneit, B. R. T. (1984). "Organic matter of the troposphere- III. Characterization and sources of petroleum and pyrogenic residues in aerosols over the western United States." *Atmospheric Environment* **18(1)**: 51-67.

Simoneit, B. R. T., Cox, R. E., and Standley, L. J. (1988). "Organic matter of the troposphere- IV. Lipids in Harmattan aerosol of Nigeria." *Atmospheric Environment* **22**: 983-1004.

Simoneit, B. R. T. (1989). "Organic Matter of the Troposphere- V. Application of Molecular Marker Analysis to Biogenic Emissions into the Troposphere for Source Reconciliations." *Journal of Atmospheric Chemistry* **8**: 251-275.

Simoneit, B. R. T., Cardoso, J. N., Robinson, N. (1990). "An Assessment of the Origin and Composition of Higher Molecular Weight Organic Matter in Aerosols Over Amazonia." *Chemosphere* **21(10-11)**: 1283-1301.

Simoneit, B. R. T., Sheng, G., Chen, X., Fu, J., Zhang, J. Xu, Y. (1991a). "Molecular Marker Study of Extractable Organic Matter in Aerosols From Urban Areas of China." *Atmospheric Environment* **25A(10)**: 2111-2129.

Simoneit, B. R. T., Cardoso, J. N., Robinson, N. (1991b). "An assessment of terrestrial higher molecular weight lipid compounds in aerosol particulate matter over the south atlantic from about 30-700 S." *Chemosphere* **32(4)**: 447-465.

Simoneit, B. R. T., Crisp, P. T., Mazurek, M. A., and Standley, L. J. (1991c). "Composition of extractable organic matter of aerosols from the Blue Mountains and southeast coast of Australia." *Environment International* **17**: 405-419.

Simoneit, B. R. T., Rogge, W. F., Mazurek, M. A., Standley, L. J., Hildemann, L. M., and Cass, G. R. (1993). "Lignin pyrolysis products, lignans, and resin acids as specific tracers of plant classes in emissions from biomass combustion." *Environmental Science and Pollution Research* **27**: 2533-2541.

Simoneit, B. R. T., Schauer, J. J., Nolte, C. G., Oros, D. R., Elias, V. O., Fraser, M. P., Rogge, W. F., and Cass, G. R. (1999a). "Levoglucosan, a tracer for cellulose in biomass burning and atmospheric particles." *Atmospheric Environment* **33**: 173-182.

- Simoneit, B. R. T., and Didyk, B. M. (1999b). "The lipid and resin composition of *Laretia compacta* Phil from the Andes of Chile." *Verlag der Zeitschrift für Naturforschung C* **54c**: 309-313.
- Simoneit, B. R. T. (1999c). "A Review of Biomarker Compounds as Source Indicators and Tracers for Air Pollution." *Environmental Science and Pollution Research* **6(3)**: 159-169.
- Simoneit, B. R. T., Elias, V. O. (2000). "Organic tracers from biomass burning in atmospheric particulate matter over the ocean." *Marine Chemistry* **69**: 301-312.
- Skoog, West and Holler (1992). Fundamentals of Analytical Chemistry. Fort Worth, Saunders.
- Stanley, J., Ayling, R., Cramer, K., Thornburg, J., Remmus, J., Breen, J., Schwemberger, J., Keng, H., and Watanabe, K. (1990). "PCDD and PCDF levels in human adipose tissue in the continental U.S. collected between 1971 and 1987." *Chemosphere* **20(7-9)**: 895-903.
- Stephanou, E. G. (1992). "Biogenic and anthropogenic organic compounds in Eolian particulates in the east Mediterranean region- 1. occurrence and origin." *Atmospheric Environment* **26a(15)**: 2821-2829.
- Stryer, L. (1988). Biochemistry. New York, W. H. Freeman and Company.
- Turpin, B. J., and Huntzicker, J. J. (1991a). "Secondary formation of organic aerosol in the Los Angeles basin: a descriptive analysis of organic and elemental carbon concentrations." *Atmospheric Environment* **25A(2)**: 207-215.
- Turpin, B. J., Huntzicker, J. J., Larson, S. M., and Cass, G. R. (1991b). "Los Angeles summer midday particulate carbon: primary and secondary aerosol." *Environmental Science and Technology* **25**: 1788-1793.
- Turpin, B. J., and Lim, H. (2001). "Species contributions to PM_{2.5} mass concentrations: revisiting common assumptions for estimating organic mass." *Aerosol Science and Technology* **35**: 602-610.
- White, W. H., Roberts, P. T. (1977). "On the nature and origins of visibility reducing aerosols in the Los Angeles air basin." *Atmospheric Environment* **11**: 803-812.
- Wiedmeyer, C. (1999). Biogenic Hydrocarbons in Texas: Source Characterization and Chemistry. Austin, Tx, University of Texas, Austin.
- Xie, S., Yao, T., Kang, S., Xu, B., Duan, K., and Thompson, L. G. (2000). "Geochemical analyses of a Himalayan snowpit profile: implications for atmospheric pollution and climate." *Organic Geochemistry* **31**: 15-23.
- Zheng, M., Wan, T. S. M., Fang, M., and Wang, F. (1997). "Characterization of the non-volatile organic compounds in the aerosols of Hong Kong- Identification, abundance and origin." *Atmospheric Environment* **31(2)**: 227-237.
- Zheng, M., Fang, M., Wang, F., and To, K. L. (2000). "Characterization of the solvent extractable organic compounds in PM_{2.5} aerosol in Hong Kong." *Atmospheric Environment* **34**: 2691-2702.

Appendix A - Daily flow rates, total sampling times and volume collected on organics sampler during BRAVO

Table A1: Daily flow rate, total sampling time, channel, and total volume collected

Date (BLK = Blank Taken)	Ambient Flow (L/min)	Sampling Time (min)	Channel (Right or Left)	Total Volume (m ³)
BB0630Q	87.20028	828	R	72.20183
BB0701Q	85.61272	1440	L	123.2823
BB0702Q	82.6231	1437	R	118.7294
BB0703Q	81.91448	1438	L	117.793
BB0704Q	80.5546	1441	R	116.0792
BB0705Q	83.8971	1439	L	120.7279
BB0706Q	83.46619	1440	R	120.1913
BB0706QBLK			L	
BB0707Q	83.8386	1437	L	120.4761
BB0708Q	83.77896	1439	R	120.5579
BB0709Q	84.34884	1439	L	121.378
BB0710Q	83.66116	1443	R	120.7231
BB0711Q	83.11063	1434	L	119.1806
BB0712Q	84.28721	1443	R	121.6264
BB0713Q	84.36899	1437	L	121.2382
BB0713BLK			R	
BB0714Q	83.63057	1439	R	120.3444
BB0715Q	83.27615	1439	L	119.8344
BB0716Q	83.71892	1442	R	120.7227
BB0717Q	84.21169	1440	L	121.2648
BB0718Q	84.0544	1437	R	120.7862
BB0719Q	84.25102	1441	L	121.4057
BB0720Q	84.1999	1436	R	120.9111
BB0720QBLK			L	
BB0721Q	83.97575	1440	L	120.9251
BB0722Q	83.71784	1379	R	115.4469
BB0723Q	110.3938	1381	L	152.4538
BB0724Q	111.441	1440	R	160.4751
BB0725Q	111.5942	1439	L	160.5841

BB0726Q	111.2876	1440	R	160.2541
BB0727Q	112.2815	1439	L	161.5731
BB0727QBLK			R	
BB0728Q	112.3535	1439	R	161.6768
BB0729Q	112.9347	1440	L	162.6259
BB0730Q	112.8982	1440	R	162.5734
BB0731Q	112.2431	1438	L	161.4055
BB0801Q	111.4033	1433	R	159.6409
BB0802Q	111.5922	1441	L	160.8044
BB0803Q	111.5178	1440	R	160.5857
BB0803QBLK			L	
BB0804Q	112.6283	1439	L	162.0721
BB0805Q	111.9348	785	R	87.86879
BB0806Q	110.2296	1394	L	153.66
BB0807Q	110.2577	1430	R	157.6685
BB0808Q	109.7091	1439	L	157.8714
BB0809Q	110.2776	1439	R	158.6895
BB0810Q	110.3354	1438	L	158.6623
BB0810QBLK			R	
BB0811Q	110.6211	1440	R	159.2945
BB0812Q	111.1931	1440	L	160.118
BB0813Q	110.4689	1439	R	158.9647
BB0814Q	110.9048	1449	L	160.701
BB0815Q	110.5011	1440	R	159.1215
BB0816Q	110.2974	1445	L	159.3798
BB0816QBLK			R	
BB0817Q	109.6518	1430	R	156.8021
BB0818Q	110.3734	1440	L	158.9376
BB0819Q	109.9546	1440	R	158.3346
BB0820Q	105.2555	1440	L	151.5679
BB0821Q	99.79947	1440	R	143.7112
BB0822Q	105.1791	1439	L	151.3527
BB0823Q	100.4109	1440	R	144.5917
BB0824Q	104.4154	1440	L	150.3582
BB0824QBLK			R	
BB0825Q	100.679	1438	R	144.7764
BB0826Q	108.9516	1439	L	156.7813
BB0827Q	111.4398	1438	R	160.2505
BB0828Q	111.5942	1438	L	160.4725
BB0829Q	112.3851	1443	R	162.1717
BB0830Q	126.3259	1411	L	178.2459
BB0831Q	116.8799	1442	R	168.5409
BB0831QBLK			L	
BB0901Q	125.1563	1440	L	180.2251
BB0902Q	118.1167	1440	R	170.088
BB0903Q	124.5847	1440	L	179.402
BB0904Q	117.9577	1440	R	169.8591
BB0905Q	125.2379	1442	L	180.593
BB0906Q	116.6449	1438	R	167.7353
BB0907Q	124.2456	1440	L	178.9137
BB0908Q	116.6828	1440	R	168.0232
BB0909Q	123.5752	1440	L	177.9483

BB0909QBLK			R	
BB0910Q	117.9418	1440	R	169.8362
BB0911Q	124.6281	1440	L	179.4645
BB0912Q	117.912	1440	R	169.7932
BB0913Q	124.4717	1440	L	179.2392
BB0914Q	118.0206	1440	R	169.9497
BB0914QBLK			L	
BB0915Q	125.4268	1440	L	180.6146
BB0916Q	117.5258	1440	R	169.2371
BB0917Q	124.6161	1432	L	178.4502
BB0918Q	117.3027	1444	R	169.385
BB0919Q	125.2318	1433	L	179.4571
BB0920Q	116.9178	1446	R	169.0631
BB0921Q	123.7392	1434	L	177.442
BBC921QBLK			R	
BB0922Q	117.6427	1449	R	170.4643
BB0923Q	125.644	1441	L	181.0529
BB0924Q	118.3256	1439	R	170.2705
BB0925Q	123.7972	1444	L	178.7631
BB0926Q	117.6083	1438	R	169.1207
BB0927Q	124.5434	1444	L	179.8406
BB0928Q	116.3706	1435	R	166.9919
BB0928QBLK			L	
BB0929Q	125.0054	1440	L	180.0078
BB0930Q	120.0388	1422	R	170.6952
BB1001Q	123.4228	1439	L	177.6054
BB1002Q	124.076	1442	R	178.9176
BB1003Q	123.0132	1436	L	176.6469
BB1004Q	124.2699	1442	R	179.1971
BB1004QBLK			L	
BB1005QBLK			R	
BB1005Q	122.8573	1431	L	175.8088
BB1006Q	123.9046	1439	R	178.2987
BB1007Q	121.6482	1441	L	175.2951
BB1008Q	123.3485	1441	R	177.7452
BB1009Q	122.4398	1434	L	175.5786
BB1010Q	123.6052	1438	R	177.7443
BB1011Q	118.7779	1443	L	171.3966
BB1012Q	123.3863	1442	R	177.9231
BB1012QBLK			L	
BB1013Q	122.6284	1437	L	176.217
BB1014Q	124.1703	1442	R	179.0536
BB1015Q	122.4398	1439	L	176.1908
BB1016Q	122.0625	1445	R	176.3803
BB1017Q	121.3456	1430	L	173.5242
BB1018Q	124.0999	1443	R	179.0761
BB1019Q	122.1379	1444	L	176.3672
BB1019QBLK			R	
BB1020Q	123.798	1438	R	178.0216
BB1021Q	123.3038	1441	L	177.6808
BB1022Q	123.1867	1494	R	184.0409
BB1023Q	122.9349	1389	L	170.7566

BB1024Q	122.9329	1436	R	176.5316
BB1025Q	122.4039	1441	L	176.384
BB1026Q	124.6482	1440	R	179.4935
BB1026QBLK			L	
BB1027Q	122.7793	1440	L	176.8023
BB1028Q	123.9112	1440	R	178.4322
BB1029Q	121.7996	1438	L	175.1478
BB1030Q	123.0084	1441	R	177.2552
BB1031Q	123.0106	1438	L	176.8892

Appendix B – IDL codes

B1: Code used for plotting trajectories

```
pro trajectoryOCBorderSA

; first plot the map

device, decompose=0

TvLCT,255,255,0,17
red = [0,0.75,0.5,0,0,0,0,0,.7,1,1,1,1,1,1]
green = [0,0.5,0,0,0.5,1,1,1,1,1,.75,.38,0,0,1]
blue = [0,1,1,1,1,1,0.6,0,0,0,0,.38,.38,0,1]

tvlct,red*255,green*255,blue*255

WINDOW,0, XSIZE=900,YSIZE=600
MAP_SET,/CONTINENT,/USA,LIMIT=[17,-111,38,-80]

Lats=[37]
Lons=[-105]
Title=['OC Trajectories - BorderSA']
XYOUTS,LONS,LATS,title,COLOR=9, $
  CHARTHICK=2,CHARSIZE=3,ALIGN=0

LATS=[29.30]
LONS=[-103.12]
CITIES=['BigBend']
PLOTS,LONS,LATS,PSYM=5,SYMSIZE=.8,COLOR=13
LATS=[29.3]
LONS=[-103.6]
XYOUTS,LONS,LATS,CITIES,COLOR=13, $
  CHARTHICK=1,CHARSIZE=.9,ALIGN=1

LATS=[25.9]
LONS=[-97.26]
CITIES=['Brownsville']
PLOTS,LONS,LATS,PSYM=5,SYMSIZE=.8,COLOR=13
LATS=[25.54]
LONS=[-97]
XYOUTS,LONS,LATS,CITIES,COLOR=13, $
  CHARTHICK=1,CHARSIZE=.9,ALIGN=0
```

LATS=[29.58]
LONS=[-95.21]
CITIES=['Houston']
PLOTS,LONS,LATS,PSYM=5,SYMSIZE=.8,COLOR=13
Lats=[30]
Lons=[-96]
XYOUTS,LONS,LATS,CITIES,COLOR=13, \$
 CHARTHICK=1,CHARSIZE=.9,ALIGN=0

LATS=[22.54]
LONS=[-102.41]
CITIES=['Ciudad de Mexico']
PLOTS,LONS,LATS,PSYM=5,SYMSIZE=.8,COLOR=13
XYOUTS,LONS,LATS,CITIES,COLOR=13, \$
 CHARTHICK=1,CHARSIZE=.9,ALIGN=1

LATS=[25.52]
LONS=[-100.14]
CITIES=['Monterrey']
PLOTS,LONS,LATS,PSYM=5,SYMSIZE=.8,COLOR=13
LATS=[25.52]
LONS=[-100.6]
XYOUTS,LONS,LATS,CITIES,COLOR=13, \$
 CHARTHICK=1,CHARSIZE=.9,ALIGN=1

LATS=[29.32]
LONS=[-98.28]
CITIES=['San Antonio']
PLOTS,LONS,LATS,PSYM=5,SYMSIZE=.8,COLOR=13
LATS=[29.5]
LONS=[-98.28]
XYOUTS,LONS,LATS,CITIES,COLOR=13, \$
 CHARTHICK=1,CHARSIZE=.9,ALIGN=.5

LATS=[28.23]
LONS=[-100.68]
CITIES=['El Carbon']
PLOTS,LONS,LATS,PSYM=1,SYMSIZE=.8,COLOR=13
Lats=[27.8]
Lons=[-101]
XYOUTS,LONS,LATS,CITIES,COLOR=13, \$
 CHARTHICK=1,CHARSIZE=.9,ALIGN=1

LATS=[32.44]
LONS=[-96.58]
CITIES=['Dallas']
PLOTS,LONS,LATS,PSYM=5,SYMSIZE=.8,COLOR=13
Lats=[32.6]
Lons=[-96.58]
XYOUTS,LONS,LATS,CITIES,COLOR=13, \$
 CHARTHICK=1,CHARSIZE=.9,ALIGN=1

LATS=[27.45]
LONS=[-97.3]
CITIES=['Padre Island']
PLOTS,LONS,LATS,PSYM=5,SYMSIZE=.8,COLOR=13

Lats=[27]
Lons=[-97.3]
XYOUTS,LONS,LATS,CITIES,COLOR=13, \$
CHARTHICK=1,CHARSIZE=.9,ALIGN=0

LATS=[31.72]
LONS=[-96.11]
;CITIES=['BB Plant']
PLOTS,LONS,LATS,PSYM=1,SYMSIZE=.8,COLOR=13
;LATS=[31.72]
;LONS=[-96.7]
;XYOUTS,LONS,LATS,CITIES,COLOR=13, \$
; CHARTHICK=1,CHARSIZE=.9,ALIGN=1

LATS=[32.47]
LONS=[-93.82]
CITIES=['Shreveport']
PLOTS,LONS,LATS,PSYM=5,SYMSIZE=.8,COLOR=13
XYOUTS,LONS,LATS,CITIES,COLOR=13, \$
CHARTHICK=1,CHARSIZE=.9,ALIGN=0

Lats=[28.86]
Lons=[-100.57]
Cities=['Eagle Pass']
Plots,lons,lats,psym=5,symsize=.8,color=13
XYOUTS,LONS,LATS,CITIES,COLOR=13, \$
CHARTHICK=1,CHARSIZE=.9,ALIGN=0

LATS=[30.391]
LONS=[-102.285]
CITIES=['Western Gas Resources']
PLOTS,LONS,LATS,PSYM=1,SYMSIZE=.8,COLOR=13

LATS=[35.429]
LONS=[-101.214]
CITIES=['Phillips 66']
PLOTS,LONS,LATS,PSYM=1,SYMSIZE=.8,COLOR=13

LATS=[30.223]
LONS=[-101.504]
CITIES=['Altura Energy']
PLOTS,LONS,LATS,PSYM=1,SYMSIZE=.8,COLOR=13

LATS=[29.442]
LONS=[-95.0025]
CITIES=['Exxon']
PLOTS,LONS,LATS,PSYM=1,SYMSIZE=.8,COLOR=13

LATS=[29.53]
LONS=[-93.573]
CITIES=['Motiva']
PLOTS,LONS,LATS,PSYM=1,SYMSIZE=.8,COLOR=13

LATS=[30.035]


```

LONS=[-94.041]
CITIES=['Mobil']
PLOTS,LONS,LATS,PSYM=1,SYMSIZE=.8,COLOR=13

LATS=[32.1554]
LONS=[-94.34]
CITIES=['Texas Utilities']
PLOTS,LONS,LATS,PSYM=1,SYMSIZE=.8,COLOR=13

LATS=[33.055]
LONS=[-95.02]
CITIES=['Texas Utilities']
PLOTS,LONS,LATS,PSYM=1,SYMSIZE=.8,COLOR=13

LATS=[31.492]
LONS=[-96.032]
CITIES=['Texas Utilities']
PLOTS,LONS,LATS,PSYM=1,SYMSIZE=.8,COLOR=13

LATS=[29.472]
LONS=[-95.252]
CITIES=['Reliant']
PLOTS,LONS,LATS,PSYM=1,SYMSIZE=.8,COLOR=13

LATS=[30.336]
LONS=[-97.041]
CITIES=['Aluminum Co']
PLOTS,LONS,LATS,PSYM=1,SYMSIZE=.8,COLOR=13

LATS=[29.413]
LONS=[-91.211]
CITIES=['Patterson']
PLOTS,LONS,LATS,PSYM=1,SYMSIZE=.8,COLOR=13

; -----
; Now start the section where we overplot traj's onto the map
; open the text file with all dates to map
openr,unit1,'c:\Back trajectories\1000m\OCBorderSA.txt',/get_lun

filename=' '
;start the loop reading days to extract
filecount=0L
while not eof(unit1) do begin
filecount=filecount+1
readf,unit1,filename
colorx=1+filecount

LATS=[37.7]
LONS=[-110.5]
CITIES=['Border SA']
;XYOUTS,LONS,LATS,CITIES,COLOR=13, $
; CHARTHICK=1,CHARSIZE=1.5,ALIGN=0

Lats8=[37.7-(.6*filecount)]
Lons8=[-110.7]
XYOUTS,LONS8,LATS8,filename,COLOR=colorx, $

```

```
CHARTHICK=1,CHARSIZE=1,ALIGN=0
```

```
filename=filename+'.txt'  
openr,unit,'c:\Back trajectories\1000m\' + filename, /get_lun
```

```
cx=0L  
header = ''  
readf,unit,header  
readf,unit,header  
readf,unit,header  
readf,unit,header  
readf,unit,header  
readf,unit,header  
readf,unit,header  
while not eof(unit) do begin  
  readf,unit,format='(a1)',test  
  cx=cx+1L  
endwhile  
close,unit  
free_lun,unit  
print,unit,cx
```

```
openr,5,'c:\Back trajectories\1000m\' + filename
```

```
header = ''  
readf,5,header  
readf,5,header  
readf,5,header  
readf,5,header  
readf,5,header  
readf,5,header  
readf,5,header  
LATS = ftarr(cx)  
LONS = ftarr(cx)  
ix=0L  
while not eof(5) do begin  
  readf,5,a,b,c,d,e,f,g,h,i,j,k,l,m  
  lats(ix) = j  
  lons(ix) = k  
  ix=ix+1  
endwhile  
LONS = -LONS  
print,lats(0),lons(0),ix
```

```
; cut traj to 3 days if it's longer  
dcheck=ftarr(2)  
dcheck(0)=72  
dcheck(1)=cx  
uplim = min(dcheck)  
uplimi=fix(uplim-1)
```

```
;OPLOT,LONS,LATS,PSYM=2,SYMSIZE=.2,color=colorx  
OPLOT,LONS(0:uplimi),LATS(0:uplimi),PSYM=2,SYMSIZE=.3,color=colorx
```

```
;result = cx/24.  
;counter = fix(result)  
;print,counter
```

```

;for jcount = 1,counter do begin
;PLOTS,LONS(23*jcount),LATS(23*jcount),PSYM=2,SYMSIZE=1,color=colorx
;endfor

close,5
endwhile

conc=''
openr,unit1,'c:\Back trajectories\1000m\OCBorderSAconc.txt',/get_lun
filecount=0L
while not eof(unit1) do begin
filecount=filecount+1
colorx=1+filecount
readf,unit1,conc

Lats8=[37.7-(.6*filecount)]
Lons8=[-108]
XYOUTS,LONS8,LATS8,conc,COLOR=colorx, $
  CHARTHICK=1,CHARSIZE=1,ALIGN=0

endwhile


image24 = TVRD(True=1)
image=Color_Quan(image24,1,r,g,b)
write_GIF, 'OCBorderSA.gif,image,r,g,b

close, /all
end

```

Appendix C – Daily Air Mass Trajectories

Daily air mass trajectories were run using the NOAA Hysplit model for each day of the BRAVO study. Trajectories were run at 8 pm CST, the middle of each daily sampling period, from a starting height of 1000m. This appendix shows each daily trajectory along with the height of the air mass.

 NOAA Air Resources Laboratory
This product was generated by an Internet user on the NOAA Air Resources Laboratory's web site. See the disclaimer for further information. (<http://www.arl.noaa.gov/hqdy/trajectories.html>)

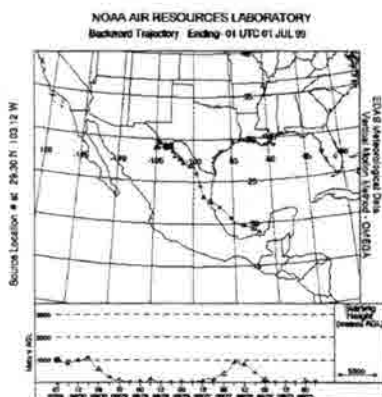



Figure C1 Air mass trajectory for Wed 6/30/99

 NOAA Air Resources Laboratory
This product was generated by an Internet user on the NOAA Air Resources Laboratory's web site. See the disclaimer for further information. (<http://www.arl.noaa.gov/hqdy/trajectories.html>)

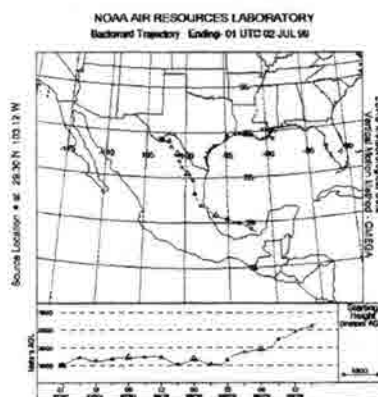


Figure C2 Air mass trajectory for 7/1/99

NOAA AIR RESOURCES LABORATORY
 Backward Trajectory Ending 01 UTC 03 JUL 99

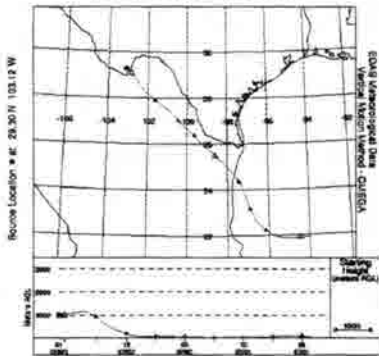


Figure C3 Air mass trajectory for 7/2/99

NOAA AIR RESOURCES LABORATORY
 Backward Trajectory Ending 01 UTC 04 JUL 99

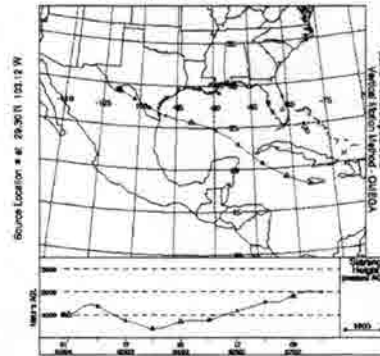


Figure C4 Air mass trajectory for 7/3/99

NOAA AIR RESOURCES LABORATORY
 Backward Trajectory Ending 01 UTC 05 JUL 99

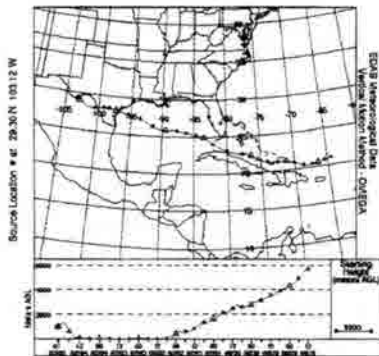


Figure C5 Air mass trajectory for 7/4/99

NOAA AIR RESOURCES LABORATORY
 Backward Trajectory Ending 01 UTC 06 JUL 99

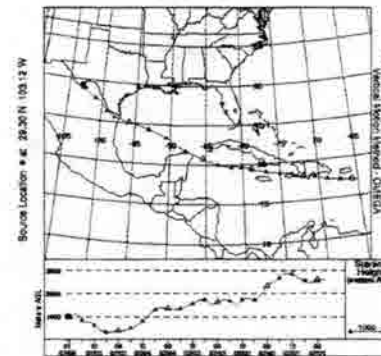


Figure C6 Air mass trajectory for 7/5/99

NOAA AIR RESOURCES LABORATORY
 Backward Trajectory Ending 01 UTC 07 JUL 99

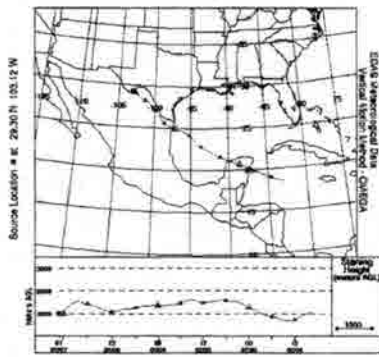


Figure C7 Air mass trajectory for 7/6/99

NOAA AIR RESOURCES LABORATORY
 Backward Trajectory Ending 01 UTC 07 JUL 99

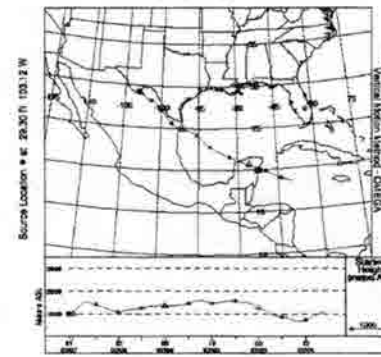


Figure C8 Air mass trajectory for 7/7/99

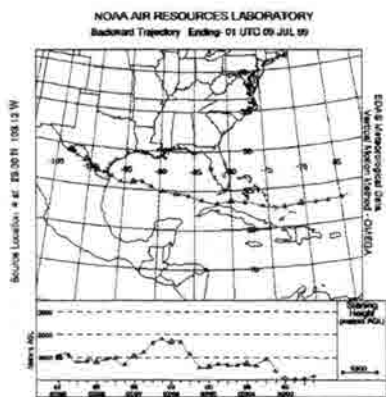


Figure C9 Air mass trajectory for 7/8/99

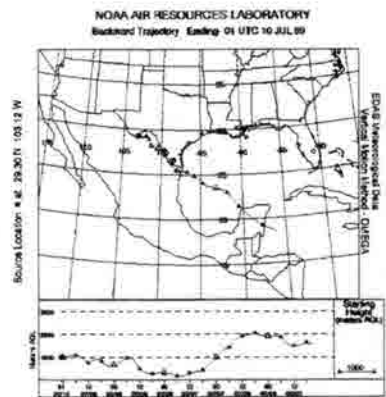


Figure C10 Air mass trajectory for 7/9/99

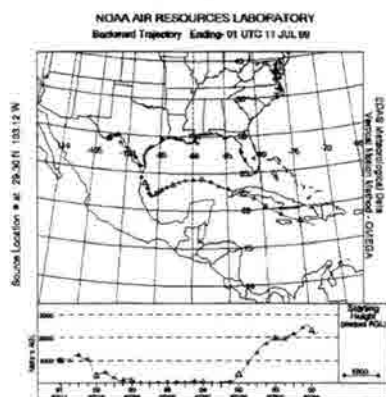


Figure C11 Air mass trajectory for 7/10/99

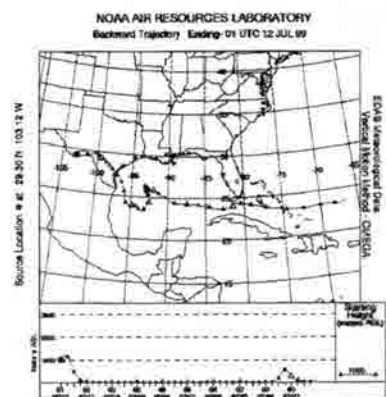


Figure C12 Air mass trajectory for 7/11/99

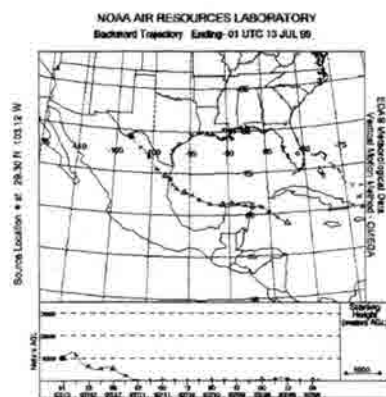


Figure C13 Air mass trajectory for 7/12/99

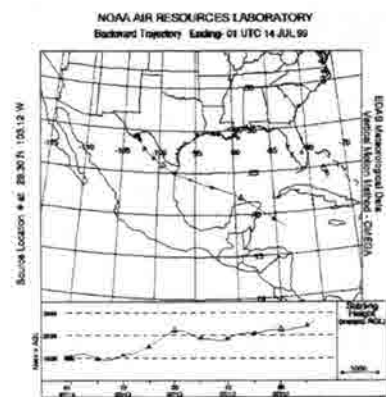


Figure C14 Air mass trajectory for 7/13/99

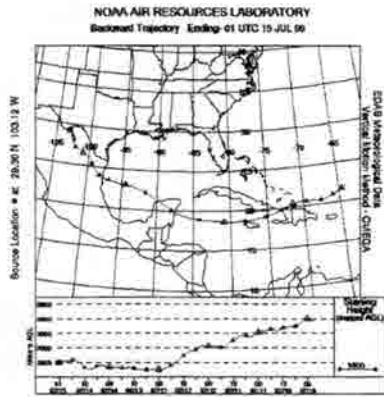


Figure C15 Air mass trajectory for 7/14/99

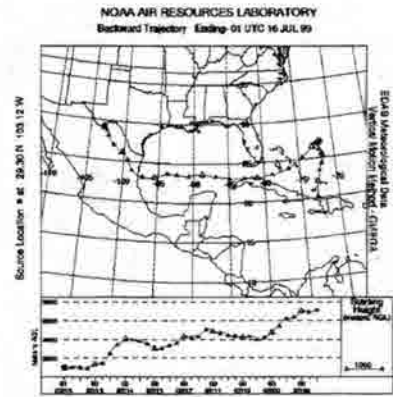


Figure C16 Air mass trajectory for 7/15/99

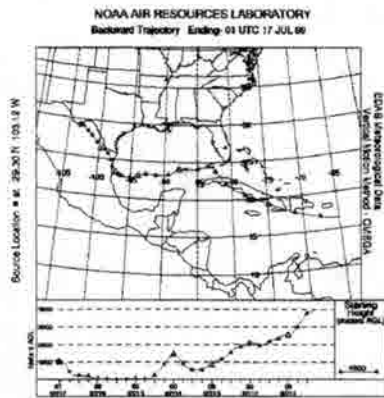


Figure C17 Air mass trajectory for 7/16/99

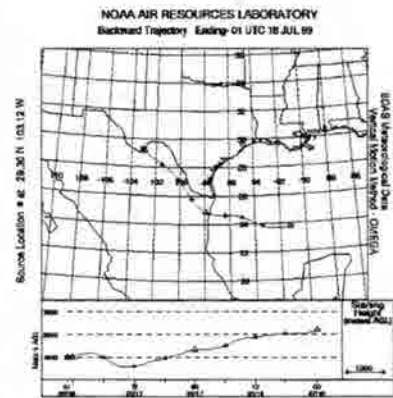


Figure C18 Air mass trajectory for 7/17/99

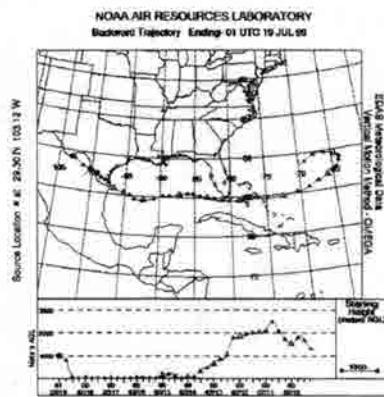


Figure C19 Air mass trajectory for 7/18/99

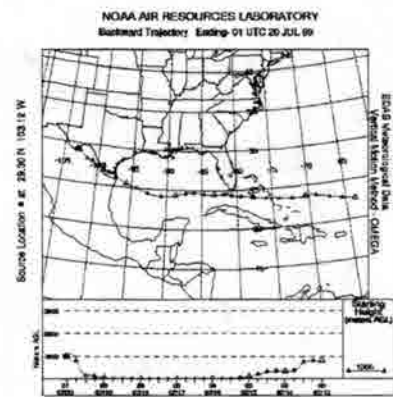


Figure C20 Air mass trajectory for 7/19/99

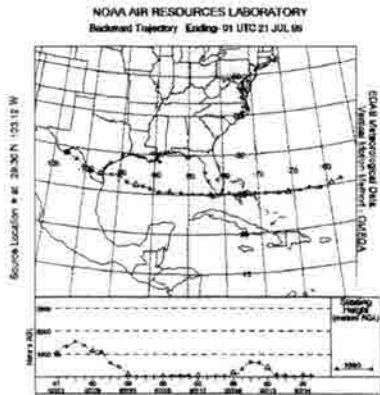


Figure C21 Air mass trajectory for 7/20/99

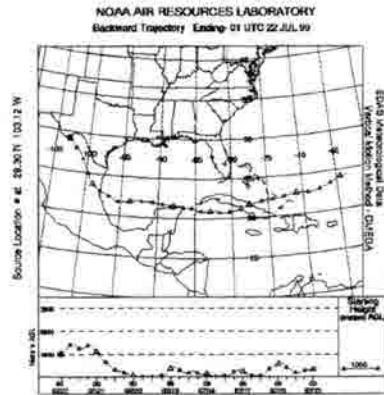


Figure C22 Air mass trajectory for 7/21/99

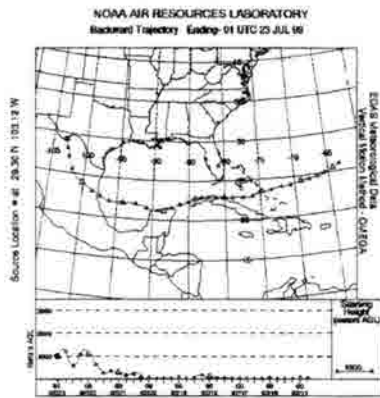


Figure C23 Air mass trajectory for 7/22/99

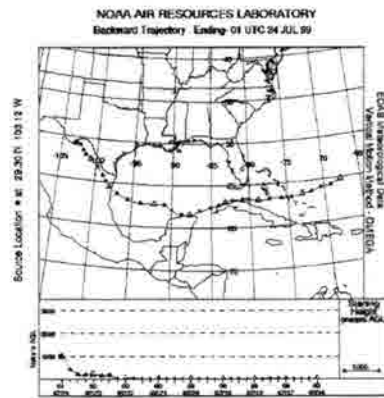


Figure C24 Air mass trajectory for 7/23/99

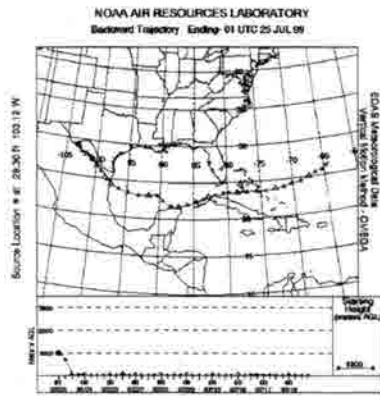


Figure C25 Air mass trajectory for 7/24/99

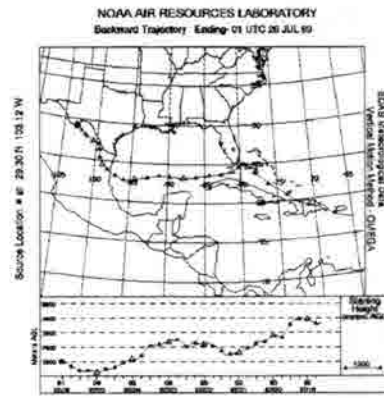


Figure C26 Air mass trajectory for 7/25/99

NOAA Air Resources Laboratory
 This product was produced by an Internet user at the NOAA Air Resources Laboratory's web site. See the disclaimer for further information: <http://www.arl.noaa.gov/ready/sta/sta.html>.

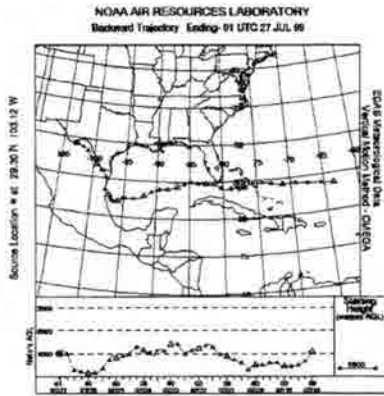


Figure C27 Air mass trajectory for 7/26/99

NOAA Air Resources Laboratory
 This product was produced by an Internet user at the NOAA Air Resources Laboratory's web site. See the disclaimer for further information: <http://www.arl.noaa.gov/ready/sta/sta.html>.

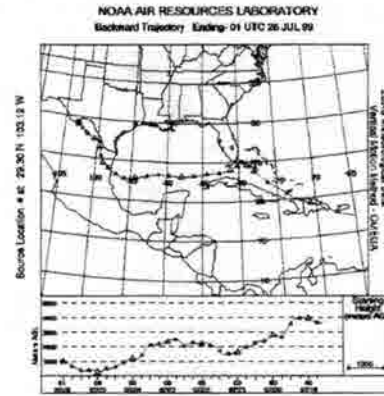


Figure C28 Air mass trajectory for 7/27/99

NOAA Air Resources Laboratory
 This product was produced by an Internet user at the NOAA Air Resources Laboratory's web site. See the disclaimer for further information: <http://www.arl.noaa.gov/ready/sta/sta.html>.

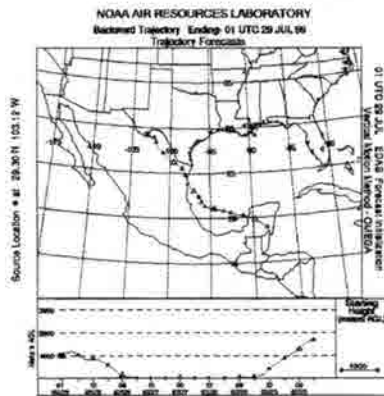


Figure C29 Air mass trajectory for 7/28/99

NOAA Air Resources Laboratory
 This product was produced by an Internet user at the NOAA Air Resources Laboratory's web site. See the disclaimer for further information: <http://www.arl.noaa.gov/ready/sta/sta.html>.

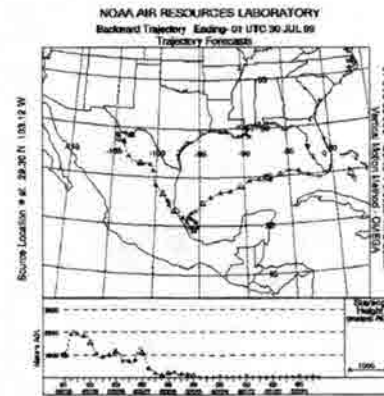


Figure C30 Air mass trajectory for 7/29/99

NOAA Air Resources Laboratory
 This product was produced by an Internet user at the NOAA Air Resources Laboratory's web site. See the disclaimer for further information: <http://www.arl.noaa.gov/ready/sta/sta.html>.

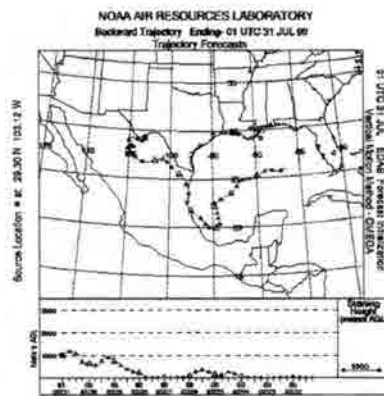


Figure C31 Air mass trajectory for 7/30/99

NOAA Air Resources Laboratory
 This product was produced by an Internet user at the NOAA Air Resources Laboratory's web site. See the disclaimer for further information: <http://www.arl.noaa.gov/ready/sta/sta.html>.

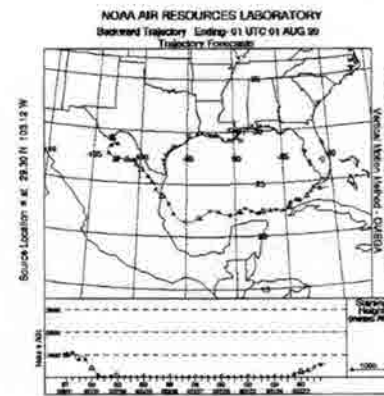


Figure C32 Air mass trajectory for 7/31/99

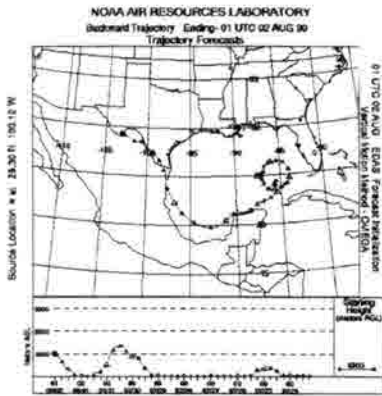


Figure C33 Air mass trajectory for 8/1/99

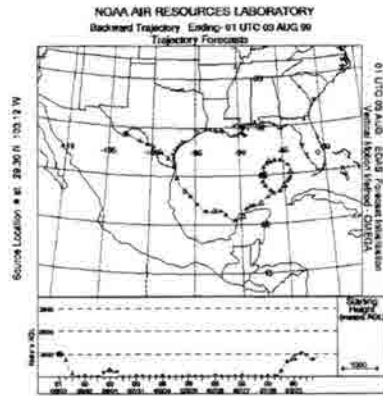


Figure C34 Air mass trajectory for 8/2/99

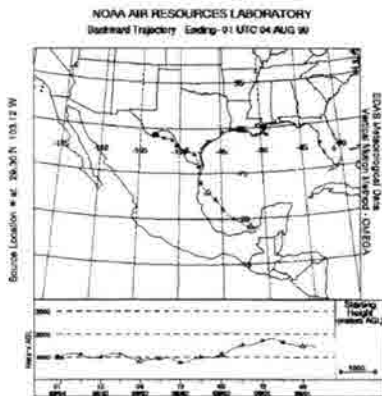


Figure C35 Air mass trajectory for 8/3/99

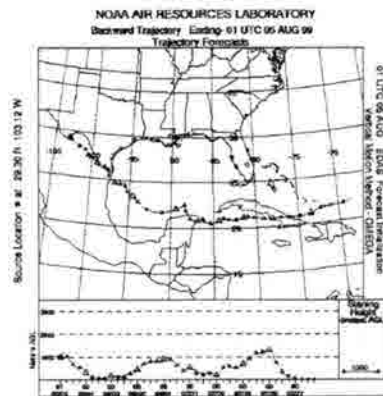


Figure C36 Air mass trajectory for 8/4/99

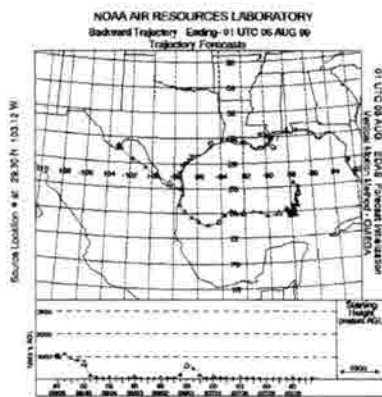


Figure C37 Air mass trajectory for 8/5/99

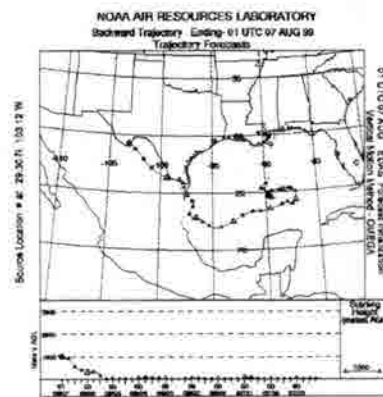


Figure C38 Air mass trajectory for 8/6/99

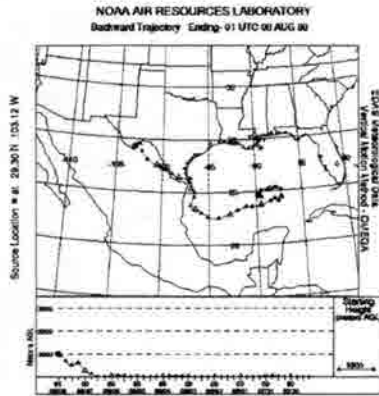


Figure C39 Air mass trajectory for 8/7/99

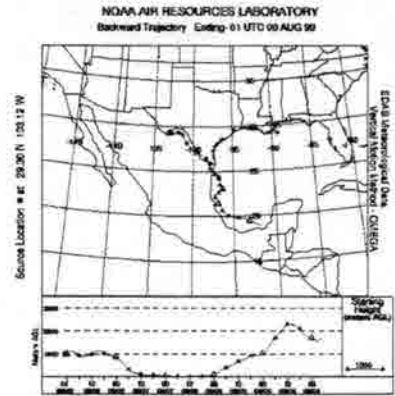


Figure C40 Air mass trajectory for 8/8/99

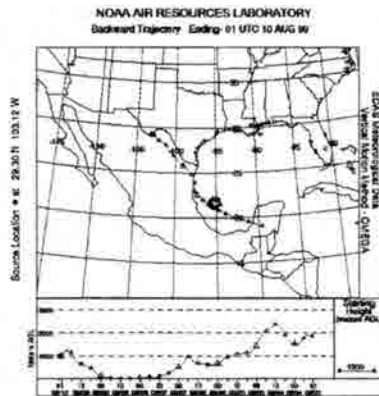


Figure C41 Air mass trajectory for 8/9/99

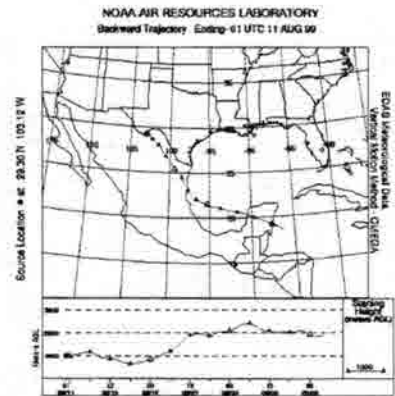


Figure C42 Air mass trajectory for 8/10/99

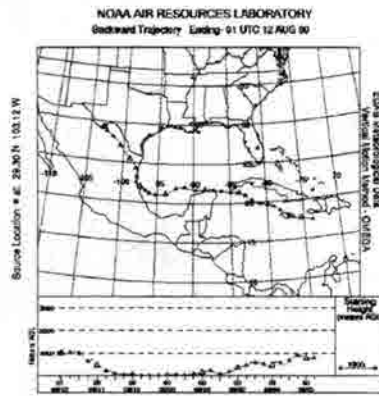


Figure C43 Air mass trajectory for 8/11/99

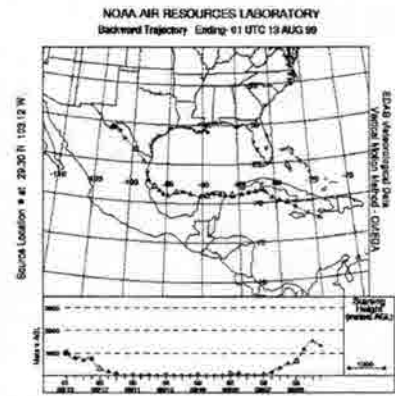


Figure C44 Air mass trajectory for 8/12/99

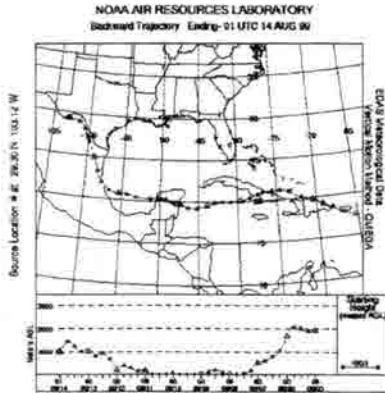


Figure C43 Air mass trajectory for 8/11/99

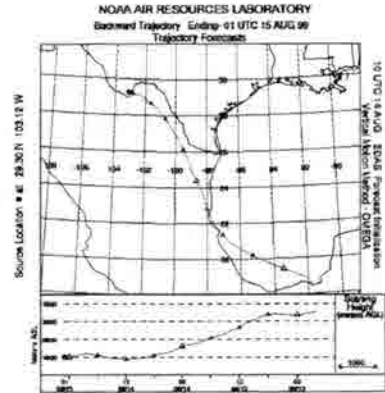


Figure C44 Air mass trajectory for 8/12/99

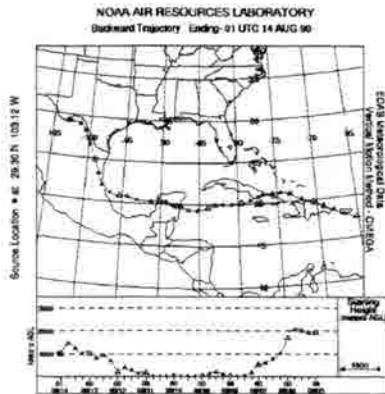


Figure C45 Air mass trajectory for 8/13/99

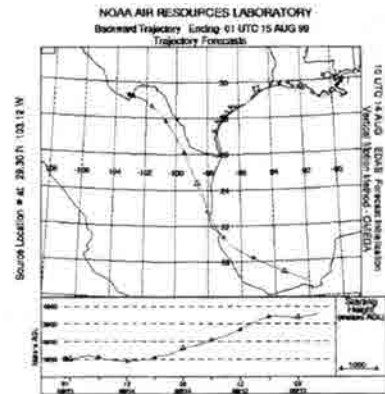


Figure C46 Air mass trajectory for 8/14/99

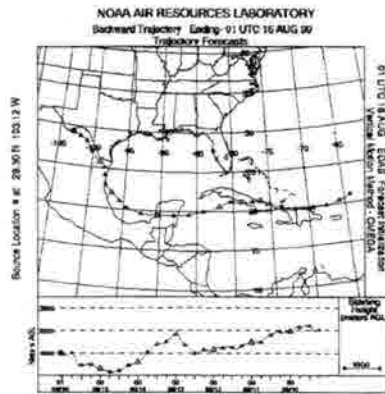


Figure C47 Air mass trajectory for 8/15/99

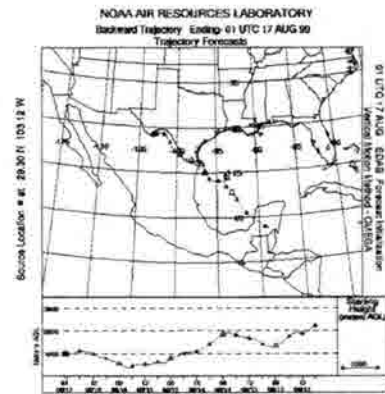


Figure C48 Air mass trajectory for 8/16/99

NOAA Air Resources Laboratory
 This product was produced by an Internet user on the NOAA Air Resources Laboratory's web site. See the disclaimer for further information: <http://www.arl.noaa.gov/help/Disclaimer.html>.

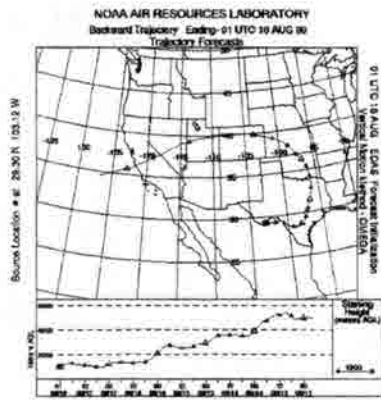


Figure C49 Air mass trajectory for 8/17/99

NOAA Air Resources Laboratory
 This product was produced by an Internet user on the NOAA Air Resources Laboratory's web site. See the disclaimer for further information: <http://www.arl.noaa.gov/help/Disclaimer.html>.

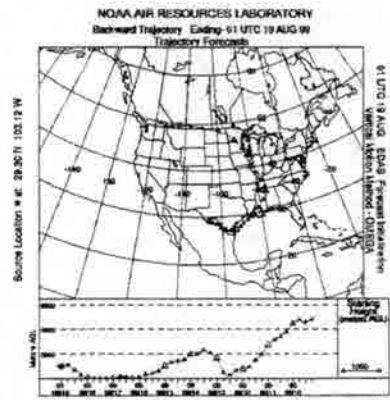


Figure C50 Air mass trajectory for 8/18/99

NOAA Air Resources Laboratory
 This product was produced by an Internet user on the NOAA Air Resources Laboratory's web site. See the disclaimer for further information: <http://www.arl.noaa.gov/help/Disclaimer.html>.

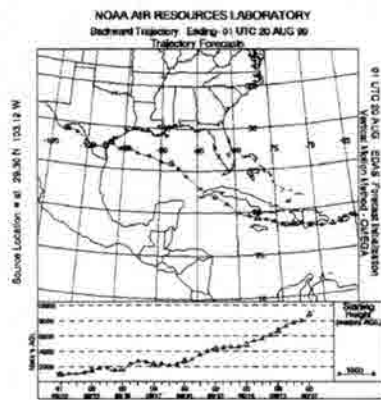


Figure C51 Air mass trajectory for 8/19/99

NOAA Air Resources Laboratory
 This product was produced by an Internet user on the NOAA Air Resources Laboratory's web site. See the disclaimer for further information: <http://www.arl.noaa.gov/help/Disclaimer.html>.

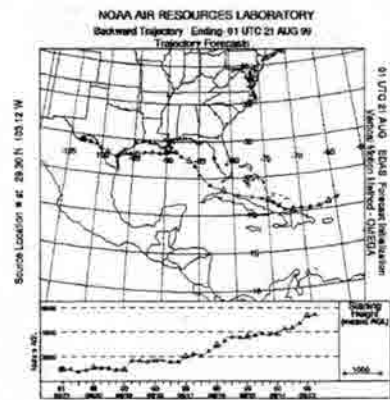


Figure C52 Air mass trajectory for 8/20/99

NOAA Air Resources Laboratory
 This product was produced by an Internet user on the NOAA Air Resources Laboratory's web site. See the disclaimer for further information: <http://www.arl.noaa.gov/help/Disclaimer.html>.

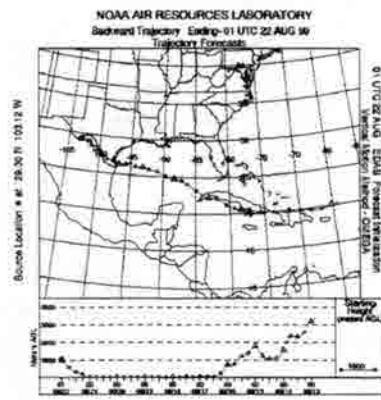


Figure C53 Air mass trajectory for 8/21/99

NOAA Air Resources Laboratory
 This product was produced by an Internet user on the NOAA Air Resources Laboratory's web site. See the disclaimer for further information: <http://www.arl.noaa.gov/help/Disclaimer.html>.

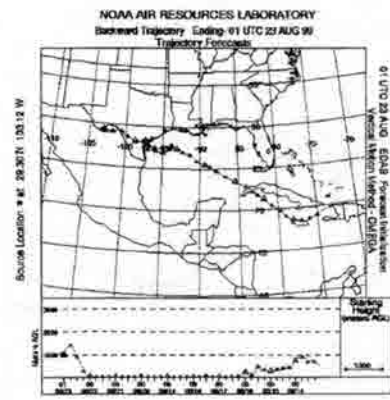


Figure C54 Air mass trajectory for 8/22/99

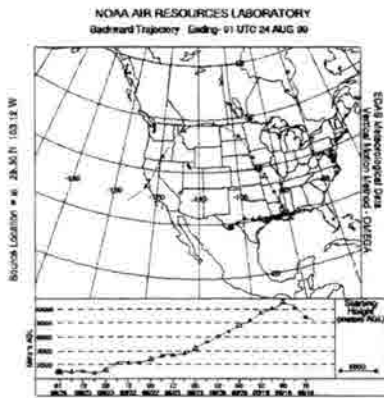


Figure C55 Air mass trajectory for 8/23/99

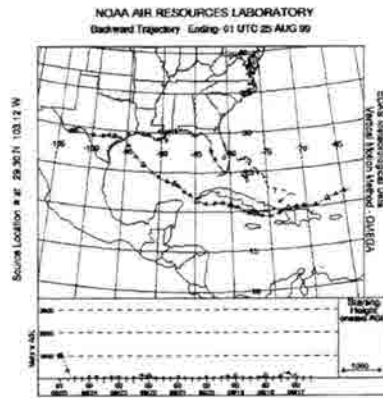


Figure C56 Air mass trajectory for 8/24/99

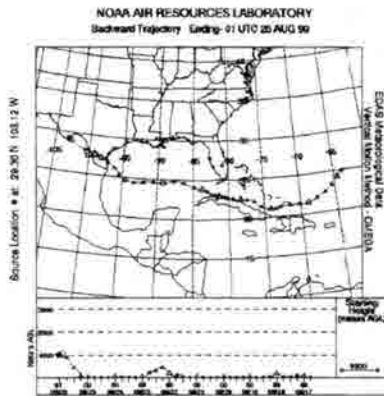


Figure C57 Air mass trajectory for 8/25/99

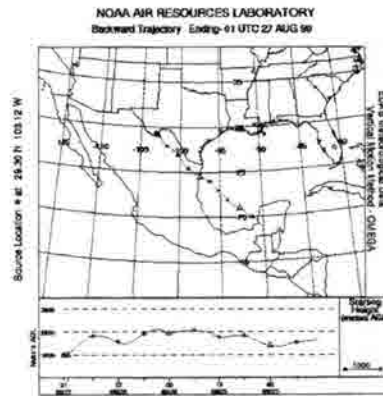


Figure C58 Air mass trajectory for 8/26/99

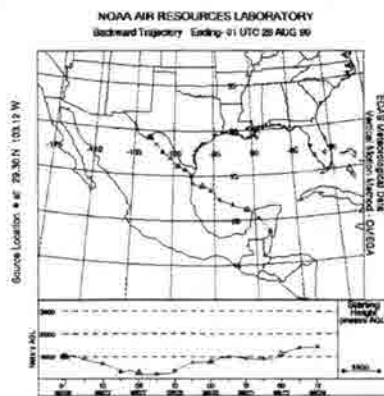


Figure C59 Air mass trajectory for 8/27/99

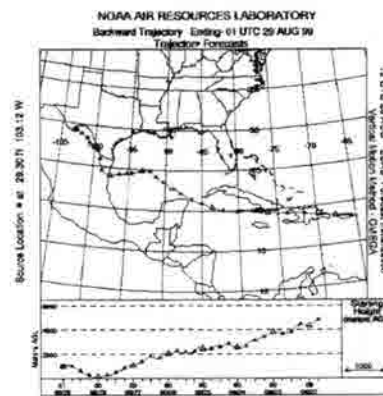


Figure C60 Air mass trajectory for 8/28/99

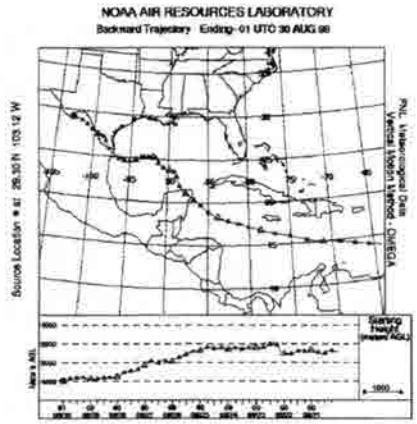


Figure C61 Air mass trajectory for 8/29/99

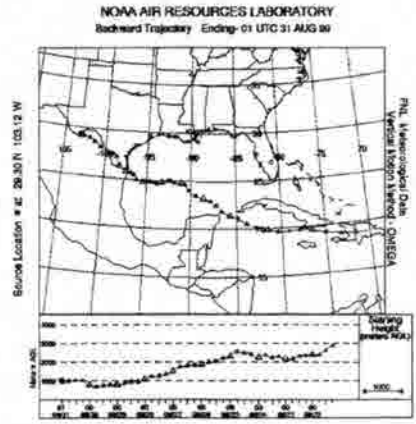


Figure C62 Air mass trajectory for 8/30/99

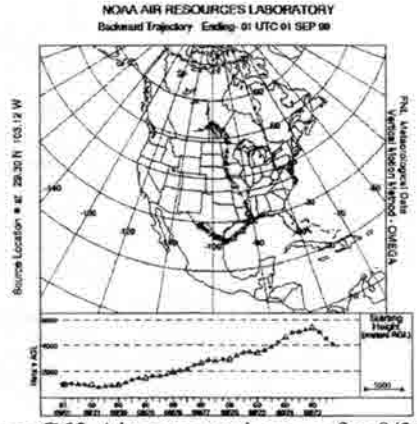


Figure C63 Air mass trajectory for 8/31/99

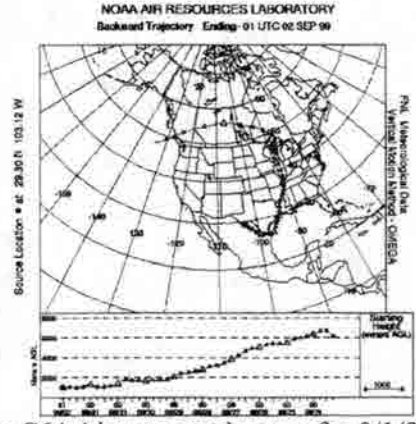


Figure C64 Air mass trajectory for 9/1/99

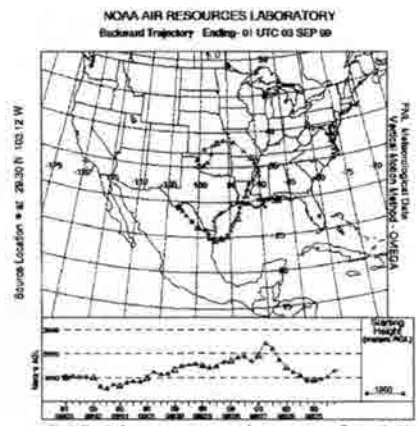


Figure C65 Air mass trajectory for 9/2/99

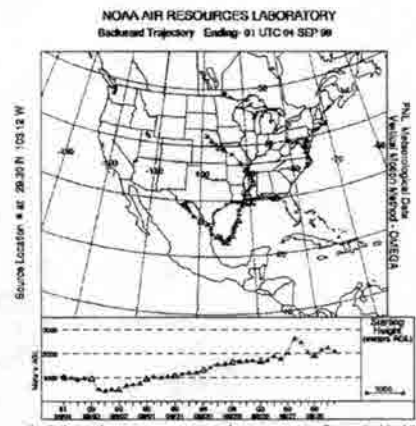


Figure C66 Air mass trajectory for 9/3/99

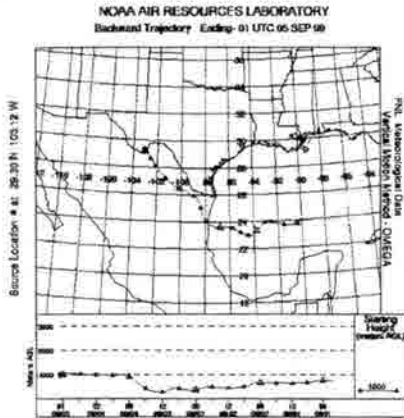


Figure C67 Air mass trajectory for 9/4/99

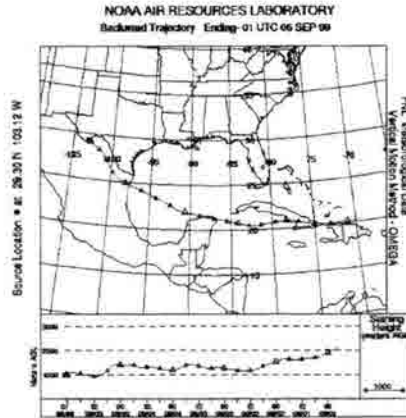


Figure C68 Air mass trajectory for 9/5/99

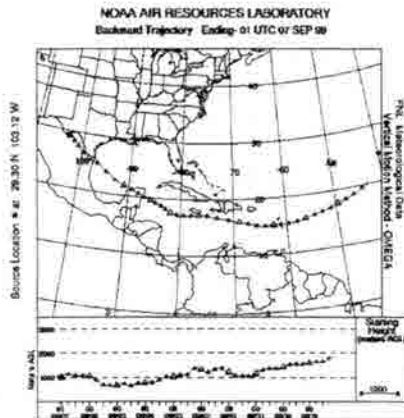


Figure C69 Air mass trajectory for 9/6/99

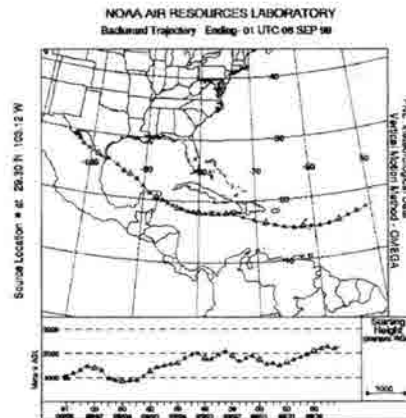


Figure C70 Air mass trajectory for 9/7/99

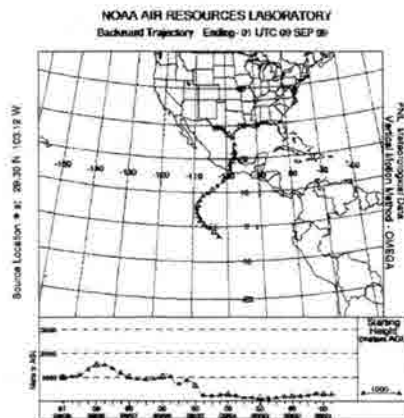


Figure C71 Air mass trajectory for 9/8/99

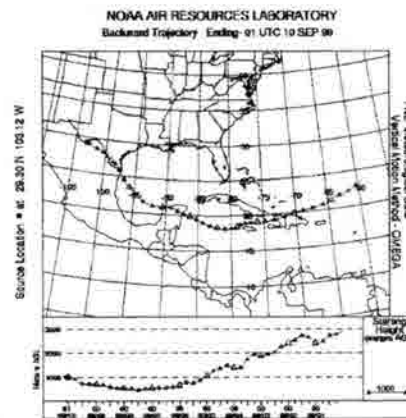


Figure C72 Air mass trajectory for 9/9/99

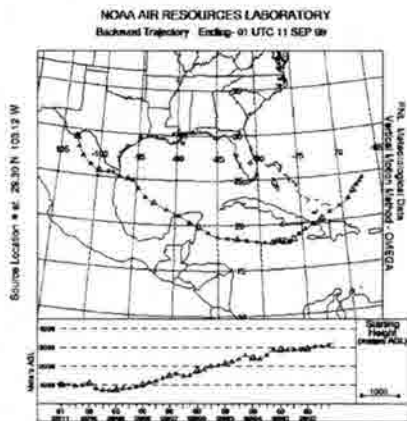


Figure C73 Air mass trajectory for 9/10/99

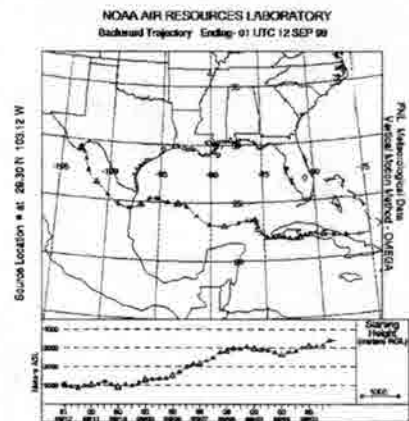


Figure C74 Air mass trajectory for 9/11/99

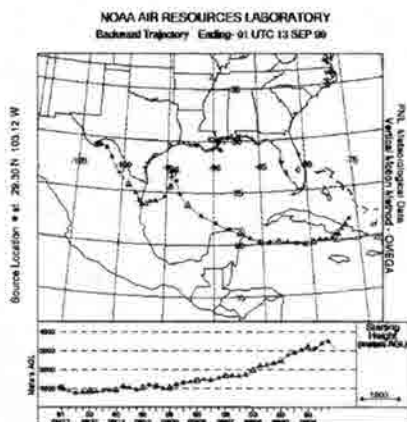


Figure C75 Air mass trajectory for 9/12/99

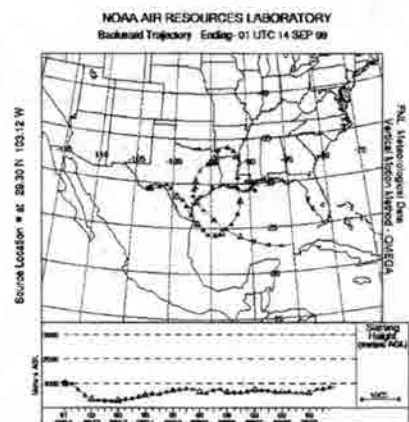


Figure C76 Air mass trajectory for 9/13/99

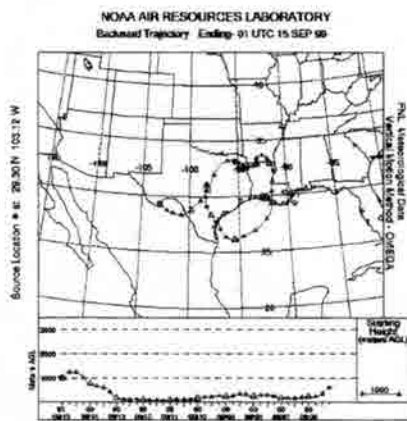


Figure C77 Air mass trajectory for 9/14/99

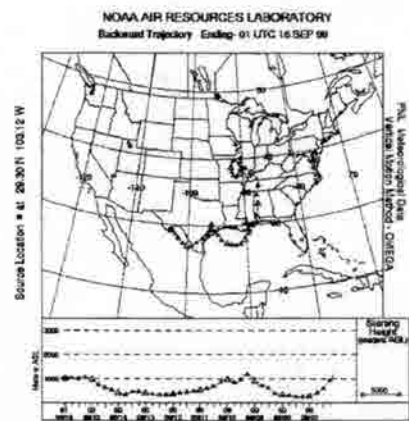


Figure C78 Air mass trajectory for 9/15/99

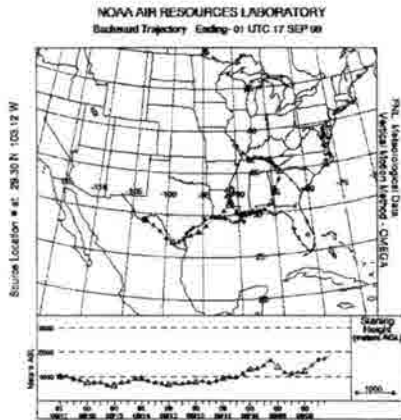


Figure C79 Air mass trajectory for 9/16/99

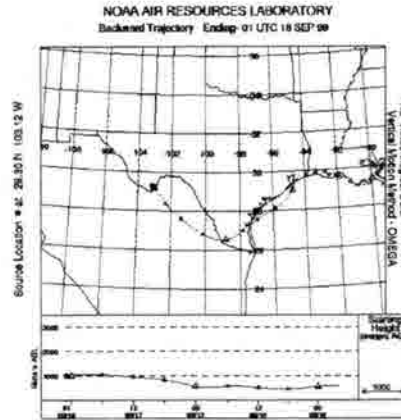


Figure C80 Air mass trajectory for 9/17/99

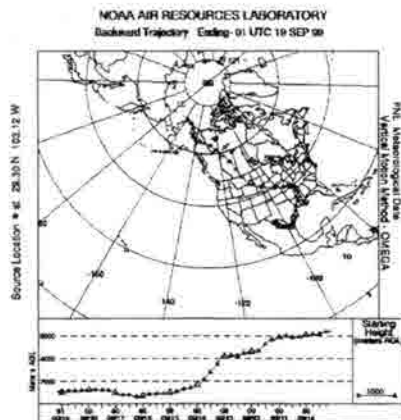


Figure C81 Air mass trajectory for 9/18/99

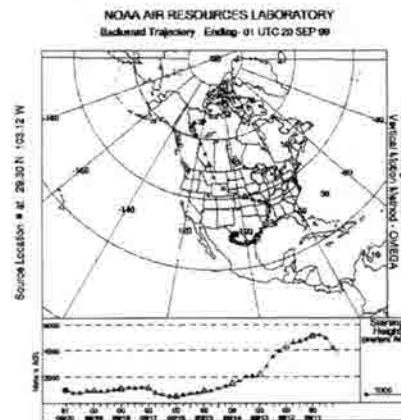


Figure C82 Air mass trajectory for 9/19/99

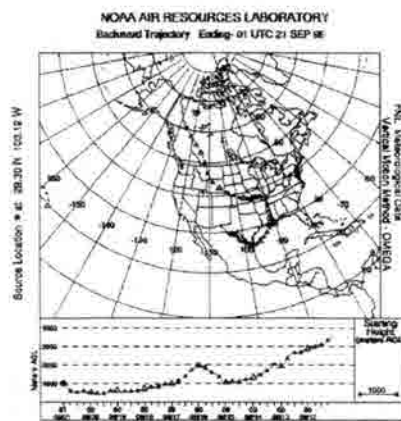


Figure C83 Air mass trajectory for 9/20/99

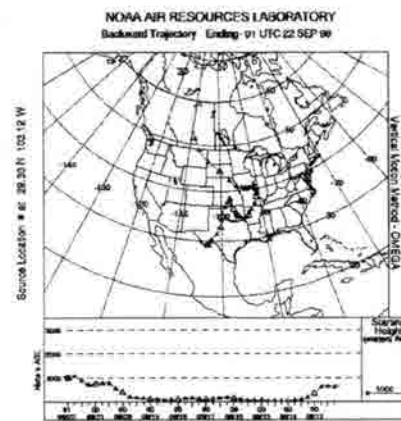


Figure C84 Air mass trajectory for 9/21/99

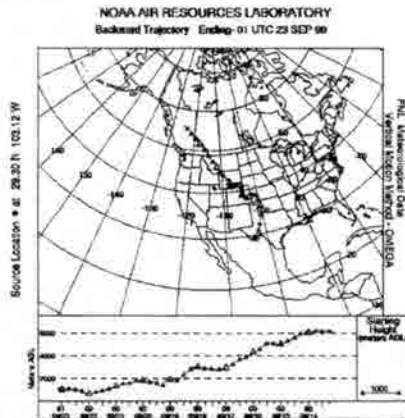


Figure C85 Air mass trajectory for 9/22/99

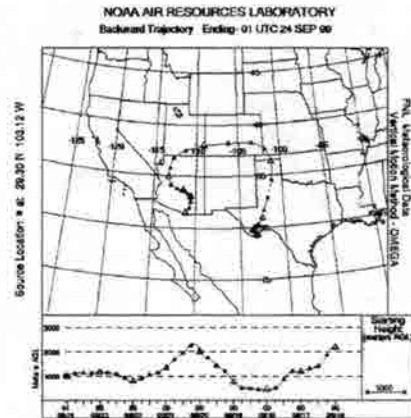


Figure C86 Air mass trajectory for 9/23/99

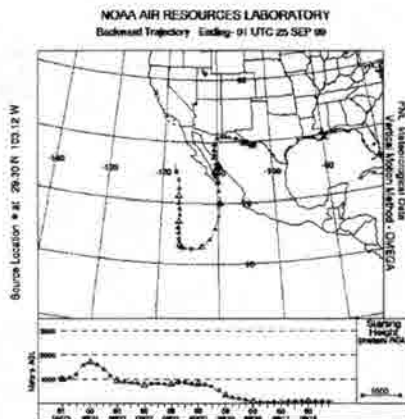


Figure C87 Air mass trajectory for 9/24/99

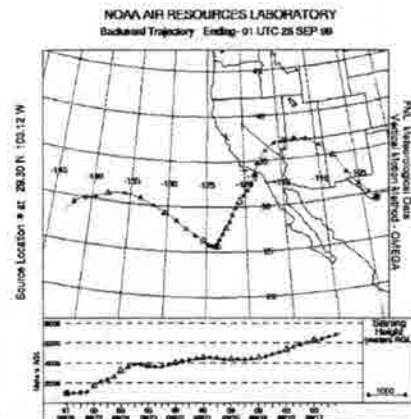


Figure C88 Air mass trajectory for 9/25/99

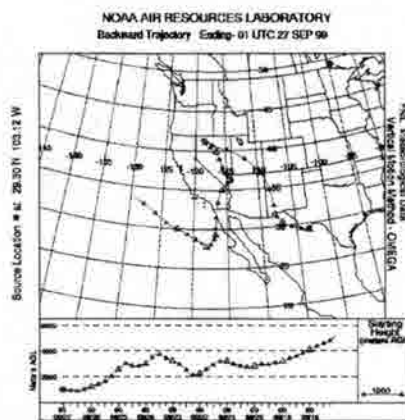


Figure C89 Air mass trajectory for 9/26/99

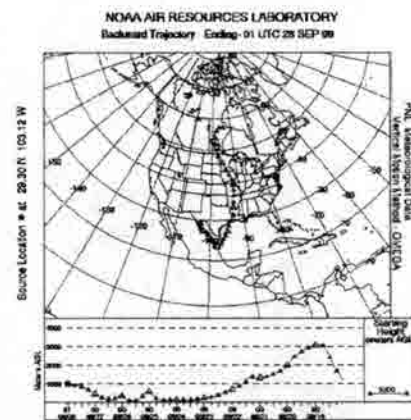


Figure C90 Air mass trajectory for 9/27/99

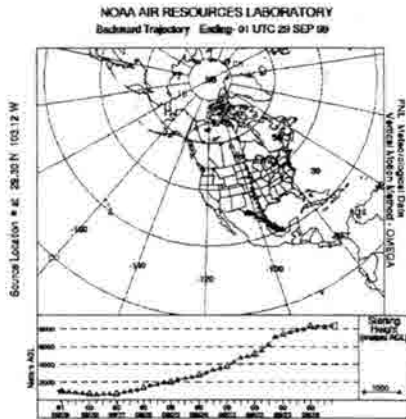


Figure C91 Air mass trajectory for 9/28/99

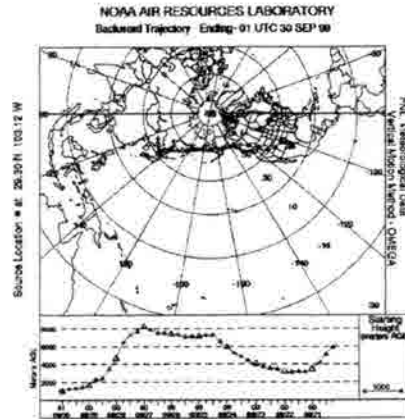


Figure C92 Air mass trajectory for 9/29/99

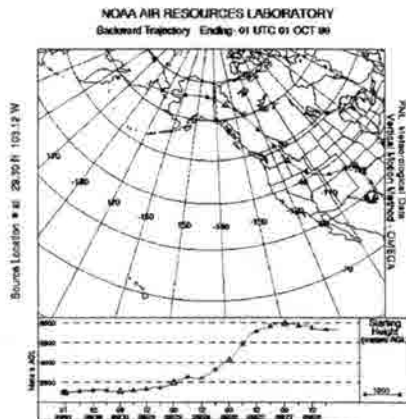


Figure C93 Air mass trajectory for 9/30/99

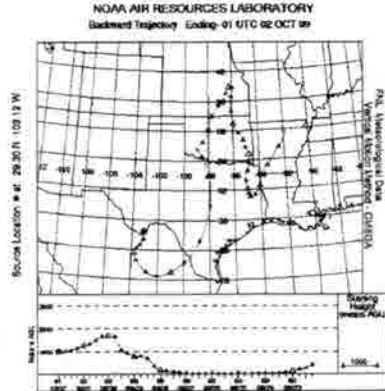


Figure C94 Air mass trajectory for 10/1/99

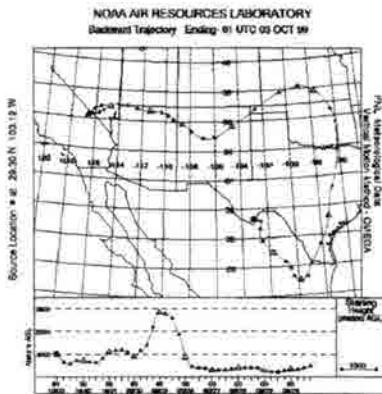


Figure C95 Air mass trajectory for 10/2/99

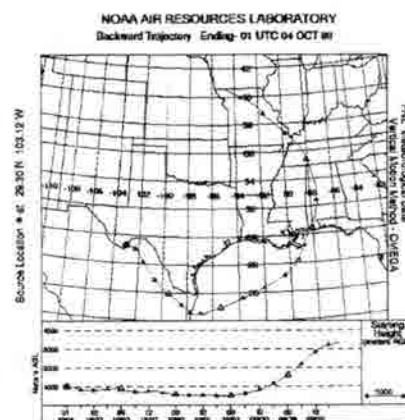


Figure C96 Air mass trajectory for 10/3/99

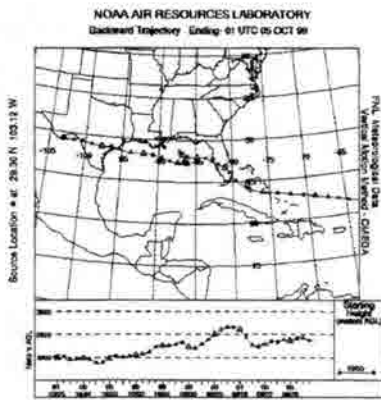


Figure C97 Air mass trajectory for 10/4/99

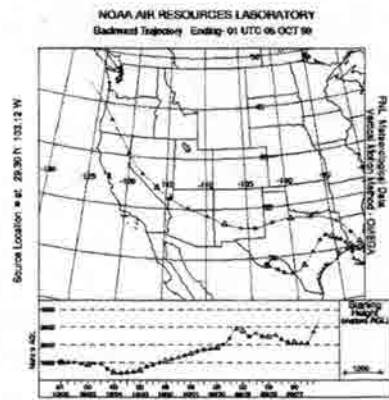


Figure C98 Air mass trajectory for 10/5/99

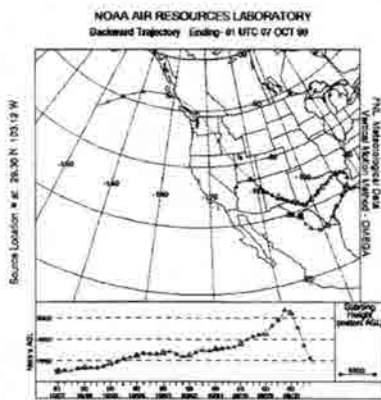


Figure C99 Air mass trajectory for 10/6/99

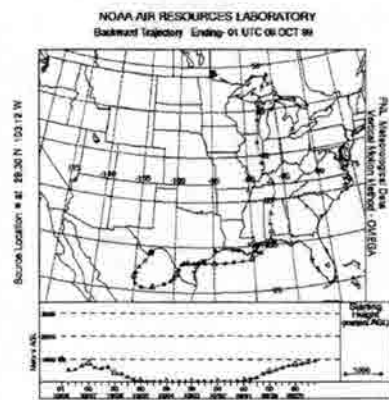


Figure C100 Air mass trajectory for 10/7/99

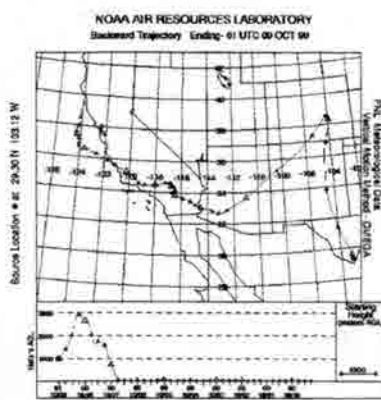


Figure C101 Air mass trajectory for 10/8/99

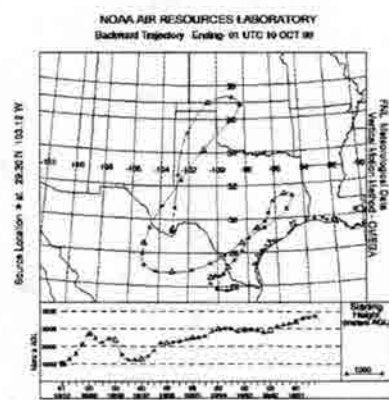


Figure C102 Air mass trajectory for 10/9/99

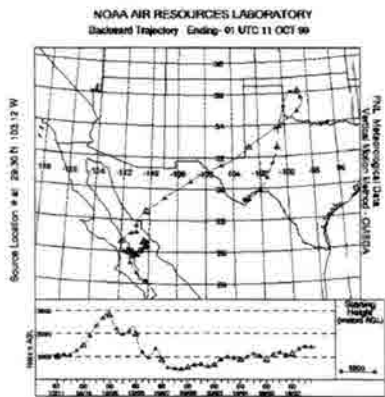


Figure C103 Air mass trajectory for 10/10/99

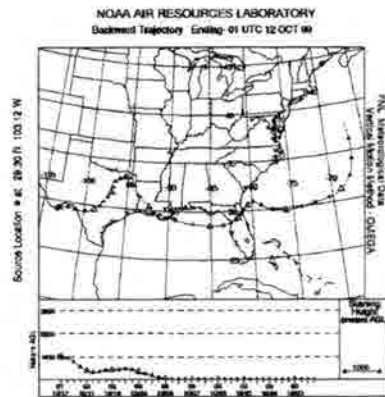


Figure C104 Air mass trajectory for 10/11/99

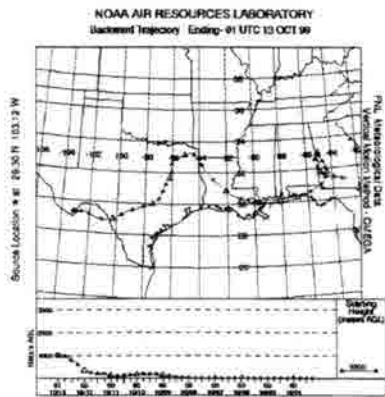


Figure C105 Air mass trajectory for 10/12/99

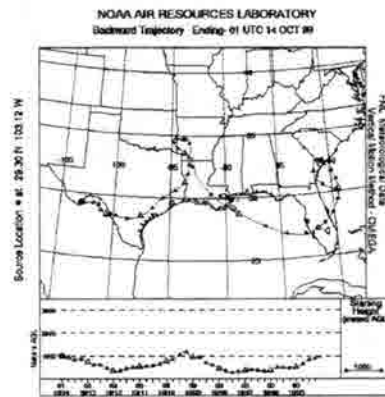


Figure C106 Air mass trajectory for 10/13/99

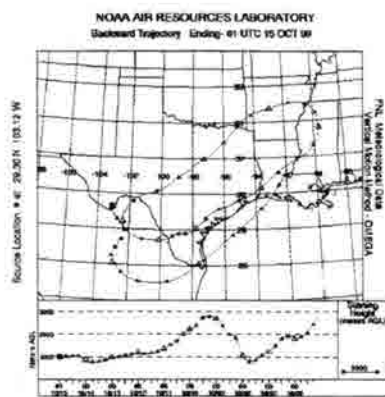


Figure C107 Air mass trajectory for 10/14/99

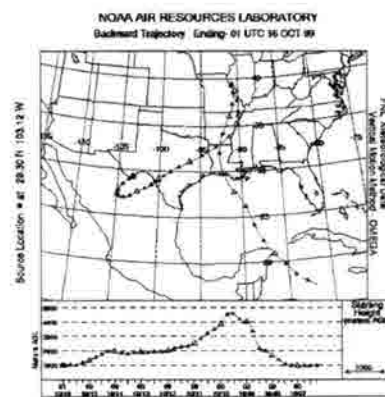


Figure C108 Air mass trajectory for 10/15/99

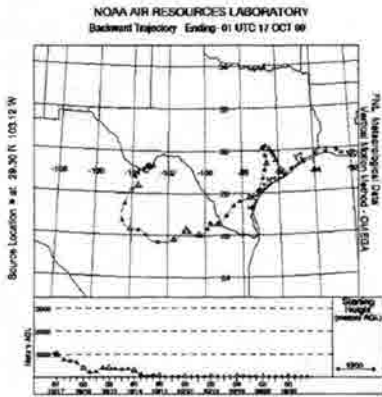


Figure C109 Air mass trajectory for 10/16/99

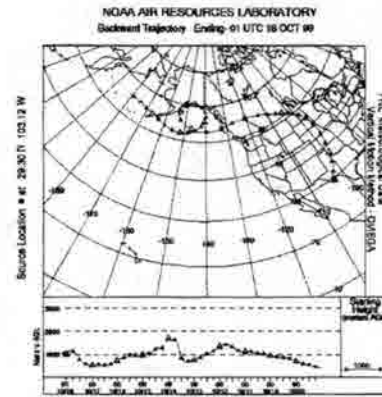


Figure C110 Air mass trajectory for 10/17/99

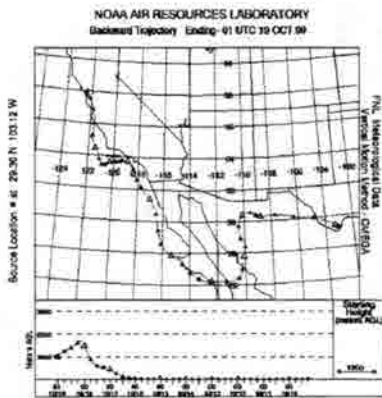


Figure C110 Air mass trajectory for 10/18/99

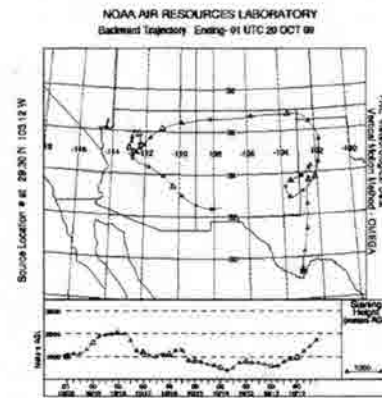


Figure C112 Air mass trajectory for 10/19/99

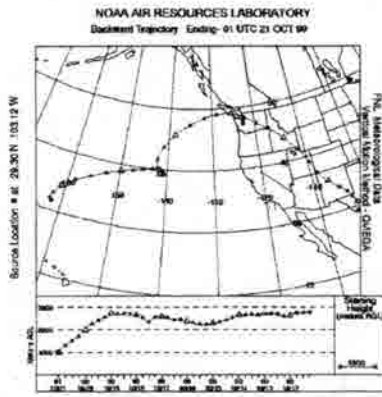


Figure C113 Air mass trajectory for 10/20/99

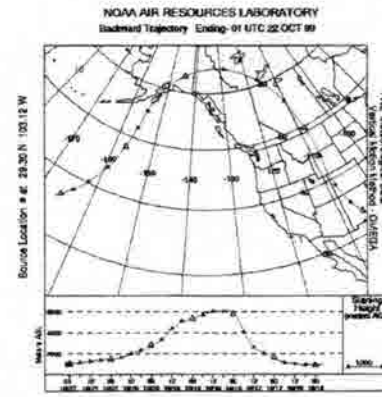


Figure C114 Air mass trajectory for 10/21/99

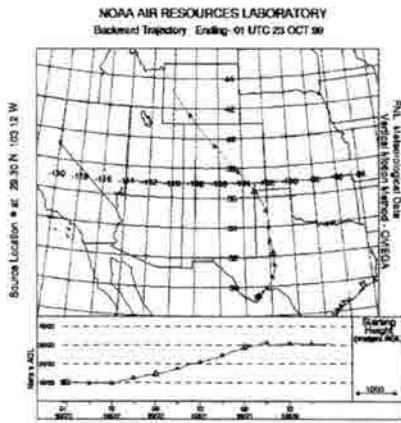


Figure C115 Air mass trajectory for 10/22/99

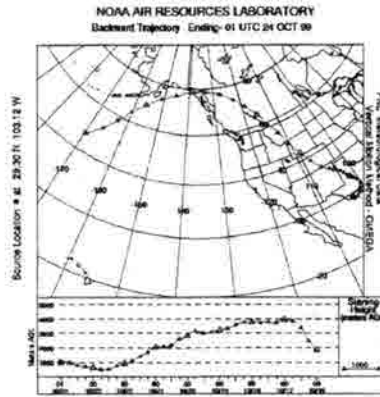


Figure C116 Air mass trajectory for 10/23/99

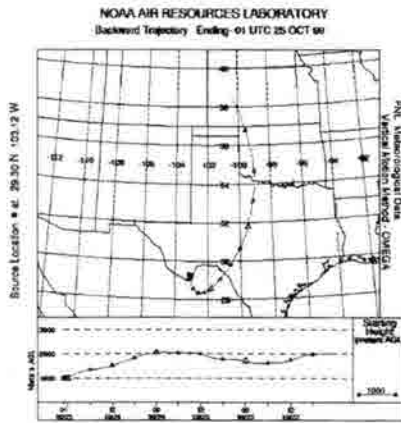


Figure C117 Air mass trajectory for 10/24/99

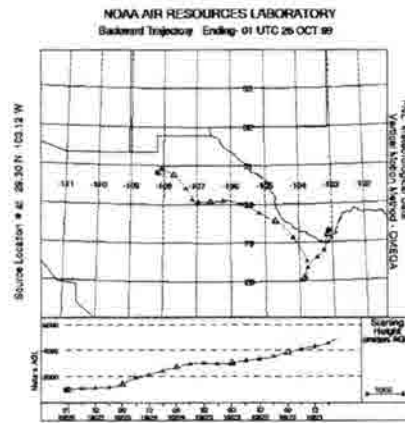


Figure C118 Air mass trajectory for 10/25/99

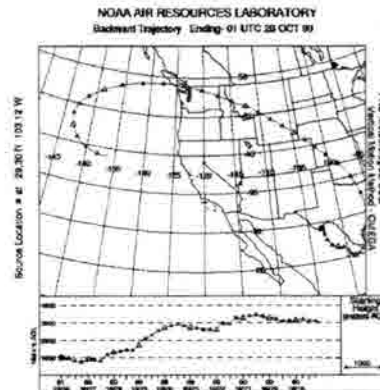
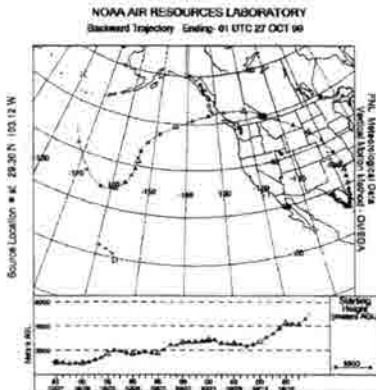


Figure C119 Air mass trajectory for 10/26/99

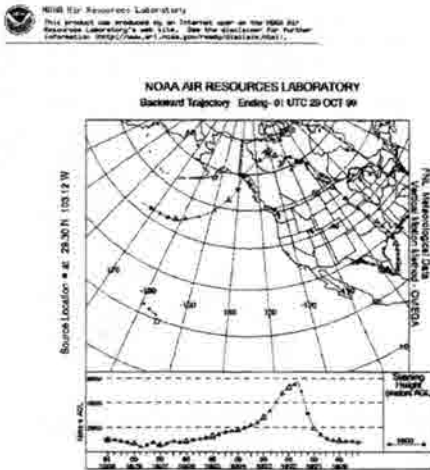


Figure C121 Air mass trajectory for 10/28/99

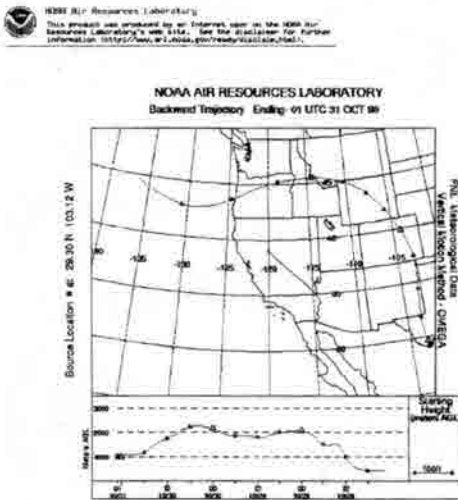


Figure C123 Air mass trajectory for 10/30/99

Figure C120 Air mass trajectory for 10/27/99

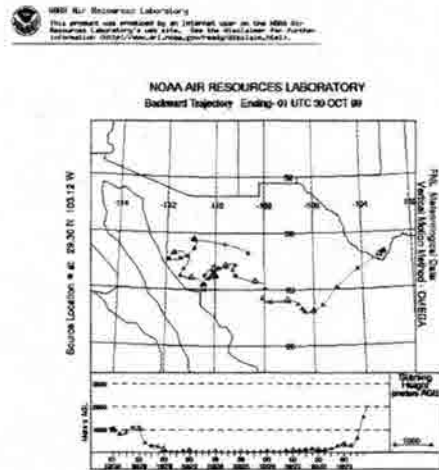


Figure C122 Air mass trajectory for 10/29/99

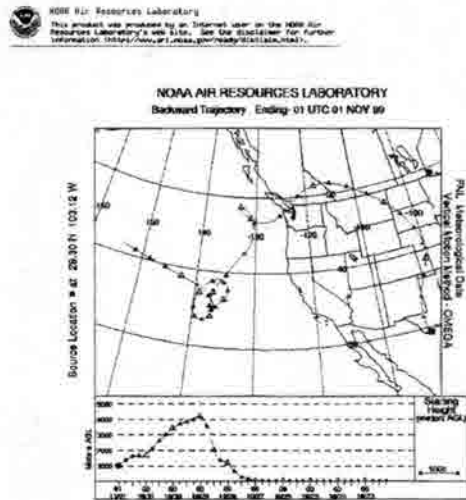


Figure C122 Air mass trajectory for 10/31/99

Appendix D – Error Calculations and Propagation

Error calculations were done starting from the errors involved in quantifying individual compound concentrations, described in section 2.5.3 and 2.5.4. Errors in OC and EC concentrations from the IMPROVE TOR combustion method are described in section 2.3.2. Errors were then propagated through all calculations using formulae stated in table E1. Statistics were also used to compare experimental means, and methods used in this work are detailed in sections 2.5.2, 2.5.3 and 2.5.4.

Table D1 Error propagation in arithmetic calculations (from Skoog et al., 1992)

Calculation	Example	Standard Deviation
Addition/Subtraction	$y = a + b - c$	$s_y = \sqrt{s_a^2 + s_b^2 + s_c^2}$
Multiplication/Division	$y = a * b/c$	$\frac{s_y}{y} = \sqrt{\left(\frac{s_a}{a}\right)^2 + \left(\frac{s_b}{b}\right)^2 + \left(\frac{s_c}{c}\right)^2}$
Exponentiation	$y = a^x$	$s_y/y = x s_a/a$

Appendix E – Species Concentrations

Table E1 Concentrations of alkanes (ng/m³) for each BRAVO composite (<DL signifies concentration below detection limit)

Alkane	MidJuly	TxMxJuly	MxJuly	BorderAug	ETxMxAug	BorderLoop	XBorder	BorderSA	SWSept1	ETxMxOct	SSEOct	NTxOct1
n-C18	0.165	<0.014	0.337	0.257	<0.019	0.177	<0.010	0.080	0.246	0.189	0.076	<0.011
n-C19	0.213	0.340	0.257	0.214	0.229	0.166	0.208	0.109	0.169	0.207	0.072	0.032
n-C20	0.274	0.582	0.426	0.179	0.290	0.214	0.127	0.110	0.246	0.195	0.034	<0.011
n-C21	0.661	1.018	0.774	0.428	0.873	0.619	0.322	0.228	0.169	0.313	0.361	0.122
n-C22	0.927	1.402	1.046	0.223	0.700	0.374	0.212	0.091	0.201	0.263	0.186	0.004
n-C23	2.226	2.857	2.282	1.827	2.174	0.828	0.977	1.069	0.786	0.618	0.409	0.055
n-C24	1.044	0.926	2.712	1.389	1.567	1.320	0.361	0.855	0.412	0.237	0.089	0.142
n-C25	1.312	1.560	1.758	1.184	1.661	0.683	0.913	1.258	0.873	0.311	0.244	0.177
n-C26	0.499	0.711	0.910	0.456	1.242	0.235	0.607	1.024	0.731	0.103	0.127	0.141
n-C27	0.525	0.817	0.926	0.604	1.540	0.253	0.770	1.445	0.583	0.237	0.334	0.338
n-C28	0.479	0.571	0.734	0.370	0.923	0.146	0.660	1.081	0.203	0.290	0.110	0.027
n-C29	0.626	0.888	1.185	0.627	0.954	0.144	0.667	1.311	0.327	0.204	0.678	0.138
n-C30	0.178	0.204	0.597	0.205	0.260	<0.032	0.340	0.675	0.127	<0.027	<0.009	<0.015
n-C31	0.703	1.221	0.772	0.666	0.307	0.070	0.351	1.069	0.319	0.137	0.383	<0.018
n-C32	0.341	0.726	0.194	0.369	0.114	<0.038	0.178	0.464	<0.047	0.109	<0.009	<0.018
n-C33	0.222	0.460	0.228	0.423	0.063	<0.038	0.182	0.432	0.169	<0.032	<0.009	<0.018
n-C18	0.165	<0.014	0.337	0.257	<0.019	0.177	<0.010	0.080	0.246	0.189	0.076	<0.011

Table E2 Concentrations of PAH (ng/m³) for each BRAVO composite (<DL signifies concentration below detection limit)

PAH	MidJuly	TxMxMidJuly	MxJuly	BorderAug	ETxMxAug	BorderLoop	XBorder	BorderSA	SWSept1	ETxMxOct	SSEOct	NTxOct1
fluorene	<0.007	<0.007	<0.011	<0.005	<0.008	<0.010	<0.005	<0.002	<0.016	<0.001	<0.004	<0.009
fluorenone	<0.007	<0.007	<0.011	0.043	0.037	<0.010	0.359	0.108	<0.016	<0.001	0.105	0.276
phenanthrene	<0.005	0.017	<0.007	0.013	<0.005	<0.007	1.087	0.012	<0.016	<0.001	<0.002	<0.006
anthracene	<0.005	0.021	<0.007	0.014	<0.005	<0.007	1.156	0.010	<0.016	<0.001	<0.002	<0.006
3-Me phenanthrene	<0.005	<0.005	<0.007	<0.004	<0.005	<0.007	0.067	<0.003	<0.01	<0.001	<0.002	<0.006
2-Me phenanthrene	<0.005	<0.005	<0.007	<0.004	<0.005	<0.007	0.087	<0.003	<0.01	<0.001	<0.002	<0.006
2-Me anthracene	<0.005	<0.005	<0.007	<0.004	<0.005	<0.007	0.036	<0.003	<0.01	<0.001	<0.002	<0.006
9-Me phenanthrene	<0.005	<0.005	<0.007	<0.004	<0.005	<0.007	0.036	<0.003	<0.01	<0.001	<0.002	<0.006
1-Me phenanthrene	<0.005	<0.005	<0.007	<0.004	<0.005	<0.007	0.054	<0.003	<0.01	<0.001	<0.002	<0.006
fluoranthene	0.089	0.022	<0.005	0.095	0.017	0.010	1.038	0.057	0.016	0.001	0.017	<0.004
Cyclopenta(def)phenanthrene	<0.03	<0.03	<0.043	<0.022	<0.031	<0.041	0.569	<0.009	<0.064	<0.005	<0.015	<0.036
acephenanthrylene	<0.004	<0.004	<0.005	<0.003	<0.004	<0.005	0.017	0.003	<0.008	<0.001	<0.002	<0.004
pyrene	0.06	0.020	<0.005	0.078	0.020	0.008	0.669	0.046	0.019	0.001	0.032	0.083
benzo[c]phenanthrene	<0.03	<0.03	<0.005	<0.003	<0.004	<0.005	<0.003	<0.002	<0.008	<0.001	<0.002	<0.004
benzo[ghi]fluoranthene	<0.004	<0.004	<0.005	<0.003	<0.004	<0.005	0.044	0.007	<0.008	<0.001	<0.002	<0.004
cyclopentacephenanthrylene	<0.004	<0.004	<0.005	<0.003	<0.004	<0.005	<0.003	<0.002	<0.008	<0.001	<0.002	<0.004
cyclopenta[cd]pyrene	<0.004	<0.004	<0.005	<0.003	<0.004	<0.005	<0.003	<0.002	<0.008	<0.001	<0.002	<0.004
benz[a]anthracene	<0.004	<0.004	<0.005	<0.003	<0.004	<0.005	0.231	<0.002	<0.008	<0.001	<0.002	<0.004
benzo[k]fluoranthene	<0.008	<0.008	<0.012	<0.006	<0.009	<0.011	0.180	<0.003	<0.018	<0.001	<0.004	<0.010
benzo[b]fluoranthene	<0.008	<0.008	<0.012	<0.006	<0.009	<0.011	0.229	<0.003	<0.018	<0.001	<0.004	<0.010
benzo[j]fluoranthene	<0.008	<0.008	<0.012	<0.006	<0.009	<0.011	0.025	<0.003	<0.018	<0.001	<0.004	<0.010
benzo[e]pyrene	<0.008	<0.008	<0.012	<0.006	<0.009	<0.011	0.135	<0.003	<0.018	<0.001	<0.004	<0.010
benzo[a]pyrene	<0.008	<0.008	<0.012	<0.006	<0.009	<0.011	0.131	<0.003	<0.018	<0.001	<0.004	<0.010
perylene	<0.008	<0.008	<0.012	<0.006	<0.009	<0.011	0.019	<0.003	<0.018	<0.001	<0.004	<0.010

Table E.3 Concentrations of alkanolic acids (ng/m³) for each BRAVO composite (<DL signifies concentration below detection limit)

Alkanolic Acid	MidJuly	TxMxMidJuly	MxJuly	BorderAug	ETxMxAug	BorderLoop	XBorder	BorderSA	SWSept1	ETxMxOct	SSEOct	NTxOct1
C8	<0.06	0.387	1.031	<0.058	0.289	0.338	<0.007	<0.008	<0.009	<0.002	0.134	<0.010
C9	9.044	10.679	5.403	8.975	1.547	1.197	4.080	4.131	1.180	0.614	3.798	2.547
C10	1.338	1.418	1.407	1.058	0.745	0.596	0.616	0.885	0.553	0.548	0.837	0.510
C11	0.213	0.187	0.187	0.193	0.120	0.080	0.105	0.122	0.086	0.097	0.158	0.121
C12	3.029	1.391	1.242	1.068	0.599	0.767	0.693	0.799	0.370	0.418	2.903	0.773
C13	0.456	0.365	0.496	0.397	0.390	0.250	0.290	0.292	0.176	0.316	0.301	0.174
C14	4.523	4.943	3.984	4.675	2.411	1.829	2.246	2.451	1.148	0.950	1.325	0.854
C15	1.214	1.070	1.360	1.827	0.929	0.789	0.789	1.161	0.430	0.407	0.530	0.428
C16	8.765	7.733	8.941	10.357	5.134	4.037	4.824	6.024	2.323	1.789	2.198	1.827
C17	0.268	0.241	0.431	0.436	0.249	0.214	0.222	0.357	0.119	0.098	0.996	0.168
C18	1.764	1.547	2.344	2.197	0.931	0.864	1.463	1.434	0.419	0.426	0.639	0.688
C19	<0.049	<0.038	0.082	<0.047	0.027	<0.006	0.056	1.251	0.015	0.018	0.039	0.036
C20	<0.049	0.095	0.121	<0.047	0.055	0.044	0.060	0.051	0.049	0.042	0.177	0.231
C21	<0.060	<0.046	0.001	<0.058	0.006	0.002	0.006	0.012	<0.014	0.011	0.038	0.032
C22	<0.060	<0.046	0.155	<0.058	0.052	0.031	0.047	0.036	0.029	0.031	0.293	0.332
C23	<0.060	<0.046	0.048	<0.058	0.013	0.011	0.013	<0.008	<0.014	0.008	0.065	0.049
C24	<0.060	<0.046	0.293	<0.058	0.057	0.065	0.097	<0.008	0.037	0.037	0.364	0.365
C25	<0.060	<0.046	0.001	<0.058	<0.010	<0.008	<0.009	<0.008	<0.014	<0.011	<0.005	<0.022
C26	<0.060	<0.046	0.228	<0.058	0.023	0.008	0.019	<0.008	0.009	<0.011	0.198	0.229
C27	<0.060	<0.046	0.033	<0.058	<0.010	<0.008	<0.009	<0.008	<0.014	<0.011	0.050	0.028
C28	<0.060	<0.046	0.643	<0.058	0.030	0.014	0.043	<0.008	0.008	<0.011	0.401	0.614
C29	<0.060	<0.046	0.001	<0.058	<0.010	<0.008	<0.009	<0.008	<0.014	<0.011	0.041	0.026
C30	<0.060	<0.046	0.635	<0.058	<0.010	<0.008	0.041	<0.008	<0.014	<0.011	0.325	0.443
C31	<0.060	<0.046	0.001	<0.058	<0.010	<0.008	<0.009	<0.008	<0.014	<0.011	<0.006	<0.022
C32	<0.060	<0.046	0.143	<0.058	<0.010	<0.008	<0.009	<0.008	<0.014	<0.011	0.070	0.109

Table E4 Concentrations of wood smoke markers, alkanolic diacids and other compounds (ng/m³) (<DL signifies concentration below detection limit)

Compound	MidJuly	TxMxJuly	MxJuly	BorderAug	ETxMxAug	BorderLoop	XBorder	BorderSA	SWSept1	ETxMxOct	SSEOct	NTxOct1
Guaiacol	<0.008	<0.007	<0.011	<0.005	<0.007	<0.010	0.051	<0.004	<0.011	0.006	<0.014	<0.006
4-Ethylguaiacol	0.288	0.488	0.210	0.157	0.271	0.559	0.280	0.157	0.407	0.522	0.900	0.230
Eugenol	<0.019	<0.018	<0.030	<0.014	0.023	0.039	0.072	<0.006	0.017	0.034	<0.037	<0.017
Isoeugenol	<0.031	<0.029	<0.048	<0.022	0.076	0.170	0.270	<0.009	0.057	0.175	<0.061	<0.028
Vanillin	0.312	0.213	0.123	0.058	0.130	0.137	0.481	0.058	0.065	0.080	0.158	<0.012
Syringaldehyde	<0.031	<0.029	0.127	0.115	0.124	0.045	0.323	0.022	0.090	0.100	<0.061	<0.028
Retene	<0.013	<0.012	<0.019	0.041	<0.013	<0.016	0.155	0.015	<0.026	<0.016	<0.025	<0.006
Citric Acid	0.084	0.113	0.161	1.681	0.931	0.240	0.739	1.908	0.417	1.467	1.334	0.044
6,10,14-trimethyl pentadecan-2-one	4.569	4.226	5.019	3.639	4.024	6.361	4.749	4.258	3.091	1.736	1.188	0.929
Levogluconan	<0.021	<0.012	<0.018	<0.022	<0.006	<0.011	1.099	<0.008	<0.013	<0.009	<0.015	<0.009
Galactosan	<0.039	<0.031	<0.035	<0.040	<0.011	<0.020	0.080	<0.015	<0.025	<0.019	<0.031	<0.017
Mannosan	<0.03	<0.022	<0.027	<0.03	<0.09	<0.016	0.242	<0.011	<0.019	<0.014	<0.023	<0.013
2(4H)Benzo furanone	0.829	0.469	0.618	0.387	0.420	0.972	0.678	0.651	0.535	0.665	0.482	1.431
Succinic Acid	<0.046	<0.033	<0.016	<0.04	0.087	0.043	0.044	<0.016	0.044	0.908	0.027	0.023
Malonic Acid	<0.046	<0.033	<0.016	<0.04	0.942	0.183	0.084	0.211	0.289	1.630	0.027	0.015
Adipic Acid	<0.046	<0.033	0.205	0.187	0.942	0.145	0.035	0.023	0.524	1.097	0.122	0.142
Azealic Acid	0.060	0.378	0.577	0.487	0.603	0.291	0.025	0.329	0.310	0.251	0.294	0.161
Oleic Acid	0.239	0.228	0.375	0.292	0.084	0.166	0.284	0.151	0.063	0.091	0.139	0.180
cholestane	<0.007	<0.004	<0.012	<0.008	<0.014	<0.011	<0.006	<0.005	<0.021	<0.010	<0.004	<0.008
17 α 21 β hopane	<0.007	<0.004	<0.012	<0.008	<0.014	<0.011	<0.006	<0.005	<0.021	<0.010	<0.004	<0.008